Computational Modeling of Barometric Pressure Fluctuation Effects on Explosive Methane-Air Mixtures in a Longwall Mine Gob

Thesis · May 2017

DOI: 10.13140/RG.2.2.22535.19360

1 author:

Samuel Lolon
Colorado School of Mines
13 PUBLICATIONS **16** CITATIONS

SEE PROFILE

COMPUTATIONAL MODELING OF BAROMETRIC PRESSURE FLUCTUATION EFFECTS ON EXPLOSIVE METHANE-AIR MIXTURES IN A LONGWALL MINE GOB

by

Samuel Atta Lolon

A thesis submitted to the Faculty and the Board of Trustees of the Colorado School of Mines in partial fulfillment of the requirements for the degree of Doctor of Philosophy (Mining and Earth Systems Engineering).

Golden, Colorado

Date _____ Signed: _____
Samuel Atta Lolon

Signed: _____
Dr. Jürgen F. Brune
Thesis Advisor

Signed: _____
Dr. Gregory E. Bogin, Jr
Thesis Advisor

Golden, Colorado

Date _____ Signed: _____
Dr. Priscilla P. Nelson
Professor and Head
Department of Mining Engineering

ABSTRACT

The coal mining industry remains a major player in electrical power generation for the United States. The U.S. Energy Information Administration (EIA) reported that coal made up the second largest share after natural gas, approximately 30%, of the total electricity generated in 2016, further, it projected to remain significant for the next several decades together with natural gas and renewable sources (U.S. Energy Information Administration, 2017). Longwall mining has become more frequently used for extracting coal seams underground due to increased safety and higher productivity (EMFI, 2010) through improved mechanization and mining system automation.

In the longwall method, the overlying strata are allowed to cave behind the working face after the coal is extracted, creating a porous zone known as gob. Due to its caving nature, the gob is inaccessible and presents a safety concern because of the potential methane and explosive mixture accumulation occurring in this zone. There have been a great number of mine fires and explosions in the United States and other countries that suggest the existence of an explosive mixture or Explosive Gas Zone (EGZ) in bleeder-ventilated longwall gob (Loane et al., 1975*;* Lynn et al., 1986; McKinney et al., 2001; Dziurzynski and Wasilewski, 2012; Brune, 2013). These events indicated that EGZs must have existed inside and around the perimeter of gobs. The risk of mine explosion will increase if these EGZs flow out from the gob to the surrounding mine entries.

As mine pressure is influenced by atmospheric pressure, the fluctuation of outside pressure can disturb the pressure differential between the internal and external gob which consequently can either escalate or lessen the EGZ outgassing from the gob. A number of studies have related major mine explosions to abrupt barometric pressure changes in the United States, South Africa, Australia, and Poland (Hosler, 1948; Boyer, 1964; Kissell et al., 1973; Fauconnier, 1992; Hemp, 1994; Wasilewski, 2014; Belle, 2014; and Lolon et al., 2015). These disastrous mine explosions

seem to happen frequently in stormy weather, which occur during late fall and winter seasons in the United States.

Numerical modeling using computational fluid dynamics (CFD) is considered the best suited approach for simulating methane air flow and mixture in the gob due to its inaccessibility, which limits the availability of gob data. CFD modeling has been widely used for mine ventilation analysis around the globe (Brunner et al., 1995; Wala et al., 1997; Balusu et al., 2002; Calizaya et al., 2004; Lowndes et al., 2005; Yuan et al., 2006; and Ren, 2010). CFD models were developed in this research to analyze the formation of EGZ in the bleeder-ventilated gob, the effects of various magnitudes and rates of barometric pressure change on the EGZ and methane outgassing, and the potential location of the outgassing. The model was built based on an actual supercritical longwall mine in the western United States, characterized by the condition of no overlying strata hanging above the shields. The ventilation parameters and gob permeability characteristics were obtained from cooperating mines which had been studied by earlier researchers in this project (Worrall, 2012; Wachel, 2012; Marts, 2015; Gilmore, 2015). Other parameters not available in the cooperating mine such as location and operating pressure of methane source, and pressure drops of regulators and other ventilation controls were obtained from reliable references or similar studies, or calculated to be deemed reasonable.

The outputs of CFD modeling indicated fringes of EGZ within the gob and several back-end crosscuts on the tailgate return under static atmospheric pressure condition, confirming an observation reported by several explosion investigations and studies of EGZ existence within the gob (Elkins et al., 2001; McKinney at al., 2001; Cario, 2006; Woodward and Sheffield, 2008; Page et al., 2011; Brune, 2013). The CFD models show that, under normal bleeder ventilation systems, it is very likely that EGZ is formed within the gob as a result of ventilation air ingressing into the

gob and mixing with methane. The CFD models further identified that the methane and EGZ outgassing occurs in barometric pressure fall scenarios. The rise of atmospheric pressures is a preferable situation with respect to EGZ outgassing; CFD models demonstrated decreasing EGZ volumes within the gob and tailgate return crosscuts associated with barometric or external pressure increases. Therefore, this research focused more on the barometric fall scenarios than the cases where it increased. The hypotheses of gob breathing and outgassing under various scenarios of pressure changes were also proved by analyzing the modeling outputs. The amount of EGZ outflow depended on the magnitude of the pressure drop. The rate of outgassing was controlled by the rate of pressure fall. The location of EGZ outgassing was mainly in the tailgate and bleeder returns.

Gob permeability is major assumption in this modeling, thus a parametric study is presented to discuss the effect of permeability on the base EGZ cases. The study shows larger EGZ volume within the gob with higher permeability. Higher permeable gob allowed more air ingression into the gob which, mixed with methane, resulted in larger EGZ. At the end, the results were validated against data provided by cooperating mines and also compared with published data.

The main objective of this research is to provide the mining industry, its stakeholders, and the body of knowledge with a better understanding of gob breathing, EGZ outgassing and the methane explosion risk associated with barometric pressure changes and, ultimately, recommendations of best practices to prevent outgassing from resulting in a mine explosion. The best practices recommended include the risk matrix, a continuous monitoring system, and Gob Ventilation Borehole (GVB) application.

TABLE OF CONTENTS

LIST OF FIGURES

LIST OF TABLES

LIST OF ABBREVIATIONS

Armored Face Conveyor …… AFC

Atmospheric Monitoring System …… AMS

Barometric Pressure…….…… BP

Bleeder Evaluation Point ……. ……. BEP

Computational Fluid Dynamics …….…….…… CFD

Code of Federal Regulations ……..… CFR

Commonwealth Scientific and Industrial Research Organization …… CSIRO

Colorado School of Mines ……..…CSM

Discrete Fracture Network ……...DFN

Energy Information Administration ……..……EIA

Explosive Gas Zone ……..... ……...EGZ

Fast Lagrangian Analysis of Continua ……FLAC

Gas Chromatograph …….....……. GC

Gob Ventilation Borehole …….……. GVB

Graphic User Interface …….....……...GUI

Headgate …….....……HG

Lower Explosive Limit …….....……...LEL

Mining Safety and Health Administration ……MSHA

National Oceanic and Atmospheric Administration ……...NOAA

Pressure Staggering Option …….. PRESTO!

Quadratic Upstream Interpolation for Convection Kinematics ……. QUICK

Renormalization Group Theory ……. RNG

Semi-Implicit Method for Pressure-Linkage Equations ……..…SIMPLE

Tailgate …….....……TG

Tube Bundle System …….....……. TBS

Ubiquitous Joint …….....……UBJ

Upper Big Branch …….....…..…UBB

Upper Explosive Limit …….....……...UEL

U.S. Bureau of Mines …….....…...USBM

User Defined Function …….....……UDF

Volumetric Strain Increment ……..……VSI

ACKNOWLEDGEMENTS

First and foremost, praise and thanks goes to my savior Jesus Christ for the many blessings undeservingly bestowed upon me. This research project would not have been possible without the financial support of the National Institute for Occupational Safety and Health (NIOSH) under contract number 211-2014-60050, and I would like to thank my advisor and mentor, Dr. Jürgen Brune for the opportunity to be a part of this project. I am very grateful for his knowledge sharing, continuous guidance of my efforts to improve my analytical thinking, writing and presentation skills. I would also like to thank my co-advisor Dr. Gregory Bogin for all discussions that ensued to help me understand better computational fluid dynamics, Dr. John Grubb, who initiated the first phase of this research project, for sharing his valuable knowledge and experience in longwall mining, Dr. Hugh Miller for his continuous encouragement and support during my study, and Dr. Neal Sullivan for chairing the committee and being available for consultation.

Further acknowledgement is due to all my predecessors in this project, Dan Worrall, Elizabeth Wachel, Jon Marts, Richard Gilmore and Saqib Saki, all of whom had invaluably contributed and set fundamental understanding of the explosibility, geomechanical model and CFD longwall model required for my research as well as many hours of HPC and MIO lessons, and fellow graduate students, Aditya Juganda, Mat Fig and Claire Strebinger for all interesting discussions. I would also like to thank Dr. Priscilla Nelson, the head of Mining Engineering Department, and the rest of the faculty for the knowledge sharing as well as Mandi, Emilia and Bruce for all their administrative assistance.

Finally, but most importantly, I wish to thank my wife, Selvi, and son, Cleon, for their continuous support and reminder of life balance, and my parents, Jan and Elisabeth, for their constant prayers.

I dedicate this work to my late father, Jan Kaleopas Lolon.

CHAPTER 1

INTRODUCTION

The coal mining industry remains a major player in electrical power generation for the United States. The U.S. Energy Information Administration (EIA) reported that the coal made up the second largest share, approximately 30%, of the total electricity generated in 2016, and though showing a decreasing trend, coal as an electricity source is projected to remain significant for the next several decades together with natural gas and renewable sources (U.S. Energy Information Administration, 2017).

The challenge of decreasing coal demand has increasingly made the coal mining industry strive for high productivity but low-cost operations. Longwall mining, a safe and highly productive coal mining method, has become more frequently used for extracting coal seams. The dimensions of longwall panels have increased to achieve higher coal recovery. Mine operators have also made great efforts in improving mechanization and automation of mining systems using advanced modern technologies. These efforts, on one hand, can increase productivity of longwall operations, but on the other hand, the increased productivity allows the coal to be mined faster. Higher mining rates may increase the amount of methane liberated at the face and in the gob, increasing fire and explosion risks. Gob methane accumulations can present a more serious concern during atmospheric pressure swings. The inability to take direct methane measurements in the gob causes uncertainty about the effectiveness of ventilation design and airflow controls to reduce or eliminate explosion risks.

The severe consequences of fire and explosion risks, including loss of lives and property damage, underscore the importance of this study. This study will evaluate risks associated with the

accumulation of explosive mixtures in the caved region under varying conditions of external atmospheric pressure, and eventually propose solutions that can be implemented to establish safer mine operations.

1.1 Introduction to Underground Longwall Coal Mining

A common underground mining technique used in the United States is the longwall method. This method is preferred due to its improved safety and high productivity, particularly for mining deeper coal seams (>1,000 ft) as it does not require the large pillars found in room-and-pillar operations (EMFI, 2010). The 2015 report issued by the U.S. Department of Energy reported that longwall mines accounted for 60% of the nation's underground coal output in 2015, with an average productivity of 4.65 short tons per employee hour (U.S. Energy Information Administration, 2016), which is almost double that of the room-and-pillar method. As of January 2016, there were 45 operating longwall mines in the United States (Fiscor, 2016).

The longwall mining method is utilized for horizontal or nearly flat-lying seams that have relatively uniform thickness and are free from major faults and discontinuities. Most commonly, U.S. longwalls use three- or four-entry gate roads for panel development. Two-entry gates are often used under deeper cover to achieve better pillar stability. A schematic of a longwall mine with a three-entry panel is shown in Figure 1.1. Development is completed by driving both gate roads and a setup room using a continuous miner, shown in the left bottom inset of Figure 1.1. Development work with continuous miners usually requires nine to 12 months, depending on the panel size. Through this section, longwall equipment components and shields are brought in to the startup room for assembly; once the installations of the longwall equipment and shields are complete, longwall mining begins and advances along the panel from the startup room towards the

recovery room (left top inset). Each panel is typically about 330 m (1,000 ft) wide and 3,100 m (10,000 ft) long.

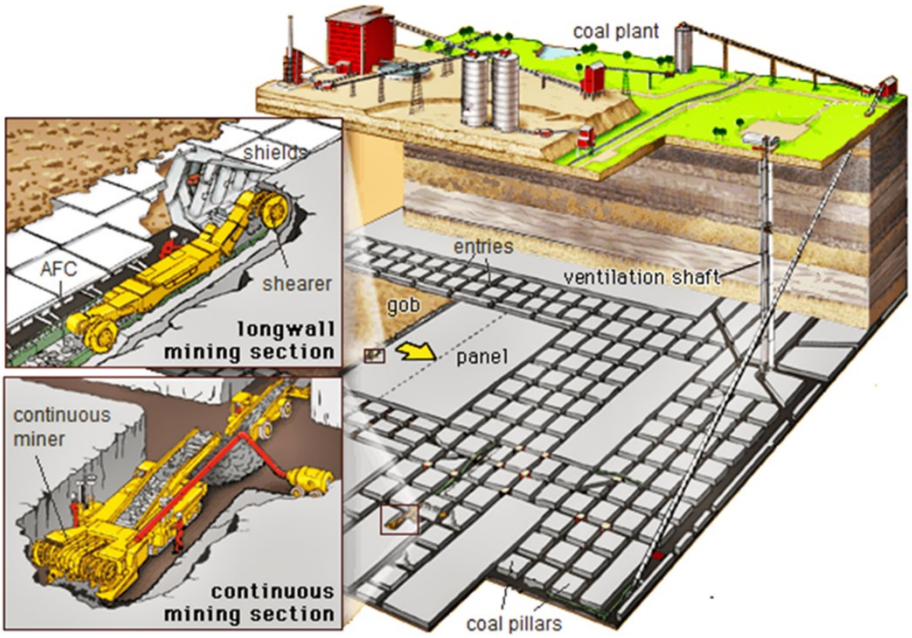

(Source: https://www.britannica.com/technology/coal-mining, last accessed 03/20/2017)

Figure 1.1: Schematic of the longwall mining method

Longwall mining is typically performed by either an advancing or retreating method. In the advancing method, the face starts from the main entries and works its way towards the back end of the panel. This method was once common in Europe. The coal production starts early with the setup room located near the main entries. Since longwall mining allows the area behind the face to collapse, the advancing type is unfavorable, as it requires great effort to maintain the main entries and the gob in good condition. In contrast to the advancing type, the retreating method is widely used in the United States and Australia. With this method, coal extraction does not begin until the panel entries are developed to the farthest end of the panel; once the development is complete, the coal extraction proceeds from the panel's back end toward the main entries, which is preferred because there is little disturbance to the main entries during mining.

The set of entries used as routes for transportation of miners, equipment and supplies is called a headgate; these entries are also used to deliver fresh air into the mine. On the opposite side of the panel, tailgate entries are used for return air. Each entry is about 3.4 m (11 ft) high and 6 m (20 ft) wide. These entries are connected every 61 m (200 ft) by crosscuts and are separated by pillars 6 m (20 ft) wide. On the back of the panel, the development entries are connected by another set of entries, bleeder entries, which typically have the same size as the headgate and tailgate entries. The dimension of pillars and entries were obtained from the mine map and the information was made available by the cooperating mine.

Figure 1.2 shows the longwall system used to extract coal from the face, which consisted of a shearer, a set of shields, and an armored face conveyor (AFC). For a 330 m (1,000 ft) wide panel, a single continuous pass of coal cutting from the headgate to tailgate takes about 45 minutes. As the shearer moves along the face, its pair of cutting drums detach coal from the face, break it into pieces, and push it all onto the AFC when the shields advance forward. The AFC transports the coal to a loading point on a beam stage loader and then to a main belt conveyor, which eventually delivers it to the stockpile located at the surface.

Figure 1.2: Typical longwall system (Joy Global, 2014)

The support system shown in Figure 1.2 consists of a side-by-side arrangement of hydraulic shields. These shields are used not only to hold the roof during coal extraction and push the face conveyor forward, but also to provide a safe workspace. Most longwall mines today utilize between 100 and 200 shields per panel. Each shield has a roof canopy supported by hydraulic jacks, and each jack is connected to AFC by a relay bar, which is also used to push shields forward. After a panel has been completely mined out, the equipment and support system are dismantled and relocated piecemeal to the next panel for reassembly. This process takes about two to four weeks.

In the longwall method, the overlying strata cave behind the shields immediately once the shields move forward. This caved area is referred to as the gob (see Figure 1.3) and mainly consists of coal, caved-in roof rocks and heaved-up floor materials representing a porous medium (Peng, 2006). Although there is no field data available to demonstrate gob condition, it is generally accepted that the gob further from the face becomes consolidated and compacted over time because of changes in stress patterns and also due to the weight of the overburden. Because of this compaction, the gob further away from the longwall face, is less permeable than the region behind the shields. This characteristic controls the fluid flow and becomes a crucial parameter in the gob study.

The gob presents a safety concern because of the potential methane accumulation in this region. Figure 1.3 shows the degasification methods most commonly used to reduce gob methane accumulation. Pre-mining degasification includes horizontal and vertical in-seam boreholes; after mining, methane is drained from the gob using gob vent boreholes. The effectiveness of these methods cannot be precisely measured, again, due to the unknown conditions of the gob (Karacan, 2008).

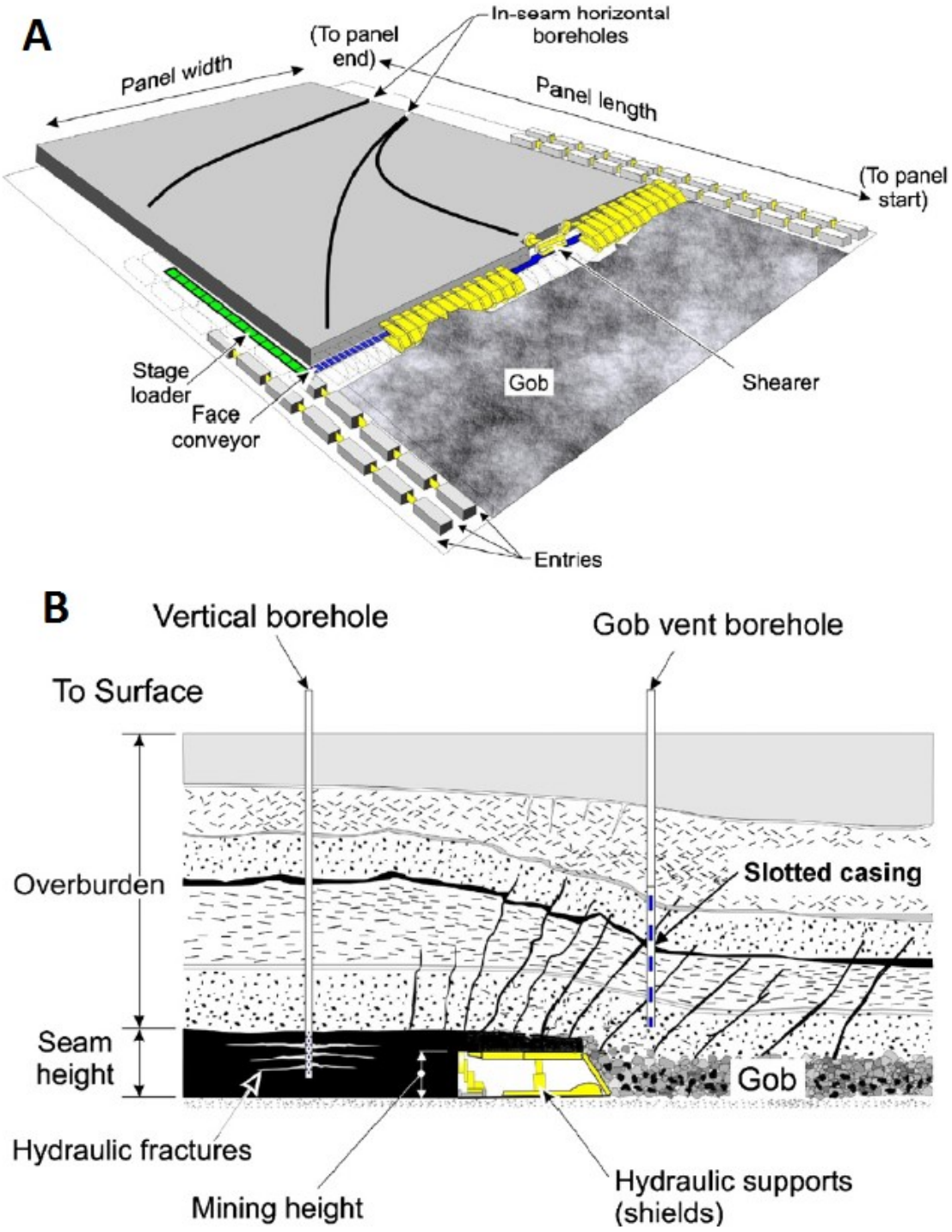

Figure 1.3: Longwall degasification (A) plan and (B) cross-section views (Karacan, 2008)

1.2 Longwall Mine Ventilation Systems

The ventilation system is the lifeblood of underground mines. It ensures safe working throughout the mine by providing sufficient fresh air for human breathing as well as diluting and carrying away contaminants, dusts, and other hazardous gases to achieve a safe mine atmosphere. In the United States, longwall mines are required to achieve methane concentration of less than 1% by volume (per 30 CFR §75.334) in active entries, 2% in bleeder entries and maintain respirable dust levels below 2 mg/m^3 in all work areas over an eight-hour shift (Colinet et al., 2010). In inactive abandoned areas and the gob, the issue of methane accumulation is commonly mitigated by combining the performance of the ventilation system and with drainage methods such as gob ventilation borehole (GVB).

There have been a variety of ventilation systems developed for longwall mining, but they can be broadly classified as either a U-type or Y-type system (McPherson, 1993). Other ventilation layouts can be variations or combinations of these two systems, including a progressive sealing and Y-systems with back return (Grubb, 2008). The main features and layout of U-type and Y-type systems in a three-entry panel are presented below. These are the common ventilation arrangements used in U.S. longwall mines, including the cooperating mine on which this study is based. Though not very common, the four-entry panel also exists; however, it is specifically used for gassy coal seams as the additional airway provides less airflow resistance overall (Krog and Bise, 2009).

1.2.1 U-type Ventilation System

U-type ventilation is sometimes referred to as bleederless. In this system, air is brought to the face from the headgate and is exhausted through the tailgate, towards the main entries. The airflow schematic is shown in Figure 1.4. The intake air is split at the headgate corner. Most of the

fresh air is directed towards the face and the remainder is used to dilute the dust and methane in the belt entry. The outby tailgate entries are used to exhaust contaminated air.

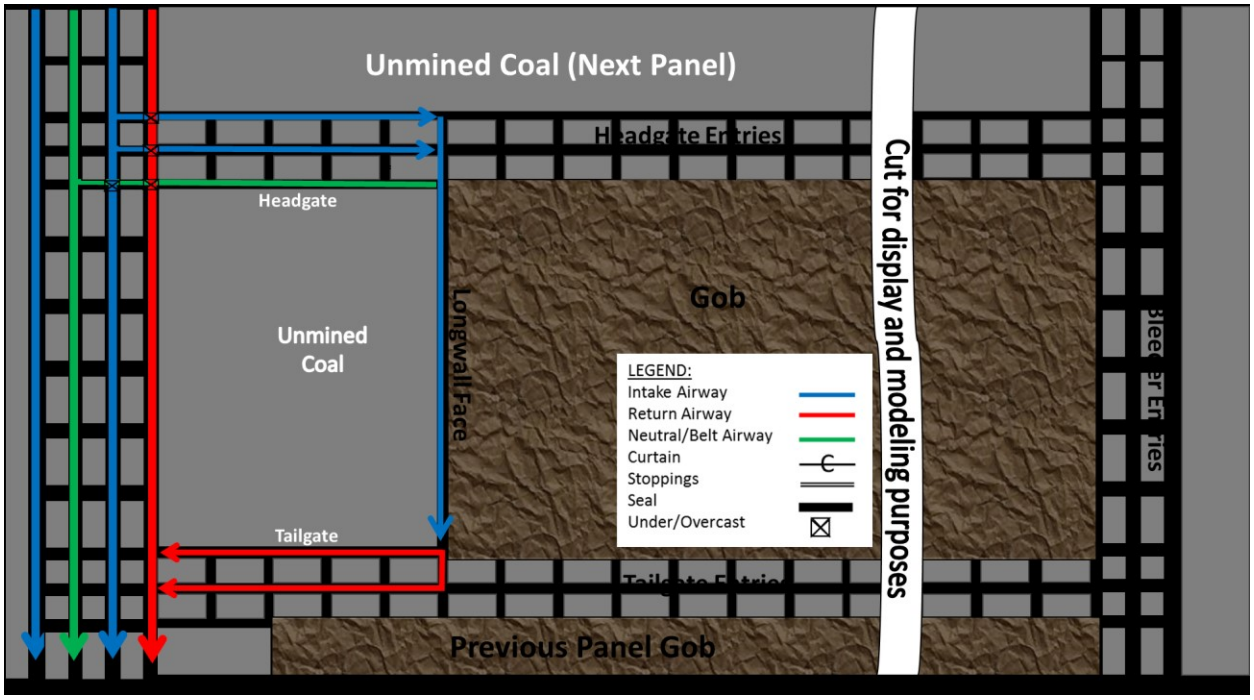

Figure 1.4: Typical U-type ventilation system

The U-type system is preferred for coal mines possessing a high tendency for spontaneous combustion (sponcom), as it limits the ingress of air into the gob. The seals are built in the crosscuts along the headgate and tailgate entries as the mine progresses. Currently, the use of the U-type or bleederless system is limited in the United States unless the mine demonstrates sponcom propensity (30 CFR §75.334). The main disadvantage of this system is that, in gassy mines, methane could accumulate in the gob.

1.2.2 Y-type Ventilation System

Most longwall mines in the United States use the Y-type ventilation system, which is referred to as a bleeder system. A typical wrap-around Y-type system uses both the headgate and tailgate entries outby the face as the intake, and the tailgate bleeder inby as the return. Figure 1.5

shows a typical setup of this system. The fresh air flushes the face and the gob. Inby the face, only two entries at the headgate and one at the tailgate are available for ventilation since the inner entries on both sides are assumed to be partially or completely blocked by caving material. The contaminated air exits through the open entry at the tailgate. This system, which allows some portions of fresh air to flow across the gob, is preferred for gassy mines because it is designed to control the gas emitted inside the gob (Kissell, 2006). The tailgate intake provides additional fresh air to dilute the gas in the tailgate corner. In contrast to the U-type system, this system is not recommended for sponcom-prone coals because the air would promote the oxidation of coal left in the gob.

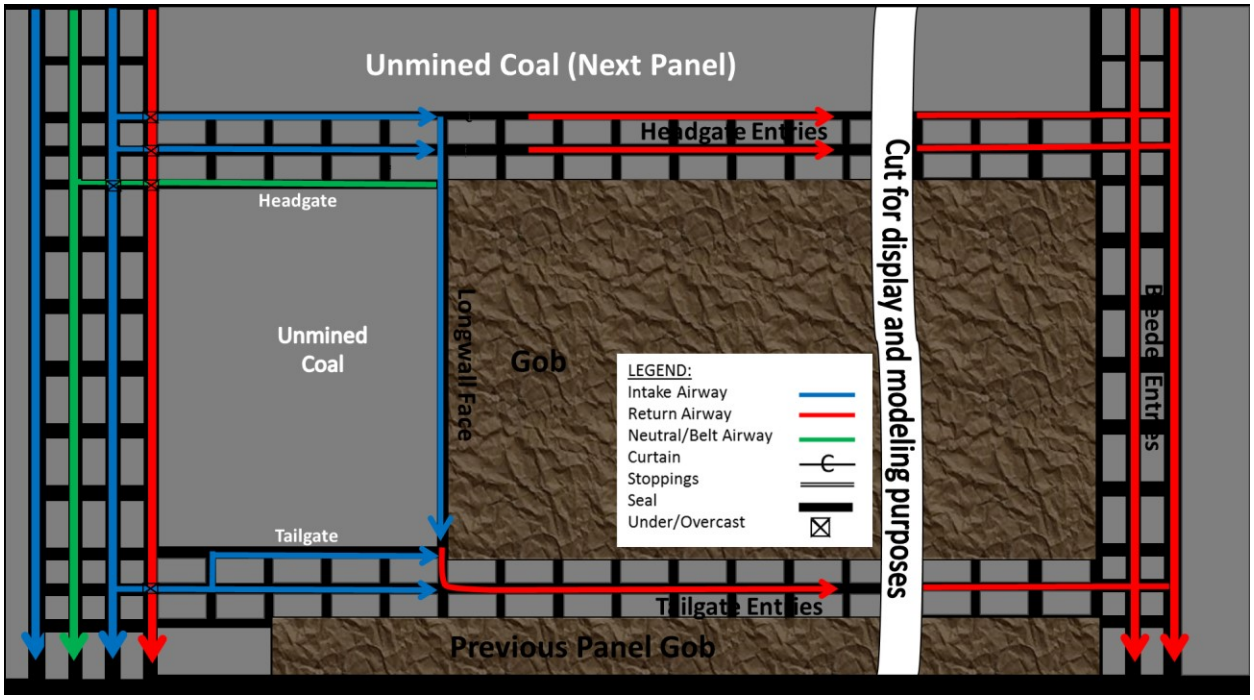

Figure 1.5: Typical wrap-around Y-type ventilation system

1.2.3 Y-type Ventilation System with Progressive Sealing

A typical modification of the Y-type ventilation system utilizes sealing or stoppings in the inby tailgate entry, as shown in Figure 1.6, compared to the conventional Y-type system, where it is open. The seals are constructed progressively in all inby crosscuts as the mine advances at the

headgate and tailgate sides (Smith et al., 1994; Grubb, 2008). This progressive ventilation system was first proposed in 1985 (MSHA, 2002). The outby tailgate entries that are used as the intake in the conventional Y-type system become the return airways in this method.

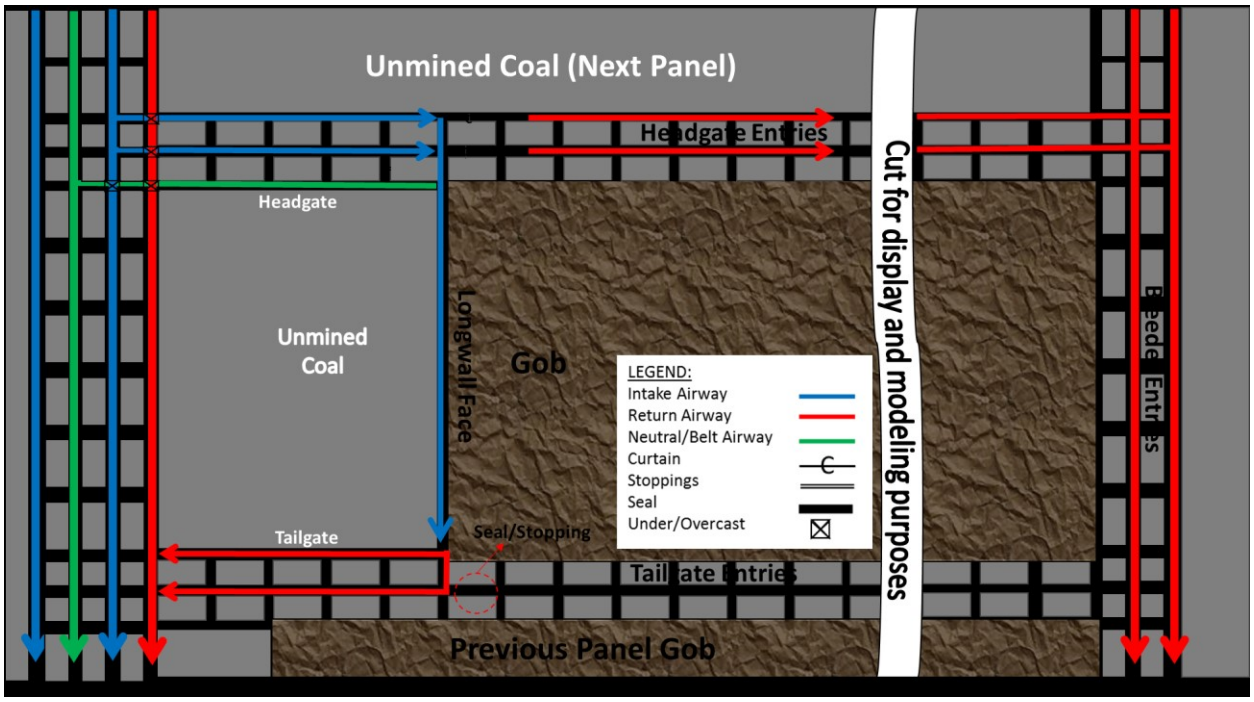

Figure 1.6: Modified Y-type system with progressive sealing

1.2.4 Y-type Ventilation System with Back Return

Another variation of the Y-type ventilation system is progressive sealing with back return. In this system, only the first inby crosscut on the tailgate is open (Smith et al., 1994; Grubb, 2008). This modification is marked in Figure 1.7. The face ventilation air at the tailgate is directed to inby the tailgate corner of the gob and passes through the first open crosscut. The purpose of having the back return is to sweep the methane that accumulates in the tailgate corner if the progressive sealing method is used.

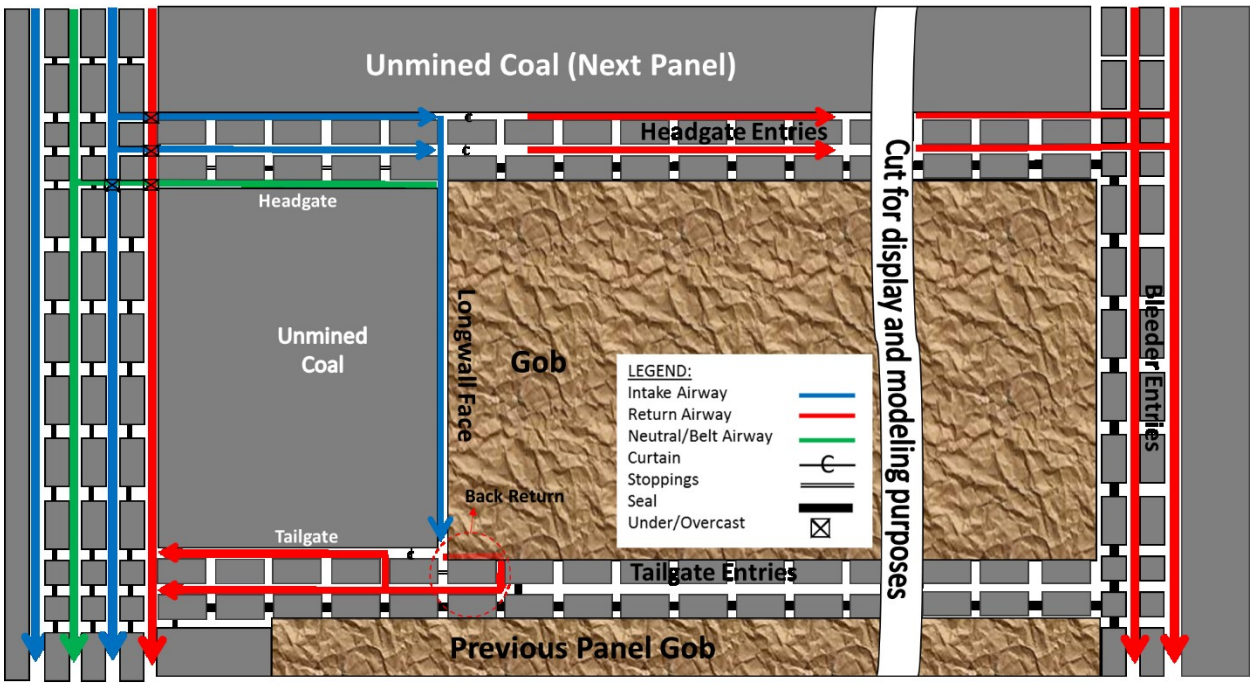

Figure 1.7: Modified Y-type system with back return

1.3 Introduction to Barometric Pressure

Barometric pressure is the pressure exerted by the weight of air in the atmosphere. As an example, the air pressure at sea level is approximately 101,352 Pa (newtons per square meter) or 14.7 psi (pounds per in^2). This means that the weight of air within a one-square-meter area, extending all the way up to the top of the atmosphere from the sea surface, contains roughly 101,352 newtons. Figure 1.8 shows the general thickness and height of the atmospheric subzones per observations by Fleagle and Businger (1980). Air pressure decreases as the altitude increases and becomes nearly nothing at the top of thermosphere region which is approximately 500 kilometers (310 miles) above sea level. Beyond the thermosphere, air does not exist, resulting in a vacuum pressure (Wallace and Hobbs, 2006). Since barometric pressure exists only in the atmosphere, the term atmospheric pressure is often used. These two terms will be used interchangeably in this dissertation.

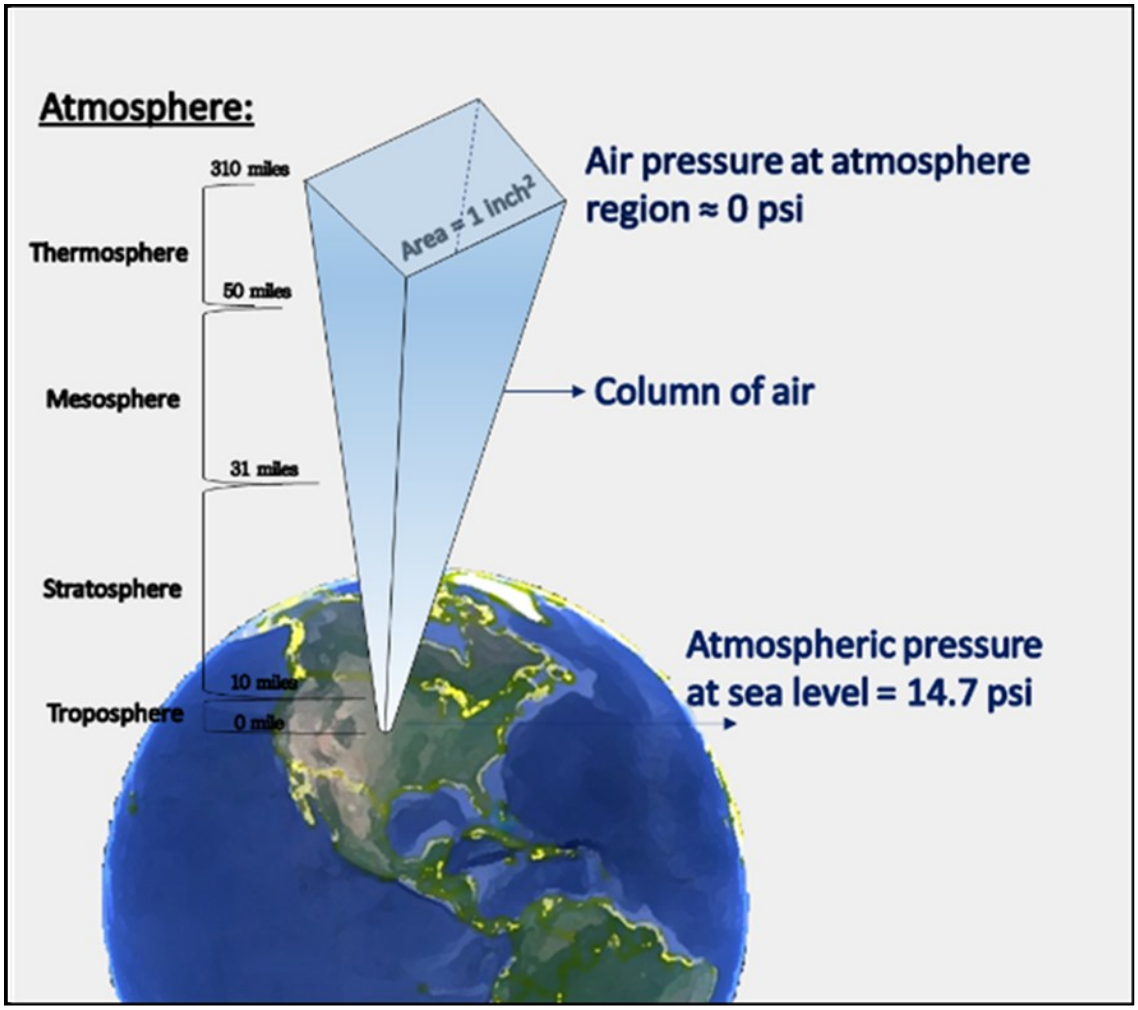

Figure 1.8: Visual representation of air pressure within the atmosphere region

Barometric pressure affects the air condition at any location within the atmosphere and in below sea-level ground, such as in deep underground mines. Since these mines connect to the surface openings via shaft or drift, barometric pressure has a great impact on mine conditions. The ventilation system in the mine is forcibly driven by the pressure difference between the fan and surface openings. The fan pressure which is usually set fixed is mechanically generated, while surface pressures are controlled by barometric condition. The changing barometric pressure will change mine pressure conditions; these changes can either assist or act against the work of a mine fan. Even without the fan, barometric pressure can facilitate natural ventilation; specifically, for a longwall mine gob or other sealed area, changes in barometric pressure can cause outflow and

inflow of gases across the boundaries of these areas. This phenomenon is known as gob breathing. Since methane is the most likely gas to accumulate in the gob, barometric pressure falls will trigger outflow of this gas from the gob and create an explosive mixture when mixing with oxygen from ventilation air that is abundantly available outside the gob. In contrast, when the pressure rises, more air ingresses into the gob, which may also change the explosibility of gob gases. In Section 3.4, a number of major coal mine explosions that have occurred during intense barometric pressure changes in the United States are presented. These explosions emphasize the consequences of gob breathing associated with barometric pressure changes. Moreover, barometric pressure fluctuations occur naturally due to constant weather changes or regular heating and cooling of atmospheric air, so gob breathing is difficult to control or mitigate by means of the ventilation system, which will be taken into consideration in this study for best practice recommendations.

1.4 Dissertation Structure and Dissemination

This dissertation comprises nine chapters, a bibliography and appendices.

Chapter 1 presents a brief introduction and general background of underground longwall mine, ventilation system, and relevant theories of barometric pressure. The synopsis of the dissertation concludes the chapter.

Chapter 2 contains an overview of the methodology and hypothetical framework on which the study is based, the motivation and the main research questions, expected outcomes, specific tasks and original contributions of the research.

Chapter 3 is a detailed literature review on the research topics of the barometric pressure, the formation of explosive methane-air mixture in the gob, cause and impact of barometric pressure fluctuation on this explosive mixture, and effects of gravity on the mixture stratification.

Chapter 4 describes the theoretical background and key components of computational fluid dynamics (CFD) modeling including its governing equations, model geometry and setup, boundary conditions, and criteria for modeling solutions used in this study.

Chapter 5 describes model validation and comparison with actual mine conditions, sensitivity of the modeling outputs to several major assumptions such as gob permeability and selected initialization method. This chapter also presents the result of mesh independence exercise to the simulation outputs.

Chapter 6 details the CFD modeling followed by discussion on the results. Several scenarios of different magnitude and rates of barometric pressures together with the details of results are presented and discussed.

Chapter 7 presents high level recommendations for operational best practices which are developed based on the modeling results given in previous chapter. These recommendations are developed within the framework of study objectives of preventing the explosive mixture outgassing and mitigating the explosion risk if the outgassing does occur.

Chapter 8 summarizes the findings and results of the study and describes the research conclusions of various scenarios conducted in CFD modeling.

Chapter 9 describes some improvements that are necessary to include in the future work of this study. These improvements correspond to the modeling parameters and assumptions, the definition of explosive range, and operational best practices.

A bibliography of cited references and appendices follow Chapter 9.

The results and findings of the study have been disseminated in the forms of conference presentations and journal publications as shown below.

1. Effect of Barometric Pressure Decreasing on Explosive Gas Zones in Longwall Bleeder Gobs, in Proceedings of the 15th North American Mine Ventilation Symposium, Blacksburg, Virginia, June 2015 (Peer-reviewed).
2. Computational Fluid Dynamic Simulation on the Longwall Mine Gob Breathing, in International Journal of Mining Science and Technology, Vol. 27, Issue 2, March 2017, published by Elsevier, B.V. with DOI: 10.1016/j.ijmst.2017.01.025 (Peer-reviewed).
3. Understanding Gob Outgassing Associated with Pressure Disturbances in Longwall Mine in Proceedings of the 16th North American Mine Ventilation Symposium, Golden, CO, June 2017 (Peer-reviewed).
4. CFD Studies on the Phenomenon of Gob Breathing Induced by Barometric Pressure Fluctuations in SME Annual Conference Preprint 16-154, Phoenix, AZ, February 2016.
5. Evaluation of Gob Pressure Response Due to Changes in Mine Atmospheric Pressure in SME Annual Conference Preprint 17-062. Denver, CO, February 2017.

CHAPTER 2

RESEARCH METHODOLOGY

2.1 Motivation for Research

The coal mining industry has long been associated with many safety concerns, including mine explosion. Historically, the mine explosion risk has been acknowledged since coal mining began. In *De Re Metallica*, arguably the most influential book of early mining methods, the dangers of "firedamp" or the methane-air mixture explosion were noted and depicted as the "fiery blast of a dragon's breath" (Hoover and Hoover, 1950). The consequences of mine explosions can include loss of life and mine closure. According to the National Institute for Occupational Safety and Health (NIOSH), a total of 494 coal mine explosions killing nearly 12,000 miners have occurred since 1839 in the United States (2016). Furthermore, many major explosions have also resulted in permanent shutdowns of the affected mines. Though mine accidents have been greatly reduced, methane explosions remain a serious risk in underground coal mines.

2.2 Research Objective and Hypothesis

The objective of this research is to provide the mining industry and its stakeholders with a better understanding of the methane explosion risk associated with barometric pressure changes as well as recommendations for preventive and mitigation methods. The methodology of computational modeling can serve as a tool for use by a mine operator to evaluate the current ventilation plan and its vulnerability to barometric pressure changes. It should be noted that modeling is not intended to give an exact prediction, but rather to give recommendations based on the trends of the simulation outputs. This approach allows users to use the simulation results as a general guideline for other longwall mines as opposed to one specific mine.

It is widely accepted that variation in barometric pressure will strongly influence the mine atmosphere and the internal gob, causing the phenomenon known as gob breathing. This research specifically demonstrates the existence of gob breathing and quantitatively evaluates its impact on explosive gas zones (EGZs) in the gob and active workings.

Figure 2.1 shows a simplified schematic of pressure conditions that occur in the gob and bleeder entries during gradual barometric pressure fluctuations (Lolon et al., 2017b). The red line represents the internal gob pressure, while the blue line shows the pressure at the tailgate return near the bleeder outlet. In a bleeder system, the blue line should be lower than the red line. The differential ΔP_s forces flow of contaminated air from the gob to the tailgate and bleeder returns. A gradual change in external pressure is presented with the gradual change of the blue line starting at t_0. Due to gob material and distance, airflow is restricted in the gob, causing the internal pressure change to lag behind the external or bleeder pressure change. At time t_1, the external pressure becomes steady, while the gob pressure continues to change until t_2 when ΔP_s is reached again between it and the external pressure. Due to this lag, the pressure differential of ΔP_b between gob and bleeder pressure, marked with green in Figure 2.1(a), is added to the system, which will induce increased methane outgassing from the gob to the bleeder. Figure 2.1(b) shows the situation with a gradual increase in barometric pressure. Here, ΔP_b works against ΔP_s, resulting in a reduced outflow at the bleeder returns. In an extreme case where either a longer time lag exists due to a highly resistant gob, or if the barometric pressure gradient is steeper, ΔP_b can exceed ΔP_s and thus induce a flow reversal where air from the bleeder and tailgate returns may flow back into gob. This is indicated in Figure 2.1(c) where the blue line crosses above the red line between t_0 and t_1.

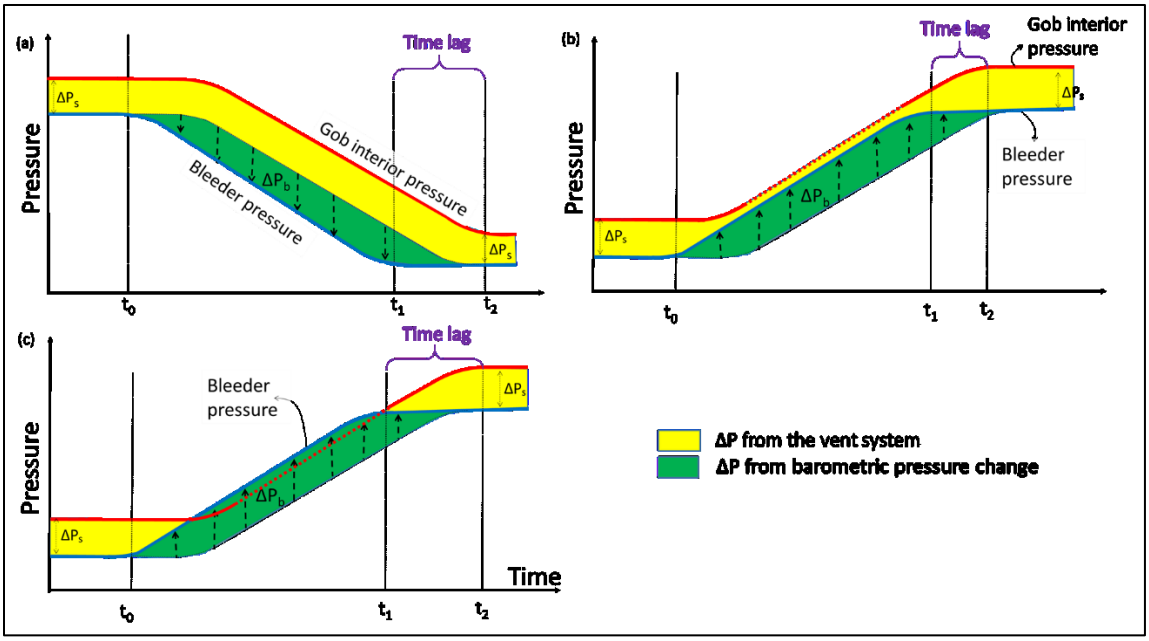

Figure 2.1: Hypothetical barometric pressure (a) drop, (b) rise, and (c) rise, longer time lag

If the external pressure changes instantly, for example, due to a fan failure, roof fall or crushed-out stopping, an additional pressure gradient ΔP_b can be produced almost immediately, as illustrated in Figure 2.2. Again, due to flow restrictions, the gob pressure has a delayed response to the external pressure changes, causing the maximum ΔP_b to occur immediately. In Figure 2.2(a), the total pressure gradient of $\Delta P_s+\Delta P_b$ in an instantaneous drop causes increasing methane outflow into the bleeder and tailgate returns. After the time lag, the pressure differential decays to the initial differential, ΔP_s. In Figure 2.2(b), an instantaneous rise of external pressure can cause an immediate negative pressure gradient ΔP_b by which external pressure becomes higher than the gob pressure. Increased air inflow from the face and headgate entries into the gob and flow reversal at the tailgate and bleeder sides are two conditions that may occur in this situation. If fresh air enters the fuel-rich inert gas body inside the gob, this will impact the size and location of the EGZ fringe between the bleeder entries and the inner gob that is fuel-rich inert.

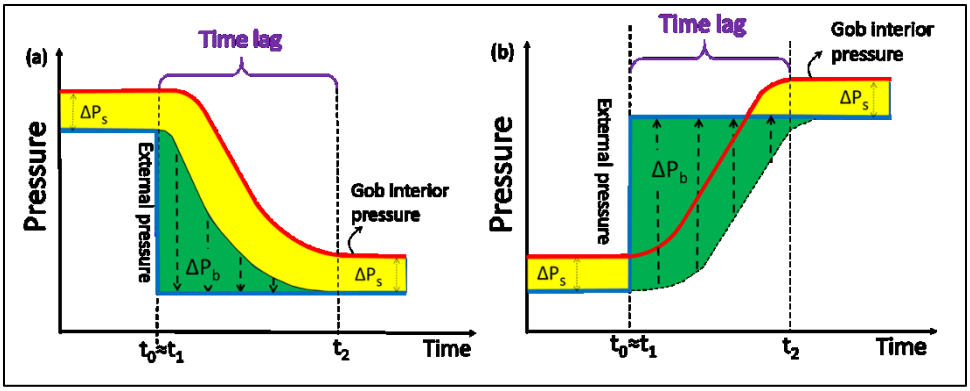

Figure 2.2: Hypothetical instantaneous barometric pressure (a) drop and (b) rise

This research investigates the hypotheses shown in Figure 2.1 and 2.2, which show that the methane gas or EGZ (if it has already been formed in the gob) will expand during barometric pressure drop and eventually flow out from the gob if the pressure continues to drop. In contrast, barometric pressure increases may trigger air ingression into the gob, which can also develop EGZs when mixed with methane. From this investigation, the researcher will determine the best practices to respond or control EGZs outgassing during periods of fluctuating barometric pressure. The control methods to be analyzed include ventilation adjustments, GVB, nitrogen injection and methane drainage. A better understanding of explosive mixture occurrence and migration in the gob during barometric pressure changes is required for the development of these preventive and mitigation strategies.

2.3 Research Questions

With the objective to provide a better understanding of the connection between barometric pressure and mine explosions, specific questions are explored in this research.

- *What is barometric pressure and how does it influence the underground mine atmosphere?*

  A clear understanding of barometric pressure, what contributing factors exist in barometric

changes, and how its changes impact the atmosphere of an underground mine are all starting points to understand the gob breathing phenomenon.

- *How does the methane gas in the gob respond to barometric pressure changes? What causes gob breathing to occur?*

  This is the main question of this research. Understanding the response of methane and other gob gases during barometric pressure changes, in respect to mass or volume, will underline the cause for the gob breathing phenomenon.

- *How can barometric pressure variations in CFD be appropriately modeled?*

  This study will be the first attempt to use computational modeling to investigate the impacts of barometric pressure variation on EGZs in the gob and its outgassing. The establishment of methodologies, assumptions and parameters for modeling barometric pressure variation in computational modeling is challenging, yet, critical for this study.

- *What suggestions can be made for preventive and mitigation methods based on the modeling results?*

  The researcher will model and test a number of preventive and mitigation methods under several pressure change scenarios, and then provide recommendations for best practices to implement in the event of fluctuating barometric pressure.

- *Are the results adaptable to other mining conditions?*

  The outputs of this research are expected to be universally applicable for various mining conditions. Sensitivity analyses and parametric studies will be performed to evaluate the versatility of the results.

2.4 Specific Aims and Research Tasks

The goal of this research is to help the mining industry achieve zero-incident operations by eliminating fatalities and accidents due to hazardous conditions of fire and explosion associated with barometric pressure fluctuations. This study benefits miners, the mining company and its stakeholders by way of providing best practice recommendations for the prevention and control of explosion risks due to barometric pressure changes in underground longwall mines. Figure 2.3 presents the tasks that will be completed to achieve this goal. Five main tasks were identified for this research, commencing with a comprehensive literature review on subjects related to the barometric pressure phenomenon, methane explosions, EGZs in the gob, and ventilation system. The findings from this literature review were used to establish methodology for the CFD modeling. The researcher concluded the study with documentation of findings and results from each task, as well as recommendations for best practices.

2.4.1 Task 1: Literature Review

A literature review provides context and base knowledge for the research. The review focused on the key subjects of methane explosions and barometric pressure, and was consecutively extended to cover related subjects of the history of mine explosions in the United States and worldwide, the phenomenon of atmospheric pressure variations, CFD modeling of explosive mixture, and the current technology for preventive and mitigation measures. The literature included books, peer-reviewed papers, internal communications, and other relevant publications accepted by well-known scientists and scholar groups. Barometric pressure data in the United States were provided by the National Oceanic and Atmospheric Administration (NOAA), for other countries, the data were mostly obtained from open sources. Important findings from the literature search will be documented for establishing modeling parameters and assumptions.

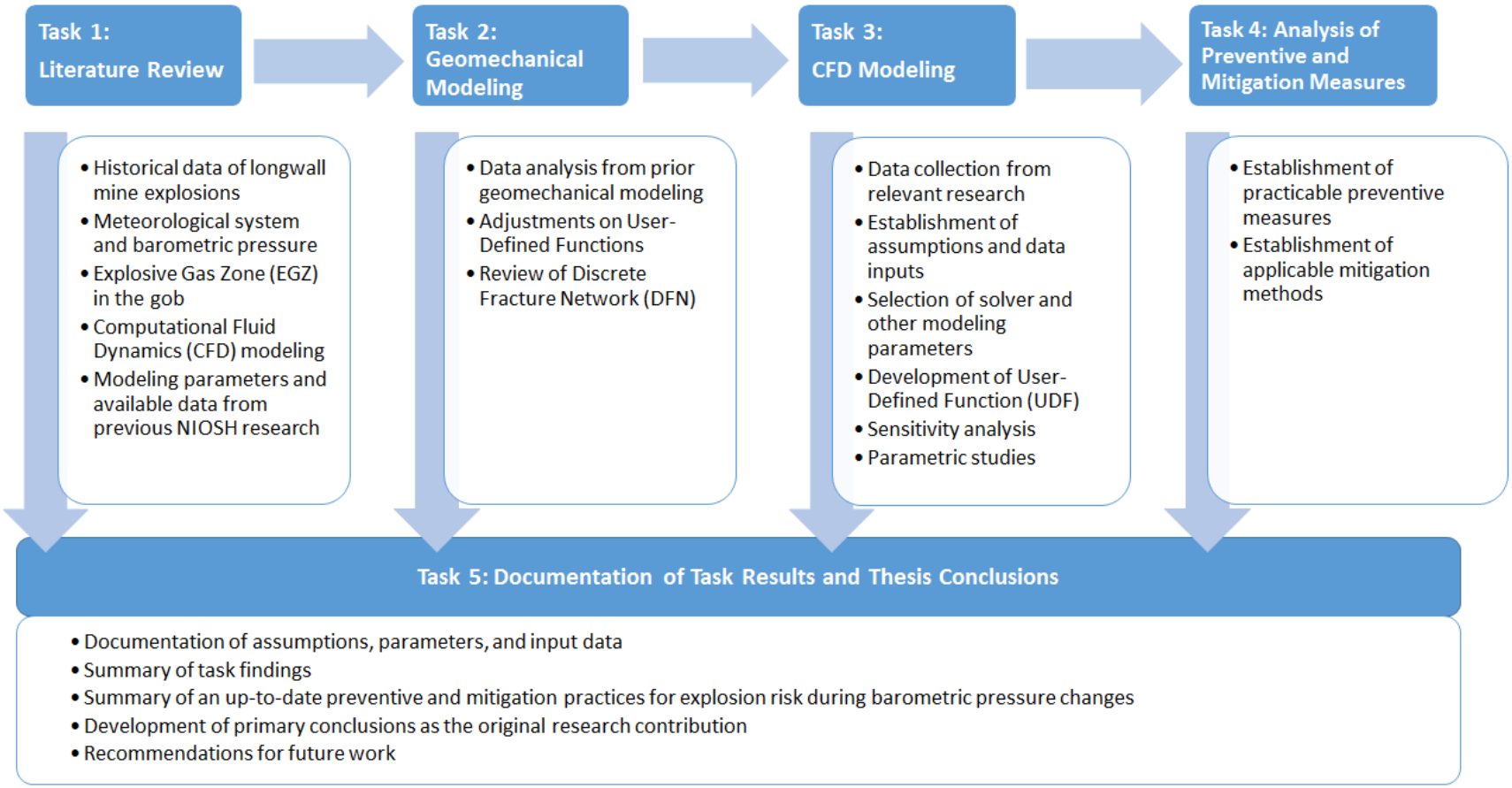

Figure 2.3: Flow of completed research tasks

2.4.2 Task 2: Geomechanical Modeling

The gob becomes one of the main focuses of this research because it is where the explosive mixture forms. Porosity and permeability are two important properties of the gob that influence fluid flow. Due to gob compaction, these properties will vary over the entire gob, and thus appropriate modeling is important to achieve accurate results of fluid flow. In Task 2, data and methodologies used by other researchers in estimating gob porosity and permeability were reviewed. Based on the researcher's review, the volumetric strain approach developed by Marts et al. (2014) had advantages over the numerical modeling approaches as it had been verified against subsidence data, thus it was selected for this modeling. This approach has been widely accepted and used for gob properties modeling. Details of this approach are shown in Section 3.2. The outputs of the estimated values of gob porosity changes were used as inputs for CFD modeling.

In addition, the researcher also reviewed a single step extraction proposed by Wachel (2012) and a recent development of fracture modeling called the Discrete Fracture Network (DFN), which was widely used in the oil and gas industry for reservoir simulation. Researchers at NIOSH (Karacan and Yuan, 2015) considered the DFN approach to be more realistic than volumetric strain modeling on the basis of the random and discrete nature of fractures. Rock rubbles and other gob materials are packed randomly in the gob void, creating fluid paths similar to discrete fractures, which leads to a consideration to use the DFN approach. This approach is further discussed in Section 3.5.4. Task 2 also included the work of revisiting assumptions and user-defined functions that were used in prior geomechanical modeling by Marts et al. (2014) and Gilmore (2015). Most of these previous assumptions remained unchanged for this study since no new stratigraphy data were available.

2.4.3 Task 3: Computational Fluid Dynamics (CFD) Modeling

Due to unsupported and active caving process, gob becomes inaccessible, which limits the field measurement to obtain information of fluid flow or methane behavior in the gob. On that account, computational fluid dynamics (CFD) modeling can be used as a predictive tool of the gob condition. CFD has the capability to model fluid flow and estimate gas concentration within any domain. In Task 3, the researcher created a longwall model, established assumptions for the modeling, evaluated the impact of methane emission from the rider seam coal and surrounding strata on EGZ in the gob, and investigated the methane behavior under barometric pressure fluctuation scenarios. The CFD models were also used for parametric studies, sensitivity analyses, and eventually for testing the performance of the suggested preventive and mitigation practices in order to make specific recommendations.

2.4.4 Task 4: Analysis of Preventive and Mitigation Measures

The main goal of Task 4 was to develop best strategies that can prevent methane explosions associated with the gob breathing phenomenon due to barometric pressure fluctuations. A potential outcome from gob breathing is the outgassing of EGZs. Ventilation strategies can be implemented to prevent and mitigate the risk of methane explosion triggered by this outcome. Task 4 evaluated the current practices and technologies commonly implemented by mine operators to prevent EGZ outflow from the gob in the event of barometric pressure fluctuations, or to promptly detect it and alert miners as early as possible. These practices included a real-time atmospheric monitoring and methane detection system, mitigation measures and gob ventilation borehole applications.

2.4.5 Task 5: Research Results Documentation

Task 5 summarized and documented the findings of Task 1 through Task 4 to establish research conclusions and recommendations. This research consisted of recommendations for best

practices on how to prevent and mitigate explosion. The documentation incorporated a literature review summary, methodologies used for geomechanical modeling, assumptions and parameters of CFD modeling, an up-to-date collection of current and recommended best practices, results of sensitivity analyses, and other important findings, all of which were summarized in the format of a doctoral thesis as the final deliverable.

2.5 Computational Fluid Dynamics Approach

Due to the caving nature of the gob at a longwall mine, little information about internal fluid flow and EGZ formation in the gob can be obtained from field measurement. A computational modeling approach using CFD provides the solutions to this problematic condition. CFD solves nonlinear differential equations such as Navier-Stokes equations in flow simulations within a discretized volume of fluid. In early years of its application, CFD was used in a wide variety of fluid mechanics-related engineering applications such as heating, ventilating and air conditioning (HVAC), automobile and aircraft, fuel cells, wind turbines, and weather science. It has capabilities to model laminar and turbulent flows, multiphase fluids, and simulate complex chemical reactions. In the mining industry, CFD has increasingly become a common tool to evaluate hazards and the effectiveness of a ventilation system. In Australia, CFD modeling was carried out by the Commonwealth Scientific and Industrial Research Organization (CSIRO) to evaluate airflow patterns on the longwall face (Ren and Balusu, 2010). These studies demonstrated the application of CFD as a tool for evaluating health and safety problems including gob gas management, inertization, and face dust controls. In the U.K., Lowndes et al. (2005) used CFD modeling to simulate the situation if a fire occurred in the longwall mine's belt entry. In the U.S., NIOSH utilized CFD to evaluate a wide range of mining operation issues including gob flow paths (Yuan et al., 2006), mine fire smoke and reverse flow (Edwards, 1999), spontaneous heating (Smith et

al., 2010) and the effect of barometric pressure on spontaneous combustion (Yuan and Smith, 2010). In addition, several educational institutions have successfully used CFD for longwall mine ventilation modeling including the University of Kentucky (Wala et al., 1997), University of Utah (Calizaya et al., 2004; Lolon, 2008), Colorado School of Mines (Worrall, 2012; Gilmore, 2015), and many others worldwide (Brunner et al., 1995; Balusu et al., 2002).

ANSYS Fluent® was selected to carry out the modeling portion of this study. This program is uniquely suited for ventilation and barometric pressure modeling because it is integrated into a convenient graphical user interface (GUI) with the capability to run customizable routines known as User Defined Functions (UDF). The researcher uses UDFs to store modeling setup, run parametric studies and boundary condition changes. ANSYS Fluent® is one of many packages incorporated into Workbench™, which is a schematic view framework that ties together multiple simulators and modelers. Other packages available and used in this study as part of Workbench™ are ANSYS Design Modeler®, ANSYS Meshing®, and CFD-Post®.

2.6 Expected Research Outcomes

This dissertation summarizes the modeling developed as a predictive tool for mine conditions as a result of variations in barometric pressure. This tool and the findings of this study can be used by mine operators to improve the safety of longwall mine operations by increasing awareness of mine explosion hazards associated with barometric pressure fluctuation, evaluating current mine conditions, and eventually implementing appropriate actions to mitigate the risk of explosion triggered by changes in barometric pressure.

This research predicts conditions of methane-air mixture in the gob before, during, and after barometric pressure fluctuations, the expected time period of outgassing or ingassing after these changes, and recommended safety measures in anticipation of methane or EGZ outgassing,

which include recommended locations for atmospheric and methane monitoring systems, frequency of gas monitoring, and emergency plans.

2.7 Original Contributions of the Research

The research presented in this dissertation will make the following contributions to the industry and the field of science:

1. The historical data of mine explosions presented in this dissertation suggest a connection between these coal mine explosions and fluctuation in barometric pressure. This increase the industry's awareness of the risks associated with barometric pressure fluctuation in underground coal mines.
2. Many studies have been aimed at eliminating the methane-air explosive mixture in underground coal operation but little work has been done to investigate the effect of barometric pressure on the mine's atmospheric condition and the explosive mixture. This research presents a novel use of CFD to analyze explosive mixture due to barometric pressure variation in the gob, and will provide better understanding of how to appropriately model this condition for future research.
3. This dissertation provides recommendation for precautions and mitigation methods that can be applied in real-world conditions in anticipation of, or as a response to, the changes in external pressure. The recommendations include monitoring systems placement and frequency, ventilation adjustment, a risk matrix and emergency plan, and other mitigations methods.

CHAPTER 3

LITERATURE REVIEW

This chapter mainly presents a literature review of seasonal variations in barometric pressure and apparently connected mine explosions. In addition, the concept of the gob breathing phenomenon and the original development of geomechanical modeling and the gob explosibility diagram are also presented.

3.1 Barometric Pressure as Seasonal Variation

As explained earlier in Section 1.3, barometric pressure is determined by the weight of air at a certain location, it decreases as altitude increases. Above the atmospheric boundary, air does not exist, creating a vacuum condition (Wallace and Hobbs, 2006). Figure 1.8 shows the general thickness and height of the atmospheric subzones per observations by Fleagle and Businger (1980). These heights vary over the earth's surface and constantly change due to meteorological systems. Under normal conditions, the vertical acceleration of air is so small that the air is perceived as strata or as atmospheric layers. This leads to a condition where atmospheric pressures at any location at the same elevation will be similar. However, this is not always true due to weather systems, some of which are active over a relatively large area. For instance, the barometric pressure of a location in the Arctic will be significantly different from that of the same elevation in the middle of the Indian Ocean due to differences in latitude, temperature and wind systems.

3.1.1 Early Studies of Atmospheric Pressure Variation

There have been numerous theories proposed to describe the reasons for barometric pressure variations. In the early 1600s, Isaac Newton recognized the connection between sea tides and the moon's gravitational pull. He considered that atmospheric air would respond in the same

way the sea responds to the gravitational forces of the moon or sun. The air pressure in the atmosphere was considered by Newton to be a result of air tides or oscillations. Detailed observations of atmospheric tides began after the invention of the barometer by Torricelli (1608-1647). Two centuries later, Lord Kelvin (1824-1907), a British mathematician and physicist, proposed a resonance theory that considered the atmosphere as having a free oscillation within a period of nearly 12 hours due to thermal influence (Lindzen and Chapman, 1969). Lord Kelvin's theory suggested that the barometric pressure tides or oscillations were mostly due to temperature and were not merely a series of gravity-triggered tides, as had been believed earlier. Lord Kelvin's theory received support from scientists and dominated thinking on atmospheric tides for almost seven decades (Lindzen, 1966).

Another prominent scientist, Lamb, conducted observations from 1910 through 1916 on the atmospheric tides and made an important proposition that the tides might, in fact, be caused by a gravitational force (Lindzen and Chapman, 1969). According to his study, a high degree of resonance is required to produce a measurable distinction between solar and lunar periods. Temperature cannot provide enough force to cause distinct oscillations; therefore, it does not contribute to barometric pressure variations as much as gravity. In contrast to Lamb's theory, Taylor and Pekeris studied atmospheric oscillation distribution in the 1930s, and found that the oscillations were a function of longitude and altitude (Lindzen and Chapman, 1969). They also noticed that the upward temperature decreased significantly as altitude increased. Lord Kelvin's proposition regained support from the work of Taylor and Pekeris. With much advanced technology, Weeks and Wilkes conducted experiments for more than a decade, starting in 1947, to obtain atmospheric oscillation and to make numerical calculations of the free oscillation of ocean waves on a spherical earth rotating at a specific velocity (Lindzen and Chapman, 1969).

Their experiment emphasized the effect of weather on barometric pressure variations. One of their widely accepted findings was that the variations of atmospheric pressure associated with weather are very localized and only affect the first 15 kilometers (9.3 miles) or so of the atmosphere. Further study by Wilkes (Lindzen and Chapman, 1969) indicated that the oscillations are influenced by temperature variations from heat transmitted upward from the ground.

3.1.2 General Concept of Diurnal and Semidiurnal Oscillations

The theory that views barometric pressure as oscillations, resonances or tides remains widely accepted by many scientists and scholars. Atmospheric tides cause horizontal divergence and inhomogeneity of air pressure over the earth's surface. The factors that trigger these oscillations are not entirely understood but numerous studies and research suggest it is the contribution of the gravitational forces of the earth, sun and moon as well as atmospheric heating and cooling (Lindzen and Chapman, 1969).

The earth's rotation causes the sun's gravitational attraction to be greater in the hemisphere closer to the sun than at other parts of the earth. This attraction acts upward against the earth's gravitational force, causing an unbalanced distribution of air pressure over the earth's surface. The position of the earth will also result in heating on one side of the earth and cooling on the other side, thus, temperatures will vary and induce air flow and atmospheric tides. These atmospheric tides will result in variations in barometric pressure.

Many early studies acknowledged the regular pattern of atmospheric pressure as a fraction of a solar day (Harris, 1954; Brier, 1965; Lindzen, 1966; Chapman and Malin, 1970). Atmospheric pressure data will indicate maxima and minima that repeat periodically every 12 and 24 hours. The 24-hour harmonic variation is the diurnal component of the atmospheric pressure, while the 12-hour is known as the semi-diurnal component. These two components can be visually

distinguished from wind fields as shown in Figure 3.1. Wind represents a disturbance caused by atmospheric pressure, and is used as a parameter to observe the diurnal and semidiurnal waves by many atmospheric scientists (Dai and Deser, 1999).

The diurnal wavelength oscillates for approximately 24 hours, indicated by the wind speed profile (short-dashed lines in Figure 3.1). The long-dashed lines represent the wind speed as affected by the semidiurnal component of atmospheric pressure. Diurnal waves usually generate higher amplitude than the semidiurnal waves, which typically have a half-wavelength of about 12 hours. The solid lines are the sum of the two components of the wind speeds. In the U.S., the atmospheric pressures are at its lowest each day around 4 AM or 4 PM and near its peak around 10 AM or 10 PM (NWS, 2015). Dai and Deser (1999) noted the contribution of the temperature to diurnal and semidiurnal waves. The temperatures in Africa and South America, which are generally warmer all year round than in the United States, intensify the diurnal amplitude. As expected, diurnal and semidiurnal pressures affect wind speed more significantly in those two regions than in the United States, as illustrated in Figure 3.1.

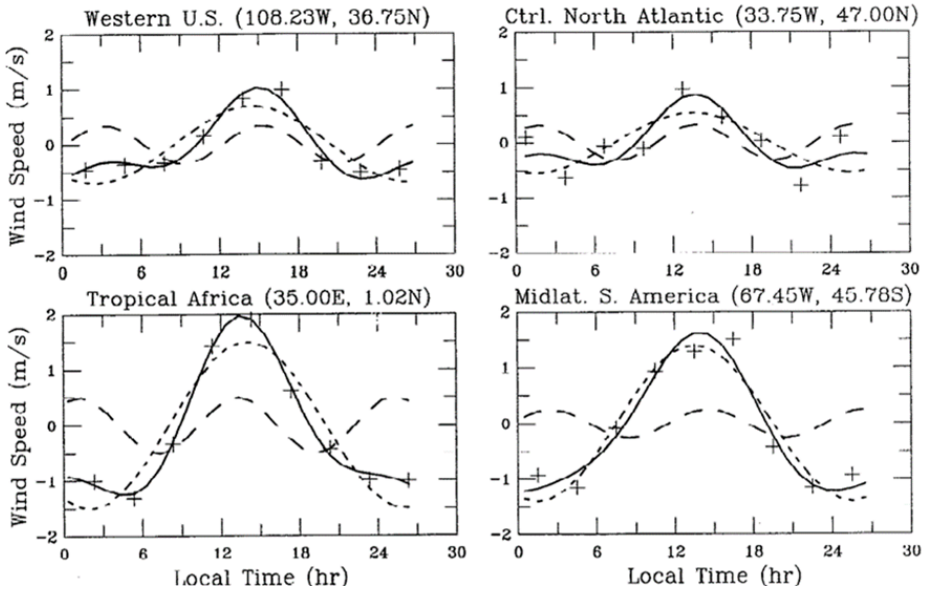

Figure 3.1: Wind speed as a factor of diurnal and semidiurnal tides (Dai and Deser, 1999)

3.1.3 Seasonal Variation of Barometric Pressure

Variations in barometric pressure result from many factors that act cooperatively or against each other in the atmospheric system. Barometric pressure can be regarded as periodic tides or oscillations in the atmosphere (Lindzen, 1966). In the combination of gravitational and thermal forces, the thermal component is considered more dominant than the gravitational (Lindzen and Chapman, 1969). The sun's position determines the thermal quantity received by the earth, which then causes variations in temperature. The temperature variation heats up or cools down the overhead air, making it either denser or less dense, and ultimately causes air movement and pressure variations. Therefore, many earlier studies have acknowledged that atmospheric pressure differs according to the integral fractions of a solar day (Harris, 1954); which are described in earlier section as diurnal and semidiurnal pressures. The diurnal and semidiurnal components primarily drive the harmonic barometric pressure variation under normal weather conditions.

Lindzen and Chapman (1969) indicated that, as opposed to always being harmonic, seasonal change can cause barometric pressures not to be truly periodic from day to day. The anomalies of barometric pressure are recognized as contributing factors in many major mine explosions worldwide. For example, investigations of South Africa's mine explosions showed that barometric pressure changes associated with cyclonic weather systems are the major contributing factor to gas explosions in mines and are much more significant than the influence from diurnal or semidiurnal pressure waves (Fauconnier, 1992). In the U.S. coal industry, disastrous mine explosions seem to happen more frequently in the winter than in the summer (Boyer, 1964; Kissell et al., 1973; Lolon et al., 2015).

The explanation for this phenomenon exists in the weather systems of both South Africa and North America. The widely accepted Köppen climate system (Köppen and Wegener, 1924)

classifies the southern region of Africa as well as North America and most European countries to be in the Mid-Latitude climate zone (Pidwirny, 2006; NWS, 2015), as shown in Figure 3.2. In this zone, frontal cyclones exist as the result of interaction between warm tropical and cold arctic fronts, and tend to be most disruptive during the winter months (Pidwirny, 2006). These cyclones are associated with freezing rain, hail, snow, and most often storms, all of which disturb normal barometric pressure conditions. Barometric pressures decrease rapidly as a storm approaches and then increase after it passes, causing much greater pressure swings than in normal daily fluctuations. Normal barometric pressure changes due to diurnal systems range between 300-400 Pa in a 24-hour period, while severe storms can result in fluctuations of 3,400-6,800 Pa over the course of two to 10 hours (Zipf and Mohamed, 2010). A very powerful thunderstorm is capable of short term rate of change as high as 3,660 Pa/hour (Francart and Beiter, 1997).

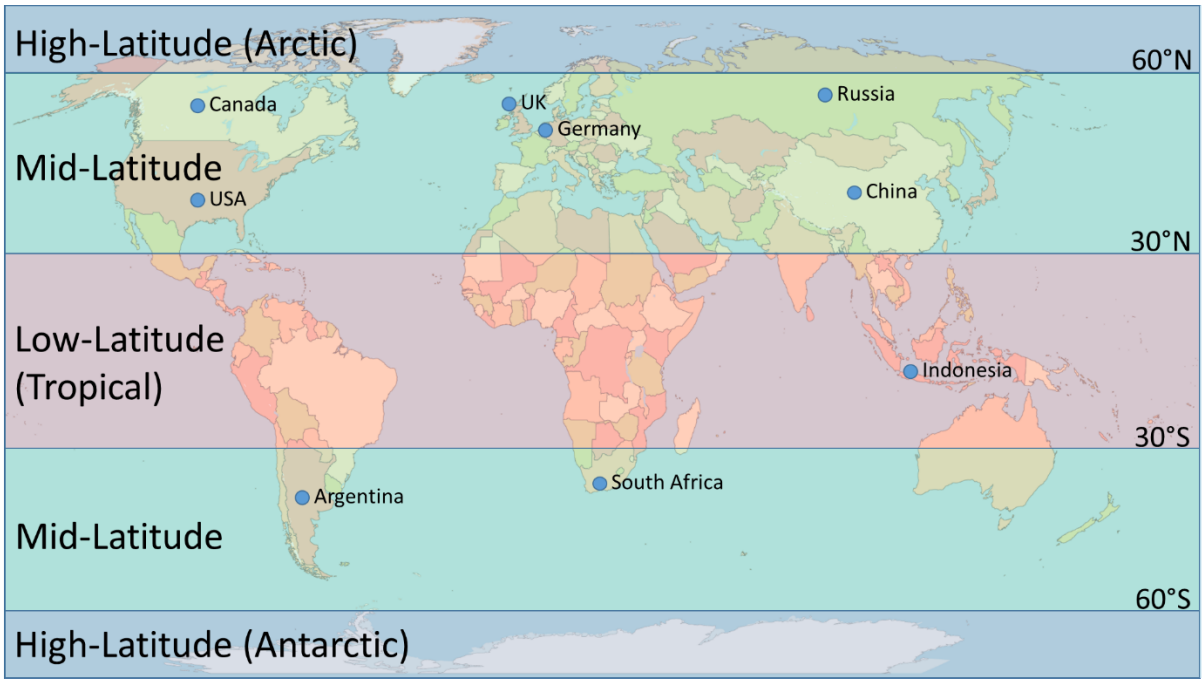

Figure 3.2: Köppen Classification climate system (drawn based on Pidwirny, 2006)

The frontal cyclones that typically occur in late fall and winter seasons support the findings of many researchers who have observed more abrupt changes in barometric pressure between

November and April than in other months of the year (Boyer, 1964; Hemp, 1994; Wasilewski, 2014; Lolon et al., 2015). The cyclone system contributes to the seasonal variation that causes greater barometric pressure fluctuations than those caused by the periodic diurnal and semidiurnal systems.

3.2 Methane and Explosive Gas Zones in Longwall Gob

Methane gas is a byproduct of the coal formation process. Within the strata, the gas is stored either in the fissures and pore structure or absorbed on coal's internal surface (Boxho et al., 1980). Methane can be released as a free gas through fracture systems in the coal seam. Coalbeds in the United States are naturally fractured, with spacing varying from 0.25 inch for the Pocahontas No. 3 coalbed in Virginia to approximately six inches for the Pittsburgh coalbeds (Cervik, 1969). Therefore, methane control is important in U.S. coal mining, particularly in longwall mining, which allows gob formation where methane can accumulate and an EGZ can potentially develop without detection.

In recent years, there have been a number of mine fires and explosions that suggest the existence of explosive methane-air mixtures or EGZ in longwall gobs (Brune, 2013). These mine fires and explosions indicated that this explosive mixture must have existed in gobs and propagated to active mine areas as it exploded. For example, a mine fire occurred in November 1998 at the Willow Creek mine owned by the Cyprus Plateau Mining Corporation. A subsequent investigation by the U.S. Mine Safety and Health Administration (MSHA) reported that the accident, which happened in the longwall tailgate area, was preceded by an orange-colored flame that appeared to move from inside of the gob toward the face area and then back into the gob (Elkins et al., 2001). Four years later, a series of four explosions occurred in the same mine; they were reported to be ignited by friction from a roof fall in the gob, suggesting the presence of an explosive mixture in

the gob (McKinney et al., 2001; Brune, 2013). In both 2005 and 2007, another mine, Consolidation Coal Company's Buchanan mine in Virginia, experienced two similar explosions. Both explosions suggest the possibility of EGZ existence in the gob, in the gob perimeter, and along the tailgate and bleeder entries (Cario, 2006; Woodward and Sheffield, 2008). In the 2010 Upper Big Branch (UBB) mine explosion, MSHA investigators believe that the methane travelled from the gob to the longwall face and was likely ignited by the friction of a shearer tail drum cutting the sandstone strata (Page et al., 2011).

In addition to the U.S. mines mentioned above, several mines, not necessarily used longwall method, in other countries have also reported similar accidents where the explosion was originated in the gob or goaf, including the Kianga No. 1 mine, Moura No. 2 and No. 4 operations in Queensland, Australia (Loane et al., 1975; Lynn et al., 1986; Windridge et al., 1994), and several Polish coal mines (Dziurzynski and Wasilewski, 2012). These accidents are all strong evidence of the existence of an explosive mixture inside and around the perimeter of the gob.

The explosibility of the EGZ is conceptually determined by the amount of methane in the air. The methane concentration must lie within lower explosive limit (LEL) and upper explosive limit (UEL) to be considered flammable or explosive. These limits are determined experimentally and vary with temperature and pressure (Turns, 2012). If the methane concentration in the air is lower than the LEL, the mixture is considered fuel lean. If it is higher than UEL, the mixture is fuel rich. The explosive mixture found between LEL and UEL, if ignited, can release energy in different amounts, depending on the mixture stoichiometry.

In 1925, the U.S. Bureau of Mines (USBM) started a cooperative program with the British Safety in Mines Research Board to study the limits of flammability and explosibility of mine gases. As part of this cooperative work, British chemist H.F. Coward and American researcher G.W.

Jones studied the flammability limits of methane-air mixtures in a laboratory using a variety of apparatus from a small pipette to large-scale 10-inch diameter and 7-foot long tubes (Coward and Jones, 1952). With different compositions of oxygen and methane concentrations, the experiments resulted in the triangle shape of the explosive areas shown in Figure 3.3. This is widely known as "Coward's triangle." If a methane-air mixture is found inside the Coward's triangle, it is explosive. The lowest methane concentration in the triangle is the LEL, and the highest the UEL. Both LELs and UELs vary by temperature and pressure. Figure 3.3 indicates that the sphere apparatus gives the greatest UEL value among other tests. The apparatus was a closed vessel in which the pressure considerably increased. The UEL value of the mixture greatly increases with rising pressure, but slightly drops with falling pressure (Kissell, 2006). This is shown in Figure 3.4. In addition, Figure 3.3 shows that no mixture of methane is flammable when the atmosphere contains less than 12.8 percent oxygen at standard atmospheric pressure and temperature.

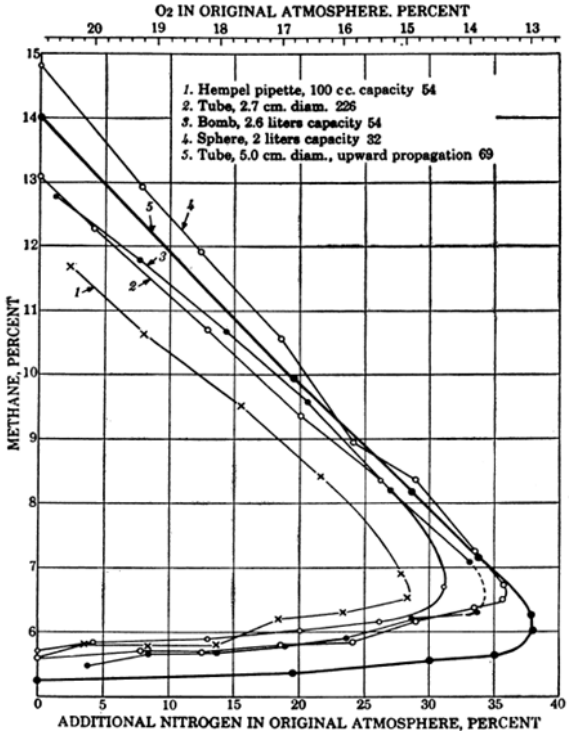

Figure 3.3: Limits of flammability of methane-air mixture (Coward and Jones, 1952).

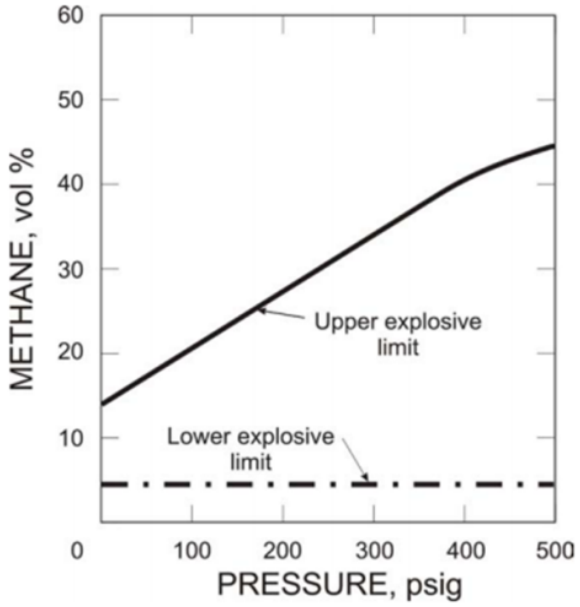

Figure 3.4: Effect of increased pressure on methane explosibility limits (Kissell, 2006)

The Coward's triangles shown in Figure 3.3 also illustrate that adding nitrogen to the atmospheric air can reduce oxygen. Being non-reactive under most conditions, nitrogen is considered an inert gas. In its gaseous form, it can shield potentially reactive materials from contact with oxygen. Therefore, adding nitrogen into methane-air mixtures can replace oxygen, and create a barrier that keeps methane and air from mixing and being explosive in the gob (Gilmore et al., 2013; Marts, 2015).

The Coward's triangle has been widely used as the basis for methane-air mixture explosibility in many gob gas modelings. Worrall (2012) developed a gob explosibility diagram based on the Coward's triangle using a color scheme (as depicted in Figure 3.5). Any mixture of methane and air can only occur below the white-colored area. The red-colored area shows an explosive composition, and the mixture in the yellow-colored area is methane-rich. Though not explosive, dilution with air can make this mixture become explosive. The mixture in the cyan-colored area is methane-lean and therefore not explosive, but it can become flammable with

additional methane introduced into the system. The green-colored zone is the composition range where methane and oxygen are not capable of forming an explosive mixture. The orange-colored zone indicates the transition from a non-explosive to explosive zone. The exact range of this transition zone is arbitrary and for visual purposes only.

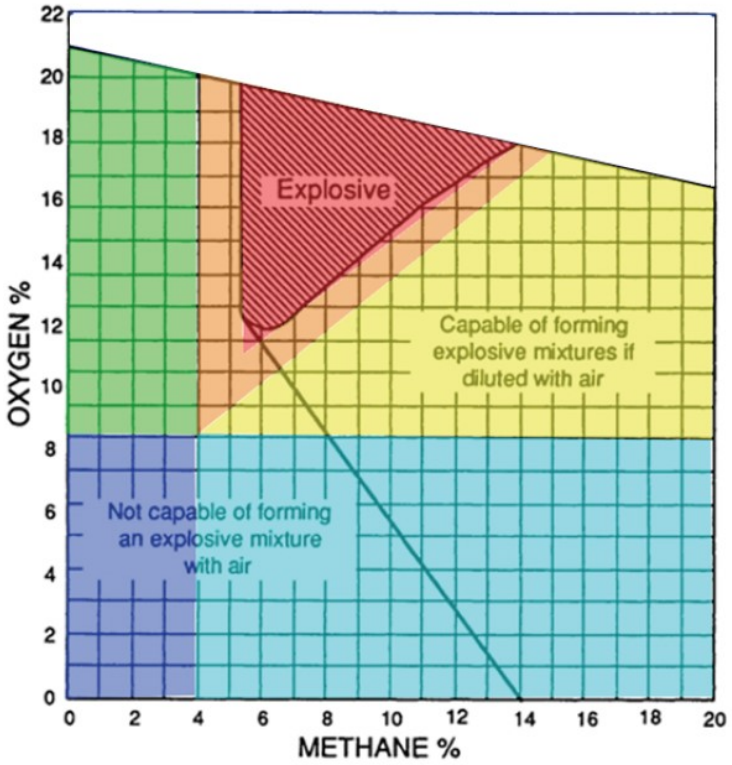

Figure 3.5: The original color-coded diagram of gas explosibility (Worrall, 2012)

Gob explosibility can be identified using the color-coded diagram shown in Figure 3.5. In bleeder panel cases, the red-colored zone of Coward's triangle is likely to exist in most, if not all, longwall gobs (Gilmore et al., 2013; Brune et al., 2015). High methane concentrations flow out from the upper rider seam or any methane sources in the gob and mix with air from the external ventilation, forming an explosive mixture or EGZ inside and around the perimeter of the gob. In bleederless ventilation cases, the formed EGZ fringe is much thinner and found to exist across the panel behind the shields only (Marts et al., 2014b).

3.3 Barometric Pressure Fluctuation and Gob Breathing

Gob breathing is the result of the pressure differential between gob internal and external pressures. For bleeder-ventilated gob, the ventilation system controls the pressure differential, and thus the gob breathing. Barometric pressure fluctuation can disturb this pressure differential, causing uncontrolled gob breathing. There are two main changes that are considered to happen with gases inside the gob during the gob breathing: volume and mass. Quantitatively, the relationship between gas volume and pressure can be simply explained by the ideal gas equation, given below:

$$PV = nRT \tag{3.1}$$

where P is pressure, V is gas volume, n is gas mole, R is 8.314 J K-1 mol-1, and T is the absolute temperature. Equation 3.1 states that the absolute pressure is directly proportional to the mole of a gas present in a domain, in this case the gob, but is inversely proportional to the gas volume. During gob breathing, external pressure changes induce expansion or shrinkage of the gas volumes inside the gob.

The volume change of gob gases is thought to occur only in the beginning of the gob breathing process. Since gob methane is continuously supplied by an inlet atop the upper seam, assumption made for this study, the external pressure changes will change the pressure differential between this methane inlet and gob, thus affecting the methane inflow rate. After a certain period of time, the inlet will push more methane into the gob when gob pressure decreases, or less when it increases. Equation 3.1 can be written in terms of the mass flow rate, $\dot{m}$, and pressure change rate, *dP/dt,* as shown in Equation 3.2.

$$\dot{m} = \frac{dm}{dt} = \frac{V}{RT}\frac{dP}{dt} \tag{3.2}$$

In this study, CFD modeling will be used to investigate whether volume change is more dominant than mass change during the gob breathing, or vice versa. The gob gas may experience volume change (i.e., gas expands or shrinks) in the beginning of the process and turn to mass change phenomenon with the increased or decreased mass inflow from methane inlet. Additionally, researcher will study the delay of gob response using the modeling. When the atmospheric pressure rises or falls, the ambient pressure in the active working areas will change almost instantaneously (Stevenson, 1968; Wasilewski, 2014), while the internal gob pressure is thought to change slowly because of the porous gob material, causing delay or time lag. This time lag measures the period when pressure differentials are considered out of normal range.

Atmospheric or barometric pressure fluctuation directly impact mine pressure. Fauconnier (1992) found that pressure changes associated with cyclonic weather systems are the major contributing factor in mine gas explosions. The diurnal and semidiurnal cycle causes a regular variation in surface barometric pressure. This variation is intensified by a cyclonic weather system, which often results in a storm that causes a quick drop and rise in the barometric pressure. The magnitude of change for such pressure fluctuations is typically higher than the fluctuation caused by regular diurnal-semidiurnal cycles (Hosler, 1948; Fauconnier, 1992). Figure 3.6 shows an example of a barometric pressure profile recorded in 2013 at a mine site in the western U.S. During a 12-month period, two fluctuation periods are identified: May through September and October through May. Barometric pressure changes are more abrupt and intense in the first period with the largest swing of nearly 2,000 Pa, and then become much steadier in the later period. The National Weather Service (NWS) reported that a major storm that occurred in the region in mid-November seemed to be the trigger for the 2,000 Pa fluctuation (NCDC, 2014).

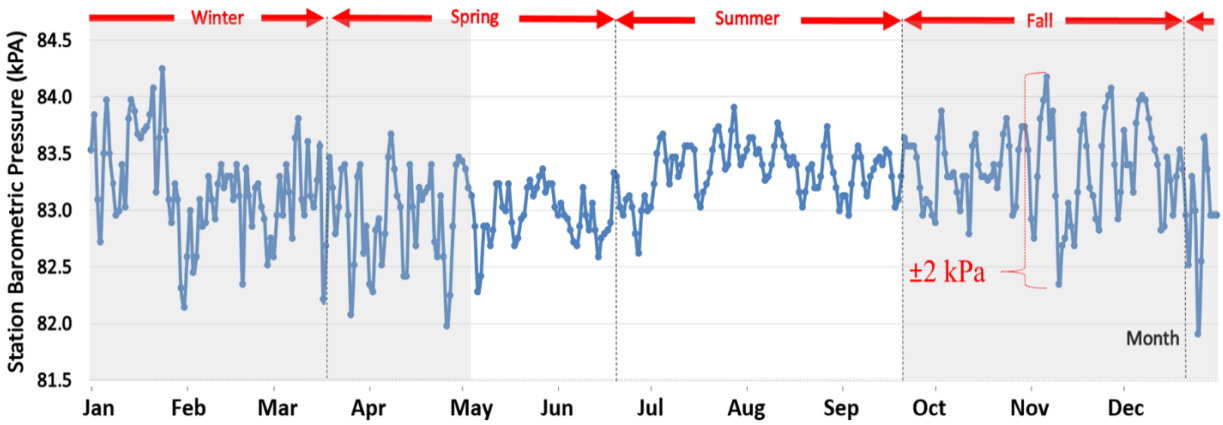

Figure 3.6: Yearly profile of barometric pressure at a Western coal mine (Lolon et al., 2015)

According to Equations 3.1 and 3.2, there are two potential conditions happening in the gob as a result of fluctuating barometric pressures: (1) the existing gases in the gob will expand or contract – volume change, and (2) methane inflow from top inlet will increase or decrease – mass change. Both conditions increase the methane outgassing or ingassing across the gob. Field investigations have demonstrated a finding of higher methane emitted during drops in barometric pressure (Carter and Durst, 1955; McIntosh, 1957; Belle, 2014; Wasilewski, 2014). Furthermore, a number of studies have related mine explosions to barometric pressure changes. Hosler (1948), Boyer (1964), and Kissell et al. (1973) conducted statistical analyses of the impact of barometric drops on several major U.S. coal mine disasters prior to 1970. Similarly, Fauconnier (1992) and Hemp (1994) studied the effect of barometric pressure drops on gas explosions in South African mines between 1972 and 1992. In agreement with these earlier studies, most disastrous mine explosions in the U.S. after 1970 were found to have occurred primarily from November through April (Lolon et al., 2015). Major disasters as defined by the MSHA are accidents with five or more fatalities. Table 3.1 lists all major mine explosions that are associated with methane explosions since 1970. Explosions caused by coal dust ignitions during blasting are excluded from the list, such as those at Finley Coal #15 and #16, Adkins #11 and RFH #1 mines.

Table 3.1: Major methane explosions in the U.S. from 1970 through 2016

Mine	Date	Mine Type[1]	Total Fatalities	Avg. Barometric Change, Pa (Preceding Days)
Itmann #3	12/16/1972	RP	5	+508 (1)
Scotia[2]	3/9-11/1976	RP	26	-1,591 (2)
Ferrel #17	11/7/1980	RM	5	-779 (1)
Dutch Creek #1	4/15/1981	LW	15	-34 (1)
Grundy #21	12/8/1981	LW	13	-914 (3)
McClure #1	6/21/1983	LW	7	+68 (3)
Pyro #9 Slope	9/13/1989	LW	10	-237 (1)
Southmountain #3	12/7/1992	RP	8	-609 (2)
JWR #5	9/23/2001	LW	13	-203 (1)
Sago	1/2/2006	RP	12	-440 (1)
Darby #1	5/20/2006	RP	5	+576 (2)
UBB	4/5/2010	LW	29	-271 (1)

Notes: [1] LW=longwall mine; RP=room and pillar; RM=retreat mine
[2] Barometric pressure trend of the first explosion

Table 3.1 outlines the average barometric pressure changes as well as the number of preceding days with noted changes prior to the explosion. For example, pressure drops of nearly 1,600 Pa and 900 Pa were recorded over the two and three days preceding the explosion at the Scotia mine and Grundy #21 mine, respectively. Figure 3.7 shows the barometric pressure trends in both mines before and after the explosion. For each explosion, daily barometric pressure records were obtained from three weather stations near the mines. These records were obtained from the National Weather Service database (NCDC, 2015). Barometric pressure values shown in Table 3.1 were selected from the closest station to the mine.

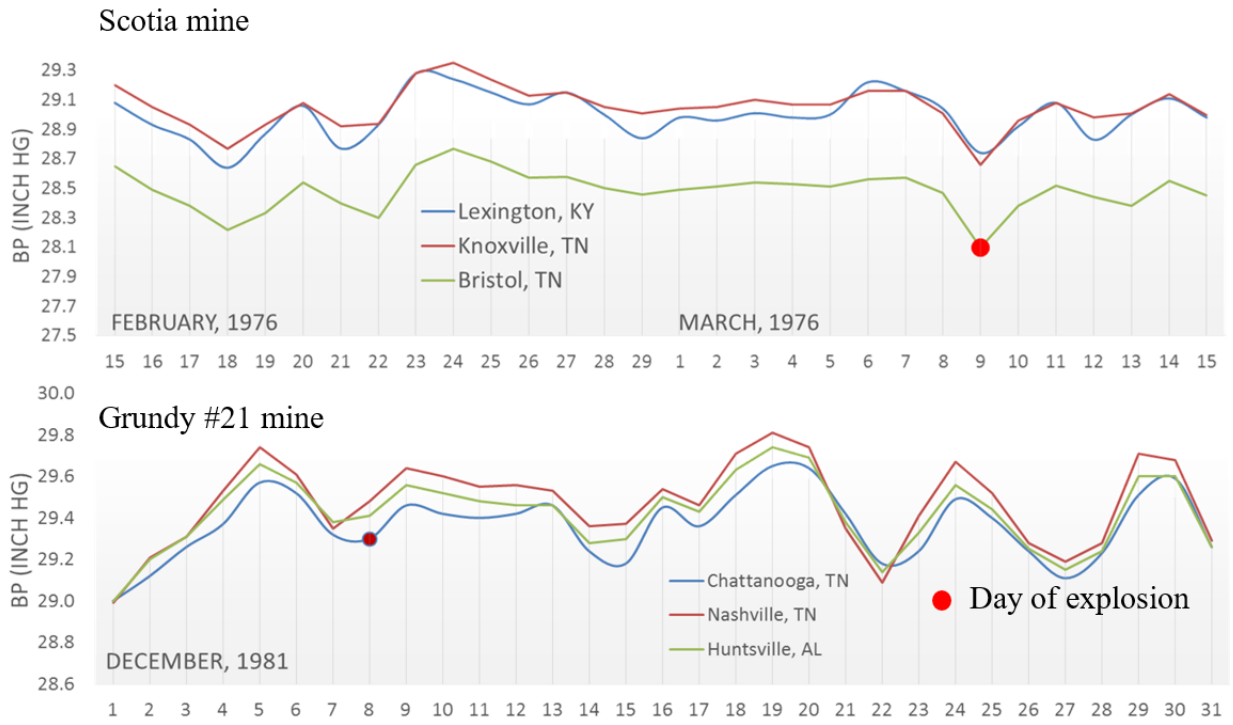

Figure 3.7: Barometric pressure data during explosions at Scotia and Grundy #21 mines

Similar to the conditions of the two mines shown in Figure 3.7, most of the explosions listed in Table 3.1 occurred during and after a barometric pressure drop in the fall and winter seasons. The Itmann #3 mine explosion appears to be an exception, however, a station near the Itmann #3 mine recorded a barometric pressure drop of nearly 1,422 Pa over a four-day period before it changed direction and went up by 508 Pa the day prior to the explosion (NCDC, 2015). Two other explosions that appeared to have increasing barometric pressure prior to the event, McClure #1 and Darby #1, happened in the late spring and summer seasons. From the NCDC database, slight barometric pressure increases were observed prior to the explosions in both mines. Investigations determined that the McClure #1 explosion was caused by inadequate ventilation to dilute methane, unrelated to a barometric pressure change (Wheatley, 1983). The Darby #1 mine explosion occurred near the seals of an abandoned area when miners were performing flame cutting outby one of the seals. This explosion may be related to the barometric pressure. The mine

had experienced rising barometric pressure starting two days before explosion, followed by a drop a few hours before the explosion (Light et al., 2007). The fresh air may have leaked into the sealed area during the rising barometric pressure, creating an explosive methane-air atmosphere behind the seals. The drop hours before the explosion may have caused this explosive methane-air mixture to leak out from the sealed area, and where it could be ignited by the cutting work just outside the seal. The explosion at the Sago mine is considered to be independent of any barometric pressure change. MSHA investigators determined that a massive lightning strike was the most likely cause for this explosion though barometric pressure drop was noted beforehand (Gates et al., 2007).

All investigation reports highlight the complexity of mine explosions. MSHA investigators often could not conclusively determine direct causes and contributing factors of an explosion. A mine explosion usually involves multiple factors such as methane accumulation, insufficient ventilation, monitoring system failure, barometric pressure, coal dust presence, human error, and many other factors. It is sometimes difficult to isolate the impact of barometric pressure changes and their contribution to each explosion. Therefore, though the historical mine explosions and barometric pressure data shown in Table 3.1 suggest that barometric pressure fluctuations contributed to the events, these fluctuations were not necessarily the primary cause for the explosions.

3.4 Current Atmospheric Monitoring System Technologies in the United States

A mine ventilation system is crucial to maintain a safe, breathable mine atmosphere. Mine operators must have their ventilation plans reviewed and approved by the MSHA before operations can commence; nevertheless, the ventilation plan is usually designed with little consideration for weather changes, and thus extreme barometric pressure variations may negate effectiveness in

eliminating hazardous gases. For this reason, a good detecting and monitoring program must be implemented in addition to a well-maintained ventilation system.

3.4.1 Gas Detector and Monitoring Systems

In the United States, Code of Federal Regulation (CFR) Title 30 regulates all mandatory safety standards for the mining industry including surface, underground, metal, non-metal and coal mining. Part 75 of the CFR covers safety requirements for underground coal mines including the mandatory application of gas detectors and a continuous atmospheric monitoring system (AMS) for monitoring smoke, carbon monoxide and methane. The term *detection* implies intermittent checks, while *monitoring* indicates a continuous measurement (Hartman et al., 1997). These systems consist of hardware and software installed in active working areas, belt lines, primary escapeways and electrical installations (30 CFR §75.334). The current regulation prescribes an alert at 1% methane and an alarm at 1.5% in active areas or 2% in bleeder or return air courses. The actions to be taken at such levels include de-energizing electrically powered equipment, adjusting ventilation and vacating personnel from the mine (30 CFR §75.323). Instrumentation available for measuring gas concentrations range from the oldest methods of using canaries and safety lamps to the most advanced methods of gas chromatography and tube bundle systems.

3.4.1.1 Personal Gas Detectors

Handheld gas detectors provide real-time measurement of gas concentration; MSHA and mine personnel commonly use this detector to monitor the methane levels in active or open working areas. The detection method is based upon either the temperature changes when gas oxidizes (catalytic) or the absorption of infrared radiation of a volume of gas. Both detector types are normally equipped with a sounding alarm to warn miners if concentrations of methane or other toxic gases exceeds a given threshold value. This handheld detector is typically used for spot

checks in active working areas or other locations where mine personnel have access. Real-time results and their light-weight design are the main advantages of handheld detectors. Figure 3.8 shows two examples of MSHA-approved handheld detectors for use in U.S. coal mines.

Industrial Scientific iTX Dräger X-am® 2500

Figure 3.8 Common handheld gas detectors used in the United States

Despite their fast results, handheld detectors have a limited range of accuracy for most gases (Grubb, 2008) depending on their detection types. For standardization, the federal regulation requires a handheld detector to have an accuracy of ±0.5% and be calibrated with a known methane-air mixture at least once a month (30CFR § 75.320 (a), (b)). The gases that can be measured include oxygen, methane, carbon monoxide, carbon dioxide, nitrogen, hydrogen sulfide and sulfur dioxide.

3.4.1.2 Equipment Mounted Detectors

In addition to handheld detectors, many gas sensors are mounted atop shearers, on continuous miners, at the tail of the longwall under the tail drive, and on the conveyor system along the belt entries. These locations are selected mainly due to their high potential for ignition sources and fire risks. The sensors can sniff out smoke as well as methane and carbon monoxide and instantaneously alert miners if certain gases have concentration above the permissible level. As these sensors are usually installed near the active cutting face, dusty and vibrating conditions can

easily interfere with sensor performance and response time, therefore, federal regulations require mine operators to maintain the sensors in proper condition with periodic checks and calibration (30 CFR §75.342 (a)). In general, each machine-mounted sensor includes a data recording unit, power supply and sensor head (Taylor, et al., 2002). Figure 3.9 shows a sensor head generally placed on shearers or continuous miners.

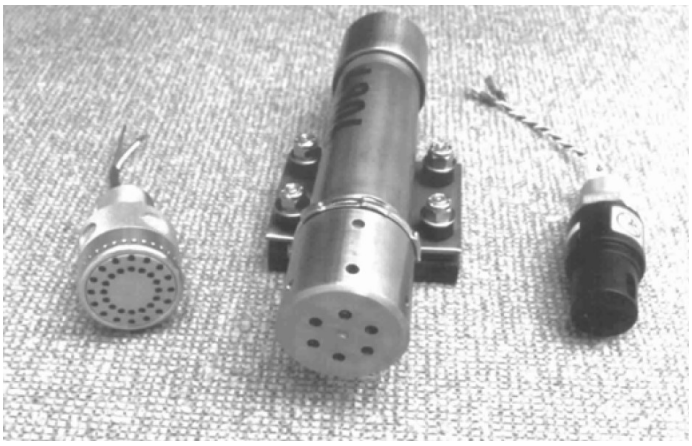

Figure 3.9: Machine-mounted sensor head (Taylor, et al. 2002)

3.4.1.3 Bag Samples and Gas Chromatographic Monitoring System

Gas chromatography requires the separation of gas components which are then analyzed based on concentrations of each component. Sampling is usually performed by drawing a gas sample into a 10-20 milliliter glass tube or syringe that has been pumped or vacuumed manually. Unlike real-time measurement devices, there is a time delay expected between sample acquisition and analysis result, depending on the time for travel from the sampling location to the gas chromatograph. Typical chromatograph instruments like that shown in Figure 3.10 are usually housed in a surface laboratory rather than placed underground, so samples must be brought to the surface for analysis. In comparison with handheld and machine-mounted sensors, gas chromatographs can detect a wider range of gas types and concentrations with high accuracy

(Timko and Derick, 2006) and provide complete analysis of hydrogen, oxygen, nitrogen, carbon monoxide, carbon dioxide and other hydrocarbons.

(Source: www.winex-instrument.com/gc4008b.php, last accessed 6/1/2016)

Figure 3.10: A typical Gas Chromatograph System

3.4.1.4 Tube Bundle Monitoring System

The primary use of a tube bundle system (TBS) is for mine fire prevention and mine atmospheric monitoring. Tube bundle system applications are widely and commonly used in Australian coal mining (Brady, 2008). Some other countries such as China, Germany, Poland and the U.K have also deployed these instruments in coal (Brady, 2008; Zipf, Jr. et al., 2013a). In the U.S., tube bundle systems are not mandatory and are thus not as common as in Australia. Only the BHP Billiton San Juan mine near Farmington, New Mexico currently employs a TBS (Bessinger et al., 2005). Another mine, the Signal Peak Energy, LLC, Bull Mountains No. 1 mine in Montana installed the system for NIOSH research purposes to investigate its application in monitoring inert sealed areas (Zipf, Jr. et al., 2013a).

The concept of TBS is similar to that of bag sampling and gas chromatography. Instead of using a special-purpose bag, samples are continuously drawn through tubes using a vacuum pump from designated locations to the surface, where they are analyzed by paramagnetic and infrared

methods with a gas chromatograph. The gases measured are usually carbon monoxide, carbon dioxide, methane, and oxygen (Cliff and Bofinger, 1998). The analysis results can be automatically obtained in a short time and at a high resolution. Figure 3.11 shows a typical flow chart and components of a tube bundle system.

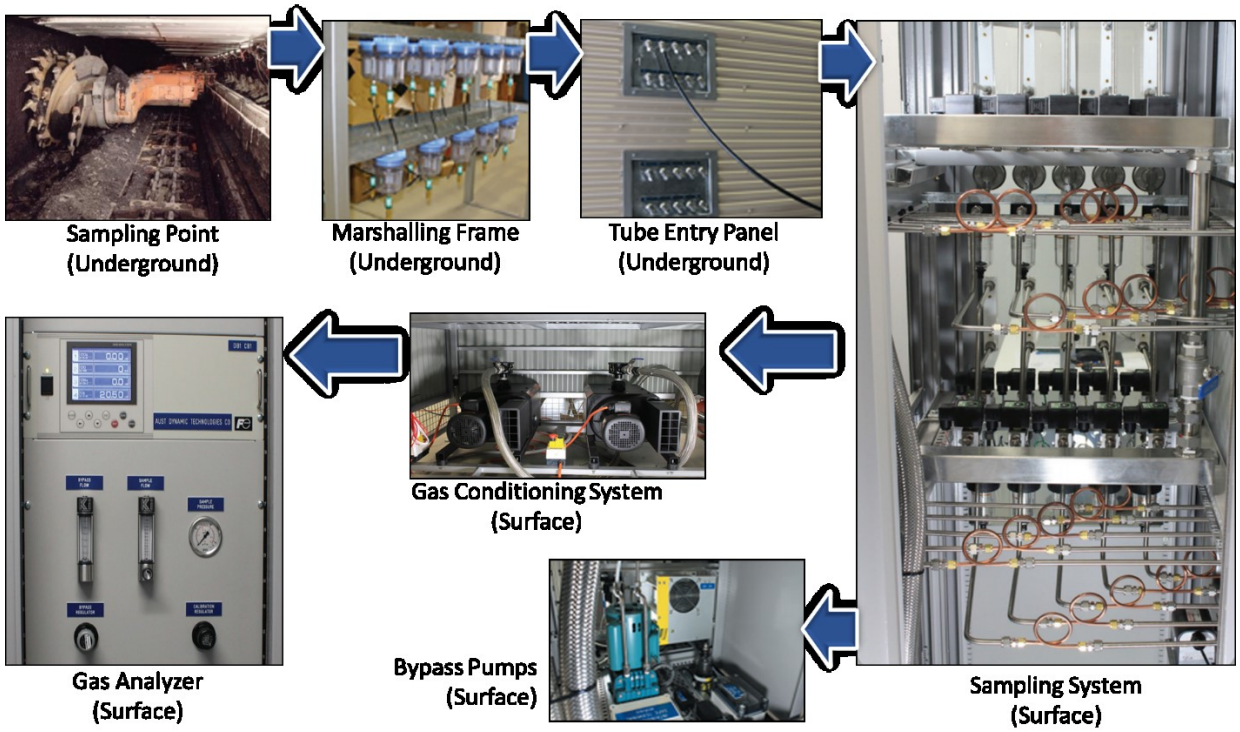

(Source: (http://www.austdynatech.com.au, last accessed 06/10/2016)

Figure 3.11: TBS flowchart and components (Australian Dynamic Technologies)

In practice, this system has limitations to detect further into the gob where the explosive mixture may occur, which makes it difficult to tackle the issues associated with the EGZ. In addition, the readout from the gas analysis is not immediate, depending upon the distance from the sampling points underground to the gas analyzer at the surface. The tubes require regular maintenance to avoid puncture and internal water condensation, both of which will negatively affect the results.

In addition to gas monitoring, TBS also monitors barometric pressure. Monitored gas concentrations in specific locations and concurrent barometric pressures can show the relationship between gas emissions and mine barometric conditions. In the investigation of the system installed at the Bull Mountains No. 1 mine, Signal Peak Energy (SPE) in Montana, NIOSH researchers observed the correlation of carbon dioxide outgassing with barometric pressure changes (Zipf, Jr. et al., 2013b). In Figure 3.12, red arrows represent sudden spikes in carbon dioxide concentration up to 10 times the typical background level of 0.5-1.0% CO_2 when the barometric pressure decreased. The same methodology can be applied to relate methane emission and barometric pressure changes in gassy mines.

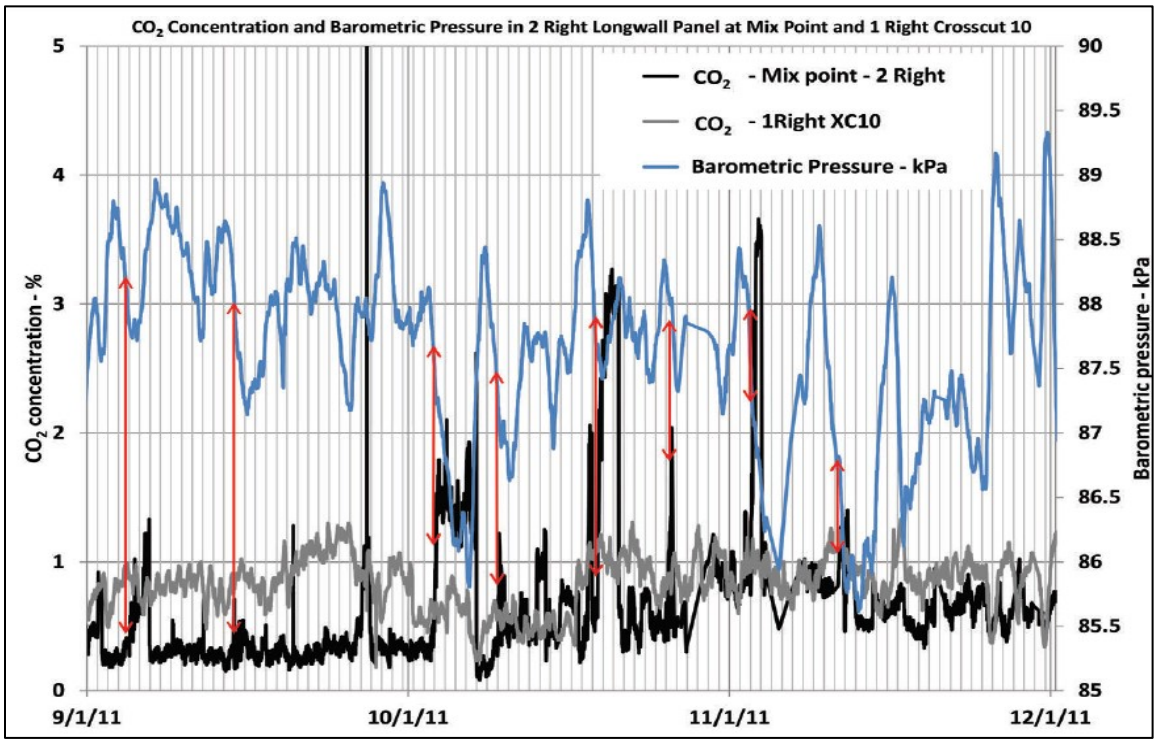

Figure 3.12: CO_2 conc. and barometric pressure from TBS at SPE (Zipf Jr., et al., 2013)

3.4.1.5 Fiber Optic Sensors

The mining industry has become increasingly attracted to fiber optics for gas sensing. The utilization of fiber optics in underground coal mines has been primarily for wireless

communication systems rather than for gas detection; however, the abundance of silica for fiber, low-cost materials, a high data capacity, good conductor characteristics and a light weight are all reasons for the development of fiber optic sensor technology.

The U.S. Bureau of Mines (USBM) developed and tested a fiber optic system prototype for methane monitoring (Dubaniewicz and Chilton, 1992). The USBM noted that fiber optics can provide a superior advantage in transmitting data compared to wire-based systems. Figure 3.13 illustrates a sensor system and the profile of fiber optic cable. The optical fiber guides light pulses to the sampling location underground; the light exits the fiber, passes a gas cell which is open to mine atmosphere and may contain CH_4, and enters the fiber connection to the detector on the surface. The detectors convert the light pulses into electrical signals that can read CH_4 concentrations present in the gas cell. Though fiber optic sensors have not been fully proven for mine utilization, the USBM prototype and tests showed promising results that may lead to the use of more standardized fiber optics sensors in underground mines.

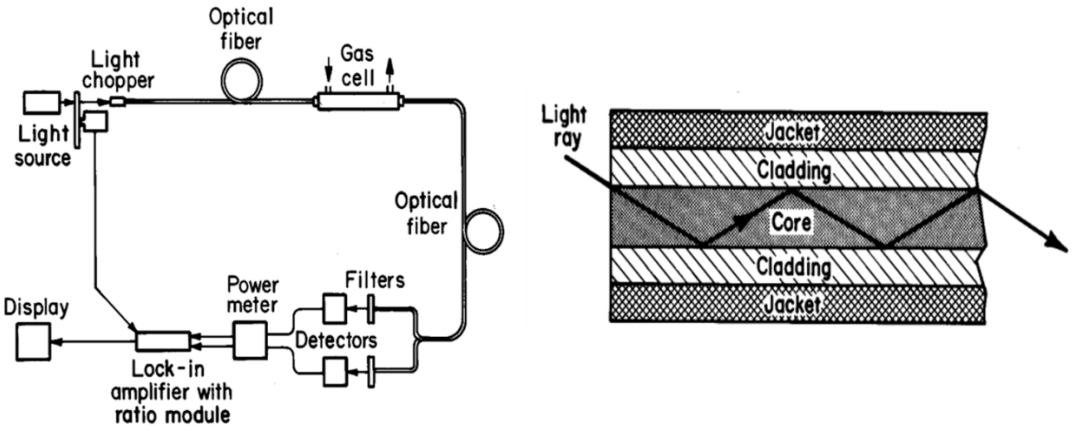

Figure 3.13: Fiber optic sensor diagram and profile (Dubaniewicz and Chilton, 1992)

3.4.2 Computational Fluid Dynamics as a Predictive Tool

Detecting methane-air mixtures and other toxic gases in the gob is vital, since investigations of several mine explosions and fires have shown that the initial ignition originated

from the gob (Brune, 2013). However, the existing sensors and monitoring systems have intrinsic limitations due to design and physical conditions. These limitations affect sensor accuracy and sensitivity. The design of handheld and machine-mounted sensors allows detection in localized areas only, which does not really reflect the overall condition of the mine or, specifically, the gob or sealed areas. Even though the mine employs monitoring systems for the gob such as TBS, the condition deeper into the gob remains unknown.

Due to the physical limitations of commonly used monitoring systems, computational fluid dynamics (CFD) has become increasingly attractive as an evaluation and predictive tool. Although studies of methane control have been conducted for many years, research on methane-air mixtures in a longwall gob using CFD codes is relatively new. Most earlier CFD studies were presented in the context of spontaneous combustion or a methane explosion in active mine workings (e.g. longwall face, entries, unsealed area). These studies utilized data collected from actual mines or laboratory experiments. The existence of the EGZ was increasingly recognized after several analyses of major mine explosions suggested the existence of an explosive methane-air mixture in the gob (Elkins, et al., 2001; McKinney et al., 2001, Cario, 2006; Woodward and Sheffield, 2008; Brune, 2013).

The use of computational programs has become more prevalent as physical gob conditions generally restrict field investigation. The U.S. Bureau of Mines initiated the development of a computer program called Gob Assistant to analyze gas flows into and out of the gob during barometric pressure changes (Foster-Miller, 1988). Further applications of CFD in gob investigations emphasized the gas flow mechanism and concentration level for spontaneous combustion analysis and methane drainage designs (Ren and Edwards, 2002; Wendt and Balusu, 2002; Ren, et al., 2005; Yuan et al., 2006). In more recent study, Yuan and Smith (2010) applied

a CFD approach to investigate the influence of barometric pressure on spontaneous heating in the gob.

Researchers at the CSM working under projects funded by NIOSH have used CFD to investigate the occurrence of explosive mixtures and gob flow pattern in different ventilation scenarios. The explosive range used in the modeling is based on Coward's triangle, as shown in Figure 3.3. Researchers have also extended the investigation to analyze the effectiveness of a nitrogen injection method in reducing EGZ in the gob (Gilmore et al., 2013; Marts et al., 2014b) and to study the effect of face ventilation, bleeder regulator settings and GVB application on the formation of EGZs (Gilmore et al., 2015; Saki et al., 2015). In addition, a range of longwall layouts such as bleeder, bleederless and progressive sealing ventilation systems have been thoroughly studied.

3.5 Porosity and Permeability of Gob and Strata

As illustrated in Figures 1.1 through 1.3, the longwall mining method uses shearer drums to cut coal in a back-and-forth path from the headgate to the tailgate. Shield arrangement provides protection for miners, the shearer, the armored face conveyor (AFC), and other equipment along the coal face. The shields advance after a complete pass from one end of the panel to the other. Both the retreating and advancing types of the longwall mining method allow overlying strata to cave behind the shields as soon as coal is extracted, and this caved area is referred to as gob or goaf (the latter term is mostly used in Australia and Europe). The gob is mainly filled with broken coal, caved-in roof and heaved-up floor rocks, which together form a porous medium.

Gob characteristics are determined by several factors, including geologic conditions of the overlying and underlying strata, panel dimensions and coal seam depth. The presence of joints, faults, and other geologic discontinuities and anomalies will change the gob properties, caving

time, and size of the broken material. The disturbance to *in-situ* conditions when extracting the coal produces abutment pressure that is heaped up around the gob. Peng (2006) stated that coal extraction by longwall mining induces a series of events: abutment pressure and roof-to-floor convergence in the entries and face area, movement of rock strata and surface subsidence. Figure 3.14 illustrates the conceptual condition of the overlying strata after the coal is mined out. Immediate response of the strata after coal extraction is failure or caving of the immediate roof. An investigation by MSHA (2002) reported that the height of the caved zone might range from one to 10 times the mining height depending on the strength, strata type, and geologic conditions of the roof rocks. Other investigations have reported a caved zone height of about four to six times the coal seam height (Mucho et al., 2000). The horizontal span of the caved zone increases as the mine retreats and broken material gradually fills the void space.

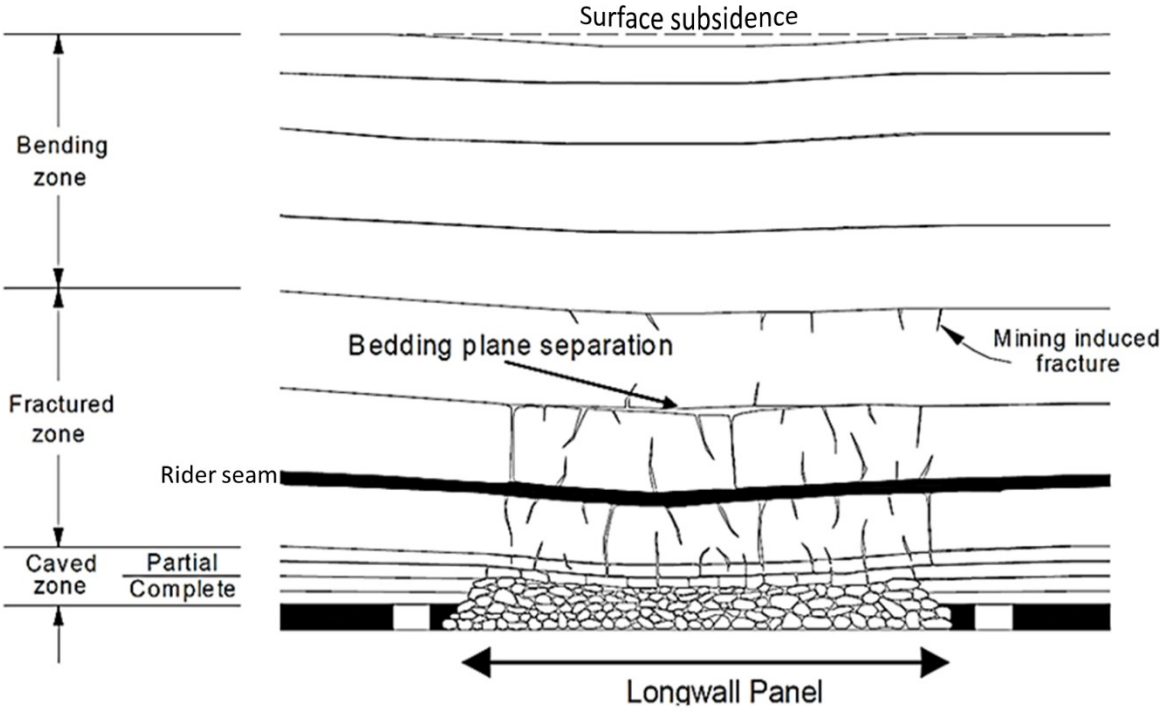

Figure 3.14: Long section view of a caved longwall panel (Esterhuizen and Karacan, 2005).

Above the caved zone, strata do not detach from the rock mass, but they are linked by cracks and fractures; this is known as the fractured zone. This zone extends from 30 to 60 times the mining height and may cause beam deformation and bedding plane separation (Esterhuizen and Karacan, 2005). Further above this zone, these cracks may no longer be present in the deformation. The strata are perceived to deform lightly without causing major cracks, but the bending deformation continues to the surface, causing subsidence.

3.5.1 Gob as a Porous Medium

As it is filled with caving materials and rubble, the gob resembles the condition of a porous medium, as shown in Figure 3.15. Porous medium is a broad subject, and its descriptions can be sometimes intuitive due to its complex system, and its exact properties are difficult to describe (Scheidegger, 1957).

Figure 3.15: Gob at two coal mines in eastern Kentucky (Pappas and Mark, 1993a)

In general terms, a porous medium can be simply defined as a portion of a solid or loose body occupied by heterogeneous or multiphase matter, of which one of the phase is not solid (Bear, 1972). In this study, the porous medium is defined in the context of the gob and overlying strata. The solid body consists of a packed form of caved rock materials distributed throughout the medium, while the non-solid body refers to the pore spaces between the rocks. An important

attribute of a porous medium is that the pores are interconnected and have apertures that are much smaller than the solid phase size (Scheidegger, 1957; Bear, 1972). The interconnected pores are sometimes known as the effective pore space. From the perspective of flow, dead-end pores are sometimes considered part of the solid matrix because the flow is practically stagnant.

In the gob, the caved roof and heaved floor materials, including unmined coal, will dominantly make up the solid phase. The materials are packed randomly, but may be rearranged as the mine progresses so that large rubble sits atop the fine rocks. This is mainly due to gravity and compaction. Considering that the pore apertures in a porous medium should be small compared to the solid phase dimension, some areas of the gob including the large voids that exist along the perimeter of the gob and extend inby behind longwall face, should not be regarded as a porous medium.

Gas flow in porous media is generally analyzed using Darcy's law, as shown in Equation 3.3, which simply states that the gas velocity is directly proportional to the pressure gradient and permeability (Bear, 1972).

$$\overline{u_g} = -\frac{k_g}{\mu_g}\left(\nabla P_g - \rho_g \bar{g}\right) \tag{3.3}$$

where u_g is the gas velocity (m/s), k is permeability (m^2), μ_g is the gas viscosity (Pa· s), ∇P_g is the pressure gradient between two referenced locations (Pa), ρ_g is the gas density (kg/m^3), and g is the gravitational constant (m/s^2). Note that the Darcy velocity is not a physical velocity, but rather a superficial velocity based on the entire cross section of the flow as if the gas is the only substance present in a given cross-sectional area.

Darcy's law is applicable and works well to low-velocity flow such as the flow through a porous system. However, as velocities increase, flow becomes turbulent and flow resistance

becomes non-linear in defiance of Darcy's law (Bear, 1972). A second term of non-linear flow resistance was then added to Darcy's law based on the work of Forchheimer for a turbulent calculation (Ho and Webb, 2006). The Forchheimer equation is given in Equation 3.4.

$$\nabla P_g = -\frac{\mu_g}{k_g}\overline{u_g} - \rho_g \bar{g} k_g^{-1/2} \rho_g |\overline{u_g}|\overline{u_g} \tag{3.4}$$

The Forchheimer equation is an extension of Darcy's law (the first term from Equation 3.4 is Darcy's equation). With advanced computer systems, calculations of porous media flow have progressed to include multiple turbulence equations as exemplified in ANSYS Fluent® codes (Tu et al., 2008; ANSYS, 2013).

3.5.2 Subsidence and Compaction

Despite being the most productive of underground coal mining methods, longwall mining has disadvantages for surface topography. Longwall mining can result in surface subsidence over a large area above the panel. The size and depth of that subsidence is governed by many factors such as longwall size, rock strata strength, rock type and mining depth. As longwall mining removes a block of a coal seam, it creates a void where the immediate roof and overburden up to the surface will move downward. An idealized sequence of a subsidence is illustrated in Figure 3.16 (Peng, 2006). Depending on the rock type, the immediate roof bends and falls quickly or soon after the coal is mined (Figures 3.16, A-D). This happens when the gob has reached interval L_o. As shown in Equation 3.5, this interval is estimated to be a factor of the thickness, density, and tensile strength of the immediate roof and the overlying strata (Peng, 2006). Fall height is often greater than the dimension of the rock fragments resulting in a disorderly arrangement (Esterhuizen and Karacan, 2007). The immediate roof failure continues to the upper strata in a bulking fashion so that bed separation potentially occurs in the overburden (Figures 3.16, E-J).

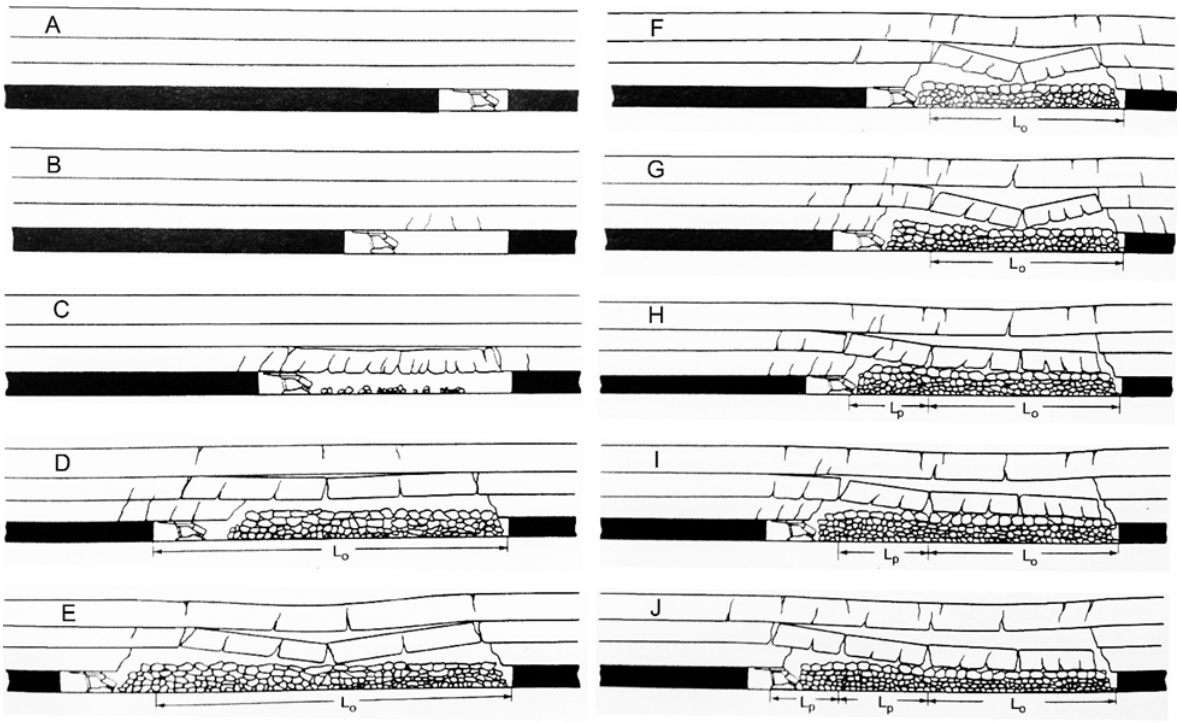

Figure 3.16: Idealized sequences of subsidence in longwall mining (Peng, 2006)

$$L_o = \sqrt{\frac{2hT}{\gamma}} \tag{3.5}$$

where L_o represents the estimated length of the initial caving (m), h is the thickness of the immediate roof (m), T is the tensile strength of the immediate roof and main roof (Pa) and γ is the weight per unit volume of the immediate roof = ρg (N/m^3).

Some of the strata weight will be held by the shields, which induce tension force and bending to the strata above the mined-out area. As the longwall face retreats further, the roof breaks periodically with a breaking length of L_p. This length varies with rock blockiness, strength, joint conditions and the gap between already-caved piles and the roof. A Peng et al. (1992) study on the Pittsburgh seam indicates that this length was, on average, 24 m (78 ft). At a certain distance, the full weight of the overlying strata eventually rests upon the gob material, showing a condition illustrated in Figure 3.14. The condition of no overlying strata hanging above the shields usually occurs in a nearly completed supercritical panel.

It is understood that subsidence directly relates to the overburden compaction. The weight of the overlying strata is transferred down to the broken materials in the gob, which subsequently compact to become more consolidated. The consolidation reduces the porous volume and thus the land surface gradually sinks down. Subsidence area and depth can provide information about gob compaction that is essential to estimate gob porosity. A number of studies have been devoted to determining gob porosity and permeability after compaction. Pappas and Mark (1993a) studied the gob compaction and porosity relationship using photoanalysis and laboratory tests. Photographs were taken of areas behind the shields in three coal mines located in Virginia and eastern Kentucky and scanned to roughly estimate rock size. Subsequent laboratory experiments were conducted using broken rock with sizes estimated from the scanning process. The experiments used a variable-pressurized chamber to analyze the porosity changes of the broken rock under compaction. The initial void ratio of gob rock fragments ranges roughly between 30% and 45% from the laboratory tests. The tests also showed that most of the gob compaction occurred shortly after the gob began to take the full load of the overlying strata. Conceptually, this condition is shown in Figure 3.16 J. The compaction caused rock fragments to be pinned or tangled and resulted in a decreased mobility of the deformation, which strengthened the material packing. This is known as strain hardening or stiffness behavior, represented by a hyperbolic profile in Figure 3.17. Many other studies also found similar strain hardening behavior of gob material under compaction (Salamon, 1990; Badr, 2004; Yavuz, 2004; Esterhuizen et al., 2010). This hardening behavior of gob material is used to match subsidence profile which gives estimated values of the porosity and permeability distributions in gob (Marts et al., 2014a).

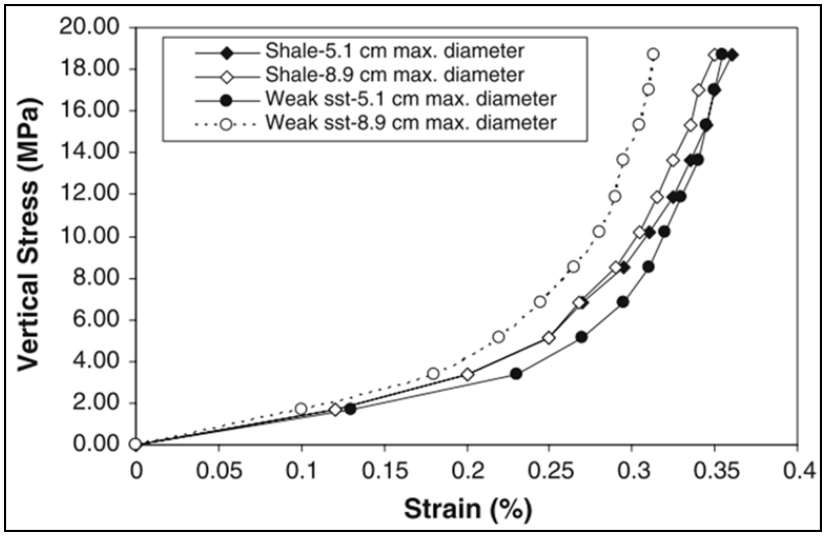

Figure 3.17: Stress-strain behavior of material under compaction (Pappas and Mark, 1993a)

3.5.3 Gob Porosity and Permeability

As explained in the previous section, when the overlying strata rests completely on the gob materials, the caved area expands laterally to the nearest entry of the outward gob and the stress pattern changes around the gob (Peng, 2006). The vertical stress increases toward the center of the gob where the load reaches maximum, changing the gob's reservoir properties, porosity and permeability. It is widely accepted that the gob becomes more compacted and less porous further into the center than the area behind the shields. This varying porosity and permeability must be accounted for in gob modeling as it controls the air flow profile.

Porosity, usually denoted by n, is the ratio of void space volume to the total volume of a porous medium. In the gob, porosity is a dynamic property that changes over time due to consolidation of the overlying burden. Initial porosity of the gob, n_o, depends on the way the fresh broken materials are arranged inside the gob. Blocky materials tend to break into large slabs and are positioned in disorderly arrangement, resulting in area with large voids. Esterhuizen and

Karacan (2007) studied gob porosity and found that it varied with shape, size, arrangement of the broken rock pile and also pressure imposed from the overburden.

Permeability, denoted by k, indicates the ability of a porous medium to transmit fluids. A common unit for permeability is Darcy (D), or more commonly, millidarcy (md), in which 1 Darcy equals 9.87 x 10^{-13} m^2. Permeability is generally expressed as in Equation 3.6 (Bear, 1972). The proportionality constant, C, is also known as Darcy's velocity.

$$K = \frac{\mu C}{\gamma} \tag{3.6}$$

where K is the permeability in m^2, μ is the gas dynamic viscosity in Ns/m^2, and γ is the gas specific weight in N/m^2.

Since porosity and permeability are technically the measures of the porous medium structures, they ought to be related. Many researchers have studied the relationship between these two parameters. The most widely used relationship is an empirical Carman-Kozeny equation (Carman, 1956). The general expression of the formula is given in Equation 3.7. The value of K_o represents the base permeability of the broken rocks and varies depending on the rock type. For open-jointed rock, it is about 1 x 10^6 md (Hoek and Bray, 1981; Karacan et al., 2005). Most, if not all, gob studies have used the Carman-Kozeny approach to estimate gob permeability, and the calculated values are relatively alike.

$$K = \frac{K_o}{0.241}\left(\frac{n^3}{(1-n)^2}\right) \tag{3.7}$$

Given that the airflow will be largely controlled by gob permeability, it is important to model the permeability distribution as opposed to a single uniform permeability. Though it is important, gob inaccessibility represents challenges in collecting compaction data behind the shields, resulting in too many unknowns when modeling a gob, particularly those associated with

gob permeability and compaction. Therefore, the use of advanced numerical approaches has become more prevalent. Advanced numerical modeling using geotechnical analysis codes such as FLAC$^{3D®}$ provides a better way to realistically predict rock mass' response to compaction. Researchers at NIOSH modeled a sequential extraction focusing primarily on the dynamic changes of permeability condition in the gob with the coal being extracted in a single step from startup room to recovery room (Esterhuizen and Karacan, 2005, 2007). Though this approach is still far from reality for an active panel, this study has provided fundamental understanding for the development of geomechanical modeling using ground subsidence data, which can output the permeability values required for CFD modeling.

Learning from NIOSH's single-step extraction model (Esterhuizen and Karacan, 2007), Wachel (2012) developed an improved approach to simulate an active progressing face through stepped extraction in 33-ft (10-m) increments. Using the FLAC$^{3D®}$ program, a commercial finite difference numerical modeling for complex geotechnical analysis, Wachel (2012) developed a curve fit of the gob permeability profiles, as shown in Figure 3.18. The permeability determination was based on the deformation zones in the overburden, which incorporated Peng's empirical equations for caved and fractured zone heights (Peng, 1992), and the strain hardening curve, which Esterhuizen and Karacan (2005) used in their gob permeability study. The permeability values range from 3×10^{-9} to 1×10^{-5} m^2.

The presence of laminated layers and weak joints was not considered in Wachel's study; thus, it oversimplified the rock mass which in reality consists of numerous anisotropic fracture and joints. A later study by Marts et al. (2014a) then used and improved this approach by using the Ubiquitous Joint (UBJ) property in FLAC$^{3D®}$ to simulate anisotropic strata. The UBJ accounts for jointed rock mass by inserting a failure plane wherever imposing stress exceeds the user-defined

joint strength (Itasca, 2013). This improved model also considered the presence of abutment pressure, in addition to only vertical stress that Wachel's study considered. Porosity is determined from gob volumetric compaction computed in FLAC$^{3D®.}$ Once porosity values are obtained, permeability is then calculated using the Carman-Kozeny formula (Equation 3.7).

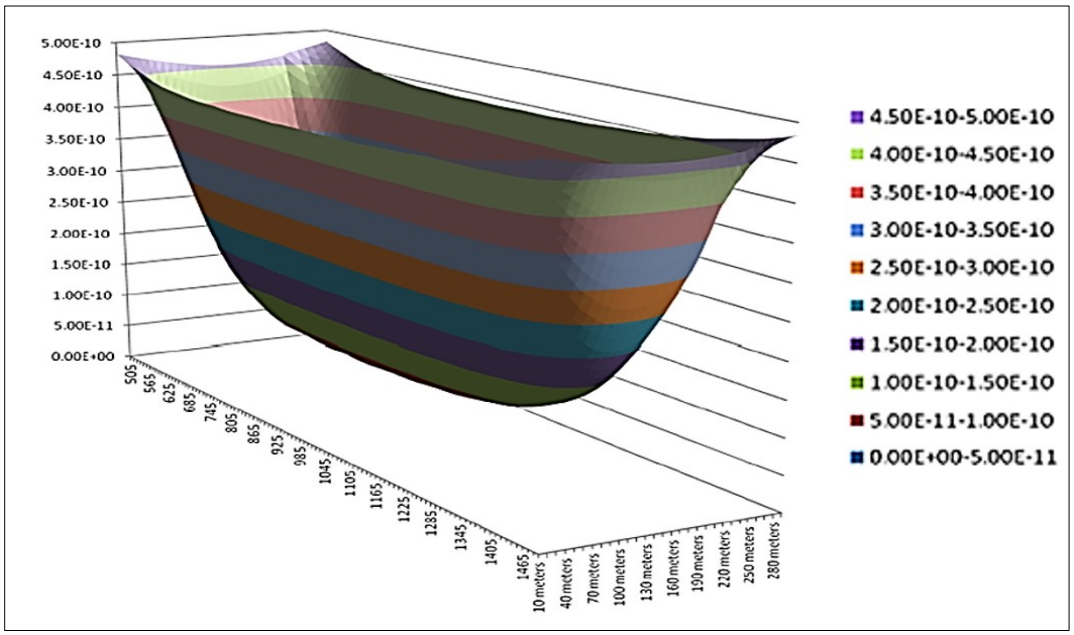

Figure 3.18: Permeability profile estimated using single step extraction (Wachel, 2012)

For validation, Marts et al. (2014a) compared the subsidence output from modeling against actual subsidence data from Mine C and Mine E. The main difference between the two mines is in their stratigraphy and rock type, both of which affect the compaction model. The modeled subsidence shows strong agreement with actual data (Marts et al., 2014a), indicating the computed porosity and permeability were within reasonable values. Figure 3.19 illustrates the porosity and permeability distribution obtained from the study. The distributions were depicted as a gradually smooth change with larger permeability existing in the gob perimeter and smaller towards the gob center.

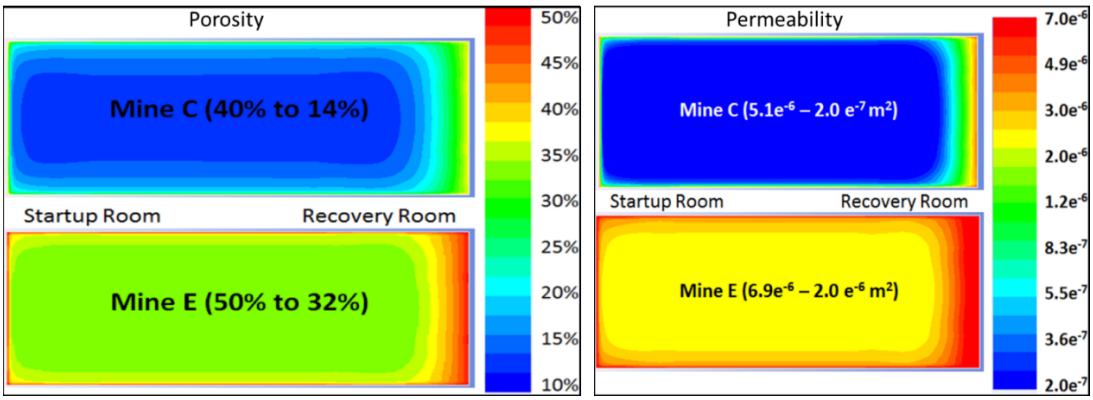

Figure 3.19: Estimated porosity and permeability for Mines C and E (Marts et al., 2014a)

For comparison, Table 3.2 shows several notable studies of gob permeability used as references in this study. Most of these studies used the Carman-Kozeny equation in either original or modified forms. The minimum value of permeability is usually assigned for the consolidated region of the gob and the maximum value is for the area behind the shields. It is noted that the differences in geological and mine operational conditions in each study contribute to the different permeability.

Table 3.2: Gob permeability values from different studies

Reference	Value Used for Gob Permeability (m^2)	
	Minimum	Maximum
Brunner (1985)	9.87×10^{-8}	9.87×10^{-6}
Ren et al. (1997)	9.87×10^{-11}	
Szlązak (2001)	5.03×10^{-9}	9.87×10^{-7}
Wendt and Balusu (2002)	9.87×10^{-10}	
Whittles et al. (2006)	9.87×10^{-10}	4.93×10^{-7}
Yuan et al. (2006)	4.93×10^{-12}	9.87×10^{-10}
Esterhuizen and Karacan (2007)	9.87×10^{-11}	9.87×10^{-10}
Lolon and Calizaya (2009)	7.17×10^{-9}	4.19×10^{-7}
Karacan (2010)	4.99×10^{-9}	7.00×10^{-7}
Smith and Yuan (2010)	2.96×10^{-11}	8.39×10^{-10}
Wachel (2012)	3.00×10^{-9}	9.97×10^{-6}
Worrall (2012)	2.00×10^{-7}	6.81×10^{-6}
Marts et al. (2014a)	1.97×10^{-7}	5.10×10^{-6}
Karacan and Yuan (2015)	2.96×10^{-11}	9.87×10^{-4}

3.5.4 Overlying Strata Porosity and Permeability

The importance of porosity and permeability estimations for the strata above the gob depends on the existence of rider seams in the overlying strata. The rider seams, in addition to the mining seam, are methane sources in a longwall mine; the methane emitted will flow to the mine workings through strata fractures.

As shown in Figure 3.14, the overlying strata do not cave but are characterized by fractures. In the oil and gas industry, strata fractures have been studied using a variety of methodologies as part of reservoir and fracture modeling. The mining industry has adopted reservoir modeling to increase gob borehole ventilation (GVB) performance. Karacan (2009) conducted a number of well tests to reconcile longwall gob gas reservoirs and the production of six GVBs drilled over three adjacent panels to strata above the gob. From the multi-rate drawdown analysis techniques, he reported permeability values of strata between 6.4×10^{-13} and 2×10^{-12} m^2. Dougherty et al. (2010) conducted a similar study using a series of boreholes. The tests provided rough estimations of strata permeability found around a borehole. They reported a permeability of nearly 1.5×10^{-11} m^2 extending to a radius of about 2,800 m (9,200 ft) from the borehole location. The permeability in the immediate vicinity of the borehole (110 m radially) was about 5.2×10^{-13} m^2.

A more recent approach by Karacan (2015) treated the strata as a porous medium with a network of random fractures. The fracture network was created using a Discrete Fracture Network (DFN) simulator and was irregular in pattern, as one should expect for random fractures. In general, the DFN model combines deterministic and stochastic discrete fractures (Dershowitz et al., 1998). Deterministic fractures are purposely created in strata based on several user inputs such as fracture size distribution, aperture, transmissivity, and directions. DFN will then use these inputs to calculate and create the main fracture network. Other smaller fractures that may be important

for methane flow are generated stochastically. An example of random, naturally occurring fracture network generated by the DFN simulator is shown in Figure 3.20.

It is important to note that field investigations (Karacan, 2009; Dougherty et al., 2010) indicate that the permeability of strata is four orders of magnitude lower compared to the gob permeability shown in Figure 3.19. With such a low permeability and its respective location above the gob zone, overlying strata may not be an area of concern with respect to explosion hazards. For this study, the permeability of strata is sufficiently modeled as a constant fixed value. Section 4.3.5 further discusses the selected value for strata permeability.

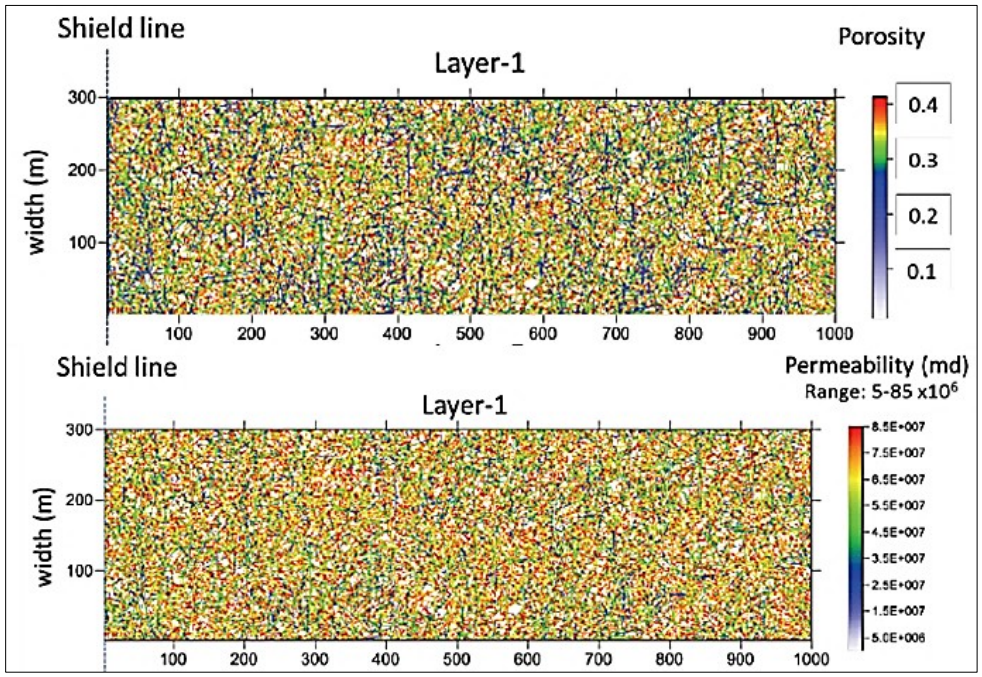

Figure 3.20: Porosity and permeability of 2-m thick zone using DFN model (Karacan, 2015)

3.6 Gravity and Buoyancy

It has been well understood that gravity influences the stratification of gas mixtures. An investigation in an actual mine determined that gas distribution further back into the gob was mostly controlled by the buoyancy effect, while gas distributions near the face were dependent on face flow rate and pressure (Ren and Balusu, 2010). Further investigation in several other longwall

panels in Australia also showed that methane tends to build up in layers towards higher elevations in the gob as the face retreats (Ren et al., 2011). With a mass weight of about one-half that of air at standard atmospheric conditions, methane is a buoyant component in the methane-air mixture. This condition is depicted in Figure 3.21. In a simple two-dimensional CFD model of two side-by-side rooms separated by a partition, one filled with pure methane and the other with air, mixture layering will occur once the partition is removed as gravity enables the methane to accumulate on top of the air. The layering can be clearly seen forming after 45 seconds of mixing. Such layering can become indistinct due to gas diffusion resulting in a completely mixing of methane and air. The methane-air flame propagation experiments conducted by researchers at the Colorado School of Mines also show the accumulation of a methane-rich mixture in the upper part of the flow-stagnant tubes (Fig et al., 2016).

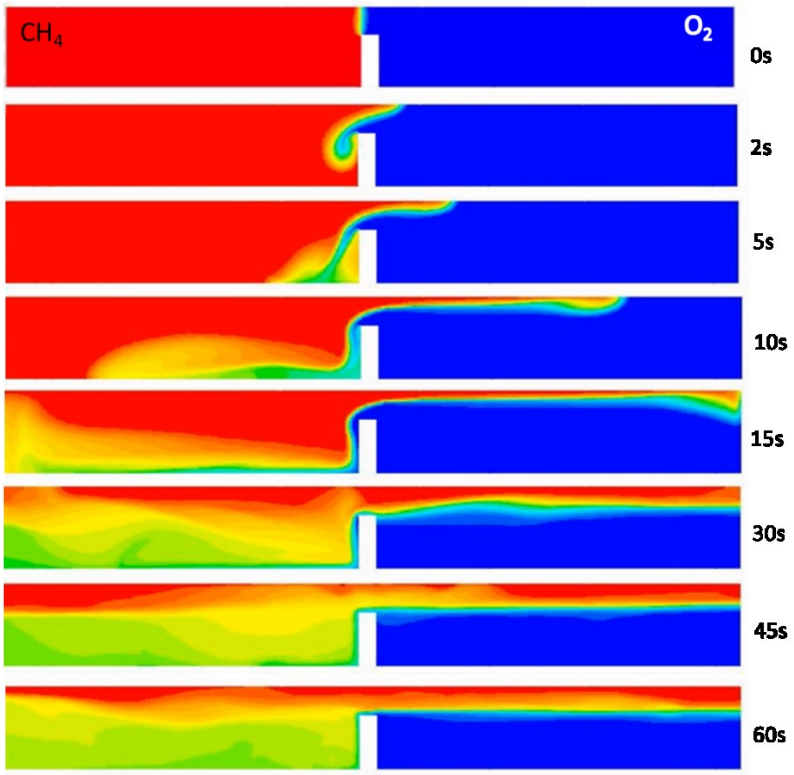

Figure 3.21: CFD modeling of methane-air separation and layering with gravity activated

Buoyancy may have a less significant effect on fluid flow in a porous medium compared to flow in an empty room. In a simulation of two simplified gob models, one is assigned as a porous medium and the other is not; a methane inlet indicates different results in respect to generated separation and total methane volume. In the absence of a porous medium, gravity causes an upward force on the methane gas within methane-air mixture that will counteract its weight. Within a porous medium, capillary force is present and can lessen the gravity effect on the buoyancy-driven flow. The capillary force can dominate the pressure gradient due to gravity depending on gas viscosity, flow velocity, and porosity (Frette et al., 1992). This finding leads to the conclusion that less gravity effect is expected for gas flow in the gob than in mine entries or gate roads due to gob materials.

Methane and air cannot be separated once they are diffused and mixed. Therefore, buoyancy will only have an effect on the unmixed gases when methane is released from relatively higher locations such as the mine roof (Kissell, 2006) and the overlying strata above the gob. Methane released from the mine floor and the lower section of the coal face or rib will immediately be picked up and diluted by the ventilation air. In this condition, buoyancy becomes negligible. Therefore, the little quantity of air flowing through the gob and an abundant supply of methane from the overlying strata will most likely create a buoyancy-driven layering in the gob.

CHAPTER 4

MODELING ENVIRONMENT AND SETUP

4.1 Introduction to Computational Fluid Dynamics Modeling

This section includes a high-level discussion of the CFD modeling setup and fundamental numerical methods implemented to solve fluid flow problems, including the governing equations of the CFD program, the selected turbulence solver, gas properties, model geometry, boundary conditions, and other modeling assumptions. Most of the selected solver and model settings are based on recommendations from previous NIOSH project research by Worrall (2012), Marts (2015) and Gilmore (2015). A commercially available CFD program, ANSYS Fluent® version 16.0, was chosen for this research, and thus the discussions on the program solver and mathematical equations were heavily based on the Fluent Theory Guide (ANSYS, 2013) and fluid mechanics theories (Tu et al., 2008; White, 2011).

4.1.1 Governing Equations of Fluid Dynamics

Most commercial CFD software programs, including ANSYS Fluent®, use a finite volume method to discretize the spatial domain into small cells and form a volume mesh or grid before applying suitable governing equations of fluid motion. The governing equations stipulate the conservations of mass, momentum and energy.

4.1.1.6 Conservation of Mass

The conservation of mass states that the mass of a fluid must neither be created nor destroyed within a volume, meaning that the mass change in a domain must be equal to the mass that enters or leaves the volume domain. This can be written in integral form as shown in Equation

4.1 (White, 2011). The equation shows that the rate of mass change within a deformable defined region or control volume (CV) is equal to the mass flux crossing the control surface (CS).

$$\left(\frac{dm}{dt}\right)_{syst} = 0 = \frac{d}{dt}\left(\int_{CV} \rho \, d\mathcal{V}\right) + \int_{CS} \rho(\boldsymbol{V_r} \cdot \boldsymbol{n}) \, dA \tag{4.1}$$

where m is the fluid mass, ρ is the fluid density, $\mathcal{V}$ is the volume, $\boldsymbol{V_r}$ is the relative velocity on the surface normal, $\boldsymbol{n}$ is the unit normal vector and A represents the surface area. The rearrangement of Equation 4.1 with Gauss's divergence theorem becomes:

$$\frac{d}{dt}\int_{CV} div \, \rho \boldsymbol{V} \, d\mathcal{V} = -\int_{CS} \rho(\boldsymbol{V} \cdot \boldsymbol{n}) \, dA \tag{4.2}$$

Gauss's divergence theorem equates the integral of volume of a vector divergence into an area integral over the surface that defines volume (Tu et al., 2008*)*. Using Equation 4.2, the surface integral in Equation 4.1 can be replaced by a volume integral

$$\int_{CV} \left(\frac{\partial \rho}{\partial t} + \nabla \cdot (\rho \boldsymbol{V})\right) d\mathcal{V} = 0 \tag{4.3}$$

The $\partial\rho/\partial t$ term corresponds to the change in mass in the control volume over time, which equals zero supposing the control volume is steady, and $\nabla \cdot (\rho V)$ = div ρV. The $\rho \boldsymbol{V}$ term is related to the mass going in and out of the control volume and driven by a certain velocity. Considering a constant control volume, Equation 4.3 can be simplified as

$$\frac{\partial \rho}{\partial t} + \nabla \cdot (\rho \boldsymbol{V}) = 0 \tag{4.4}$$

Equation 4.4 is the general form of the mass conservation. In the Cartesian coordinate system with the velocity vector, $\boldsymbol{V} = ue_x + ve_y + we_z$, it can be expressed as

$$\frac{\partial \rho}{\partial t} + \rho\frac{\partial u}{\partial x} + \rho\frac{\partial v}{\partial y} + \rho\frac{\partial w}{\partial z} + u\frac{\partial \rho}{\partial x} + v\frac{\partial \rho}{\partial y} + w\frac{\partial \rho}{\partial z} = 0 \tag{4.5}$$

4.1.1.7 Conservation of Momentum

The conservation of momentum states that the change of momentum over time must be equal to the sum of forces applied on the fluid, which can be written as Equation 4.6.

$$\frac{d\boldsymbol{P}}{dt} = \sum F = ma \tag{4.6}$$

where $\boldsymbol{P}$ is the momentum of the fluid, F is the force acting on the fluid element, m is the fluid mass, and a is the acceleration. Further expansion of the above equation for each of the Cartesian coordinates gives Equations 4.7 – 4.9 (Tu et al., 2008):

$$\left(\rho\frac{\partial u}{\partial t} + \rho\frac{\partial u}{\partial x} + \rho v\frac{\partial u}{\partial y} + \rho w\frac{\partial u}{\partial z}\right) = \frac{\partial \rho}{\partial x} + \frac{\partial}{\partial x}\left(2\mu\frac{\partial u}{\partial x} + \kappa\nabla\cdot\boldsymbol{V}\right) + \frac{\partial}{\partial y}\left[\mu\left(\frac{\partial u}{\partial y} + \frac{\partial v}{\partial x}\right)\right] + \frac{\partial}{\partial z}\left[\mu\left(\frac{\partial u}{\partial z} + \frac{\partial w}{\partial x}\right)\right] + \rho g \tag{4.7}$$

$$\left(\rho\frac{\partial v}{\partial t} + \rho\frac{\partial v}{\partial x} + \rho v\frac{\partial v}{\partial y} + \rho w\frac{\partial v}{\partial z}\right) = \frac{\partial \rho}{\partial y} + \frac{\partial}{\partial x}\left[\mu\left(\frac{\partial u}{\partial y} + \frac{\partial v}{\partial x}\right)\right] + \frac{\partial}{\partial y}\left(2\mu\frac{\partial v}{\partial y} + \kappa\nabla\cdot\boldsymbol{V}\right) + \frac{\partial}{\partial z}\left[\mu\left(\frac{\partial v}{\partial z} + \frac{\partial w}{\partial y}\right)\right] + \rho g \tag{4.8}$$

$$\left(\rho\frac{\partial w}{\partial t} + \rho\frac{\partial w}{\partial x} + \rho v\frac{\partial w}{\partial y} + \rho w\frac{\partial w}{\partial z}\right) = \frac{\partial \rho}{\partial z} + \frac{\partial}{\partial x}\left[\mu\left(\frac{\partial w}{\partial x} + \frac{\partial u}{\partial z}\right)\right] + \frac{\partial}{\partial y}\left[\mu\left(\frac{\partial w}{\partial y} + \frac{\partial v}{\partial z}\right)\right] + \frac{\partial}{\partial z}\left(2\mu\frac{\partial w}{\partial z} + \kappa\nabla\cdot\boldsymbol{V}\right) + \rho g \tag{4.9}$$

where μ is the laminar viscosity and κ is the kinematic viscosity. Equations 4.7 – 4.9 are known as the Navier-Stokes equations for a three-dimensional flow field.

4.1.1.8 Conservation of Energy

The conservation of energy states that the amount of energy remains constant within a domain, though it can be converted from one form to another. Conservation of energy equations must be solved to account for temperature changes, species mixture and buoyancy within the gravity field. The equations are derived from the consideration of the *first law of thermodynamics* (Tu et al., 2008) that indicates the change of energy (E) is equal to the sum of the heat added to the system (Q) and the work done by the system (W).

$$\frac{d}{dt}(\rho E) = \frac{dQ}{dt} + \frac{dW}{dt} \tag{4.10}$$

The expansion of the conservation of energy equation for fluid flow used by ANSYS Fluent® is reflected in Equation 4.11 (Worrall, 2012; ANSYS, 2013):

$$\frac{\partial}{\partial z}(\rho E) + \nabla \cdot \big(V(\rho E + p)\big) = \nabla \cdot \big(k_{eff,c}\nabla T - \sum_{i=1}^{n} h_i J_i + (T \cdot V)\big) + S_h \qquad (4.11)$$

where the term $k_{eff,c}\nabla T$ corresponds to conduction in the fluid, $\sum_{i=1}^{n} h_i J_i$ corresponds to diffusion enthalpy transfer, $(T \cdot V)$ corresponds to viscous dissipation, and S_h is the volumetric heat source.

4.2 CFD Environment Settings

4.2.1 General Settings

The ANSYS Fluent® program provides a number of options for simulating fluid flow, under two main solvers: pressure-based and density-based. The pressure-based solver was initially developed for low-speed incompressible flows, and density-based for high-speed compressible flows. In later versions of Fluent, the pressure-based solver is available for compressible flow and yields superior performance (ANSYS, 2013). The pressure-based solver was selected for use in this study due to its flexibility in priority setting for solving equations and that it requires less computational memory than the density-based solver. The selected solver takes momentum and pressure sequentially before solving energy and species (ANSYS, 2013). The complete settings for the selected solvers and model parameters are shown in Table 4.1.

Table 4.1: Selected solver and model settings in Fluent

ANSYS Fluent® Setup	**General Settings**
Solver Type	Pressure-based
Velocity Formulation	Absolute
Time	Steady and Transient
Turbulence Model	Realizable *k-ε,* Standard wall, viscous heating
Species transport	Methane-air mixture
Gravity	On
Energy	On

Both steady and transient cases are used in this study. The steady-state scenario sets the base case, or initial condition of the mine, before any changes in barometric pressure. All other simulation scenarios with time-dependent barometric pressure changes are completed using the transient approach.

4.2.2 Turbulence Model

In fluid mechanics, fluid flow regimes can be categorized as laminar, intermediate, and turbulent. As opposed to a laminar flow, turbulent flow produces random, chaotic and swirled flow with formation of eddies. The Reynolds Number, N_{RE}, is a dimensionless criterion used to establish the regime of a fluid flow. It is given by Equation 4.12:

$$N_{RE} = \frac{\rho DV}{\mu} \tag{4.12}$$

where ρ is fluid density, μ is dynamic viscosity, D is conduit diameter, and V is the fluid flow velocity. Laminar flow exists for $N_{RE} \leq 2{,}000$ while turbulent flow $N_{RE} > 4{,}000$ (Hartman et al., 1997).

ANSYS Fluent® offers several model options for turbulent flow since there is no single universally accepted turbulence model that is superior for all problems (ANSYS, 2013). The selection of turbulence mode depends on the physics of flow, the complexity of interaction between fluid species, the accuracy, available computing resources and expected simulation time. Detailed information about all the models can be found in the Fluent Theory Guide (ANSYS, 2013). While previous researchers (Worrall, 2012; Gilmore, 2015) recommended that the RNG k-epsilon (k-ε) model be used in longwall gob simulations, the realizable k-ε model has been demonstrated to be superior for similar longwall gob problems in this study. The realizable k-ε model produces solution convergence and stability with the gravity function being activated.

ANSYS reported that this model provides the best performance of all the *k*-*ε* models for flows with complex features (ANSYS, 2013).

4.2.3 Material Settings

In the initial modeling of EGZ formation, the mixture species consist of methane ($CH_{4(g)}$), oxygen ($O_{2(g)}$), nitrogen ($N_{2(g)}$), carbon dioxide ($CO_{2(g)}$) and water vapor ($H_2O_{(g)}$). Carbon dioxide and water vapors could exist in the gob as a result of the spontaneous combustion of coal. Since coal combustion will not be modeled in this study, the mixture species will exclude both carbon dioxide and water vapor. To simplify the species for the bleeder-ventilated gob case, the oxygen and nitrogen components are replaced by air species ($H_2O_{(g)}$) in Fluent. Table 4.2 shows the properties for material properties and mixture species.

Table 4.2: Fluent material settings

Parameter	**Material Settings**
Species	Methane and Air
Density	Compressible (Ideal-gas)
Specific Heat	Mixing-law
Mixture Thermal Conductivity	Constant: 0.0454 W/m-K
Viscosity	Ideal-gas-mixing-law
Mass Diffusivity	Kinetic-theory

The appropriate ideal-gas density formulation is selected for compressible flow. Fluent uses the formula shown in Equation 4.13 in calculating density changes.

$$\rho = \frac{p_{op}+p}{RT/M_w} \tag{4.13}$$

where p is the gauge pressure predicted by Fluent, p_{op} is the operating pressure, R is the universal gas constant (8.314 J/K-mol), T is the operating temperature and M_w is the molecular weight. It is noted that Fluent recommends a positive non-zero pressure be used at the model's boundary conditions if the ideal-gas density is used; therefore, all simulations, regardless whether it is an

exhaust or blower system, are modeled in the positive pressure system. Operating pressure is also adjusted to 90,500 Pa based on elevation of the cooperating mine, which is approximately 1,000 m (3,300 ft) above the sea level.

4.2.4 Solution Method Settings

The Fluent solution method settings are given in Table 4.3. Four algorithms for pressure-velocity coupling are available in Fluent. The default Semi-Implicit Method for Pressure-Linked Equations (SIMPLE) is selected from all available algorithms due to its robust capability for getting converged and stable solutions (ANSYS, 2013). From a series of exercises, the researcher found that SIMPLE works best with the buoyancy-affected flows. The SIMPLE algorithm applies a relationship between pressure corrections and velocity to derive a pressure field while maintaining mass conservation.

Table 4.3: Fluent solution settings

Parameter	**Solution Settings**
Pressure-Velocity Coupling	SIMPLE
Gradient	Least Square Cell-Based
Pressure	PRESTO!
Momentum	2nd Order Upwind
Turbulent Kinetic Energy (k)	2nd Order Upwind
Turbulent Dissipation Rate (ε)	2nd Order Upwind
Species	2nd Order Upwind
Energy	2nd Order Upwind
Under-Relaxation Factors	Default

The least square gradient scheme is used to interpolate spatial discretization. The discretization is mainly needed for constructing values of a scalar at the cell faces and for computing diffusion terms and velocity derivatives. Using this scheme, the solution is assumed to vary linearly by interpolating the value at the cell center to the cell faces. The accuracy of the least square cell-based scheme is superior to that of other gradient methods and is less expensive than

other methods available in Fluent (ANSYS, 2013). The interpolation scheme used for calculating cell-face pressure is PRESTO! (PREssure STaggering Option). The scheme is recommended by ANSYS for flows involving steep pressure gradients caused by a porous medium or porous jump and for highly swirling flows occurring along the longwall face.

The remaining transport equations including momentum, turbulent kinetic energy, dissipation rate, species and energy are second-order upwind discretization, the minimum recommendation by ANSYS for final results. A higher order scheme will result in better accuracy. The first-order discretization assigns the face value equal to the value of the upwind cell centroid. From the simulation results, a noticeable difference can be observed between the first-order and second-order methane contour plots. Stability and convergence difficulties are encountered when using a third order discretization scheme.

4.2.5 Gravity

The gravity function is turned on in the current models with a value of 9.8 m/s^2 in -*z* direction. Positive *z* direction is upward in the model. For realizable *k*-ε turbulent scheme, the effects of buoyancy on *k* are always included when inputting a nonzero gravity. The generation of turbulence due to buoyancy for an ideal gas is given by:

$$G_b = -g_i \frac{0.09\rho k^2}{\rho \varepsilon Pr_t} \frac{\partial \rho}{\partial x_i} \tag{4.14}$$

where Pr_t is the turbulent Prandtl number for energy (default value is 0.85), g_i is the component of the gravitational vector in the i^{th} direction, k is the turbulent kinetic energy, and ε is the rate of dissipation.

The degree of buoyancy effect on ε is determined by the constant $C_{3\varepsilon}$, which is calculated in Fluent according to the following equation:

$$C_{3\varepsilon} = tanh \left|\frac{v}{u}\right| \quad (4.15)$$

where v is the velocity component parallel to the gravitational vector, and u is the component perpendicular to the gravitational vector. The value of $C_{3\varepsilon}$ is 1.0 if the main flow direction of buoyant gas aligned with the direction of gravity and 0 if it is perpendicular to the gravitational vector.

4.2.6 Solution Convergence Approach

The steady-state and transient simulations reach convergence if the solution no longer changes with subsequent iterations. The minimum convergence criteria as recommended by ANSYS are as follows:

- Overall mass, momentum, energy and scalar balances are achieved
- Discrete conservation equations (momentum, energy, etc.) are fulfilled in the entire model
- Iteration residuals must decrease to a specific tolerance:
    - Energy residual decreases to 10^{-6}
    - Species residual decreases to 10^{-5}
    - All other residuals decrease to 10^{-3}

A converged solution is not necessarily a correct solution. Therefore, further iterations and evaluations of the solution are performed to ensure a true convergence. In addition to monitoring the residuals and variables of interest, overall heat and mass conservation are also checked. ANSYS suggests that the net imbalance should be less than 1% of the smallest flux through the domain boundaries. Table 4.4 the mass flow rate through all inlet and outlet boundaries in the

current models as reported by the ANYS Fluent®. The net mass imbalance in the entire model is -5.8 x 10^{-4} kg/s, which is three orders of magnitude less than the smallest influx at methane inlets.

Table 4.4: Overall mass balance of the current base case model

Parameters	Mass Flow Rate (kg/s)
Total Headgate Inflow	50.312366
Total Tailgate Inflow	5.3495626
Total Bleeder Outflow	-53.869978
Headgate Outflow	-2.4980629
Methane Inflow	0.70552737
Net Imbalance	-5.8 x 10^{-4}

A steady-state case is run to provide solutions for an initial base condition. This solution will subsequently be used for the simulations of barometric pressure changes which involve time-dependent iterations. The transport equations of species and energy, and then gravity options are turned on one after another during the iterations until the convergence criteria are achieved. Figure 4.1 shows the residual profile of the steady-state iteration for the bleeder model. The iterations begin by solving flow and turbulence equations, then the transport equation for methane species, followed by energy and gravity options at 75, 100, and 225 iterations, respectively. The profile jumps in the residuals correspond to changes made during the iteration process. Pressure adjustments are necessary to achieve certain flow rates that match ventilation data. Further iterations are needed for a true convergence by monitoring pressures at certain locations (*i.e*. all boundaries and six monitoring points in the gob) and percent change in methane gas volume. An evaluation of the solutions suggests that convergence can be reached with 10,000 iterations with convergence limits 1 x 10^{-5} for continuity, 1 x 10^{-6} for velocities, 1 x 10^{-10} for energy, 1 x 10^{-5} for species, and 1 x 10^{-4} for turbulence and epsilon. The methane concentration at the bleeder outlet during the iterations is shown in Figure 4.2. The flat portion of the graph starts at 1,500 iterations and beyond.

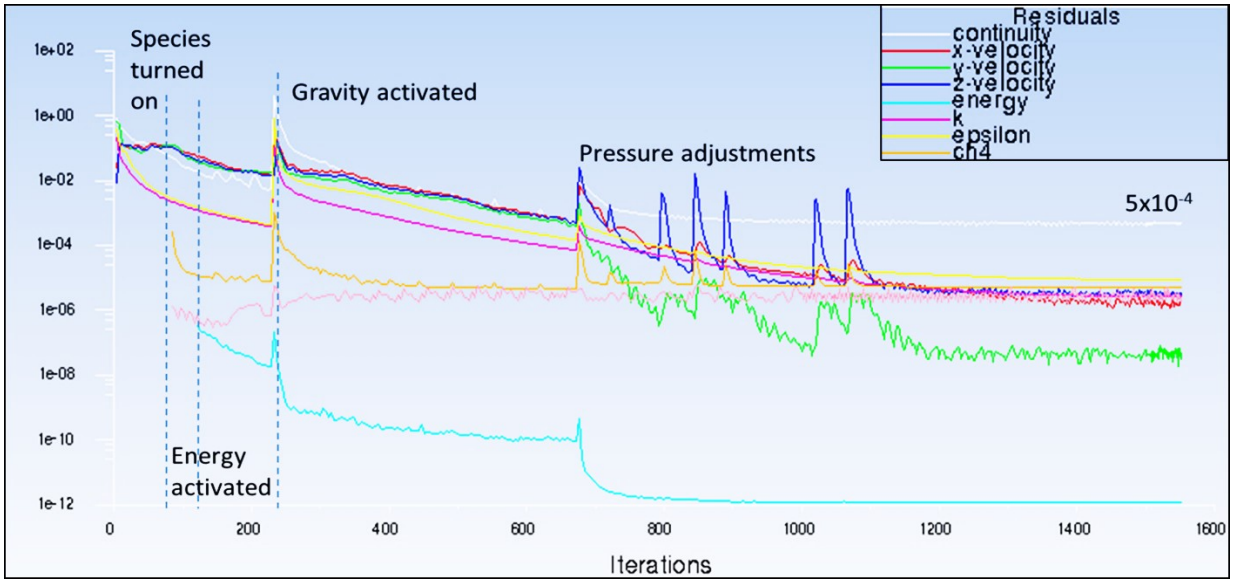

Figure 4.1: Residual history of the steady-state bleeder model

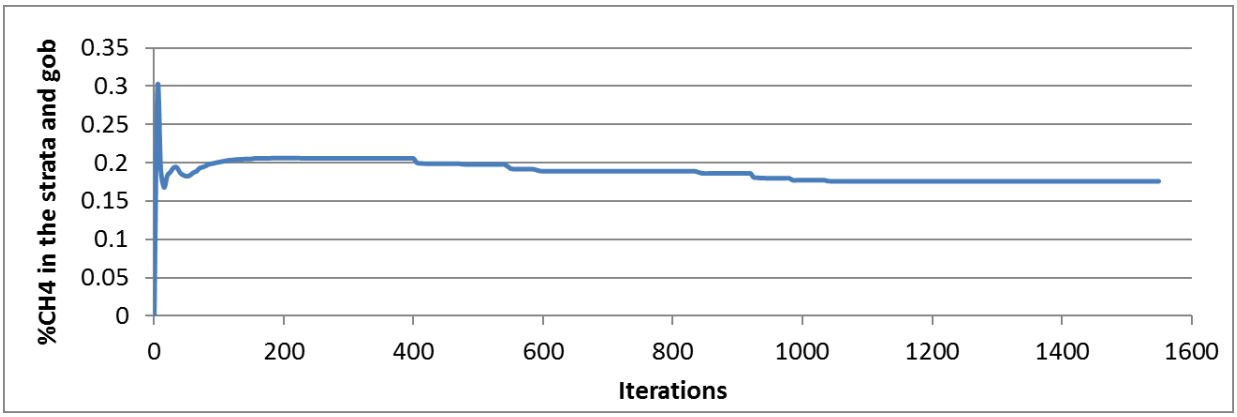

Figure 4.2: Monitored methane concentration in the iteration process

4.3 Geometry and Ventilation Setup

The CFD model is developed based on data available from cooperating mines in the Western U.S. including Mine C (Grubb, 2008; Worrall, 2012) and Mine E (Gilmore, 2015). The collected data consist of mine layouts, ventilation requirement, and gob caving characteristics.

4.3.1 Ventilation Layout

The ventilation condition of the mine for the base scenario is depicted in Figure 4.3. The simulated mine uses a three-entry bleeder ventilation system with both headgate and tailgate sides

serving as air intakes. The outermost tailgate entry is not modeled as it is assumed to cave along with the previous gob and thus be sealed, leaving only two entries on the tailgate of which one is modeled as the gob void.

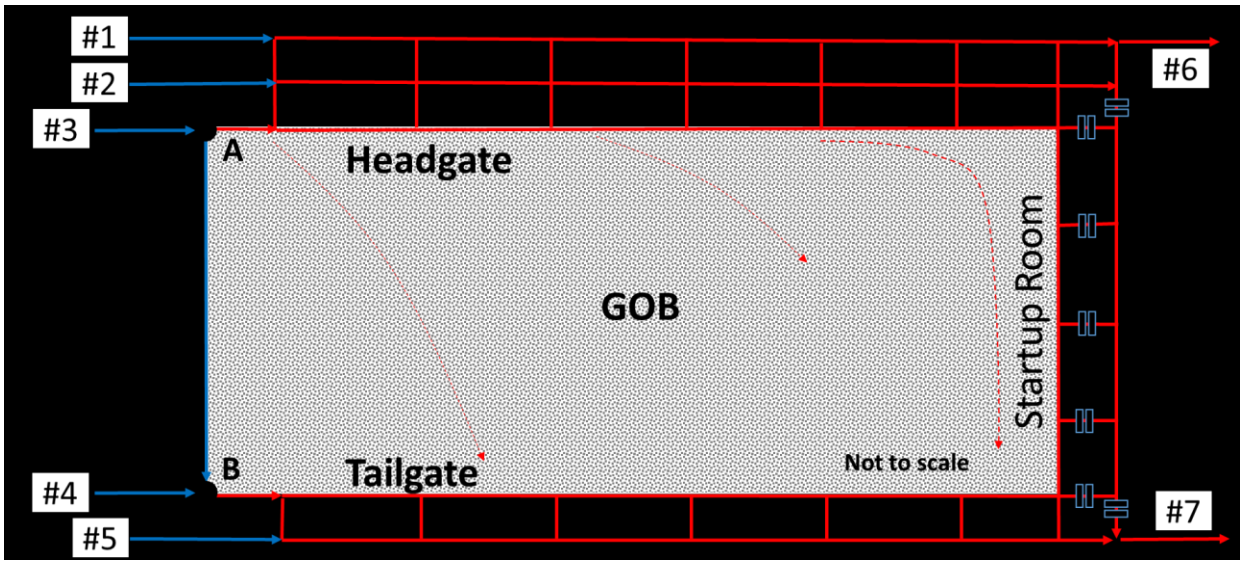

Figure 4.3: Simulated bleeder ventilation system

Entries 1 through 5 supply fresh air, which is then exhausted through entries 6 and 7. The longwall face progresses from right to left, with headgate entries at the top and tailgate entries at the bottom. Entries 1 and 2 supply 4.7 m^3/s (10,000 cfm) each to the panel and entry 3 supplies 38 m^3/s (80,500 cfm), of which about 13% leaks into the gob at point A. The remaining 33 m^3/s (70,000 cfm) ventilates the longwall face. Both entries 4 and 5 add another 4.7 m^3/s (10,000 cfm) of fresh air from the tailgate side to dilute the methane accumulation that may exist at the inby face at point B. Outlets 6 and 7 receive 4.7 m^3/s (10,000 cfm) and 47 m^3/s (100,000 cfm), respectively. A bleeder shaft is assumed to be located near outlet 7, where 90% of the total air in the model exits. Several regulators for ventilation control are set up in the bleeder entries near the start-up room to correspond to their locations in the cooperating mine. In practice, the condition of the inner bleeder entry next to the start-up room can be wholly or partially caved, limiting the passing air flow.

The methane inlet is placed at the top of the strata and assigned a constant pressure of 4,630 Pa pushing about 1.01 m^3/s (2,140 cfm) of methane down to the gob. The permeability of the strata is about six orders of magnitude smaller than the smallest gob permeability. As regulated by federal laws (30 CFR §75.323), the methane concentration should not exceed 1% in an active area or an intake air course and 2% in bleeder or other return air courses, otherwise the operation will be disrupted by ventilation adjustments to lower the methane. In this modeling, the methane concentration at outlets is set to 1.9% limit.

4.3.2 Model Geometry and Dimension

In ANSYS Fluent®, the solution to a problem is found by solving the governing equations iteratively in a volume domain of pre-determined geometry and boundary conditions. The ANSYS Design Modeler® (DM) is used to create the model parts independently. These parts are then meshed in ANSYS Meshing® using a modular mesh approach developed by Gilmore (2015). The next step is to import and assemble the meshed components together in Fluent using a user-defined function (see Appendix A) to create a single longwall panel model. In many cases, the geometry of the model parts is simplified by ignoring unnecessary details such as posts or cribs along the mine entry. If possible, such exclusions are then compensated by adjusting other tuning parameters, such as wall roughness.

The longwall model shown in Figure 4.4(a) consists of a supercritical panel with a gob surrounded by mine entries. In Appalachian coal seams, a supercritical panel is characterized by a panel width exceeding 1.2 times the mine depth, which will cause the full overburden weight to rest fully on the gob (Peng et al., 1992). The model is a simplification of the actual mine panel, as shown in Figure 4.4(b). The panel is 6,800 m (22,400 ft) long and 366 m (1,200 ft) wide, consisting of mine entries and longwall face, the gob and a fractured zone above the gob. In ANSYS DM®,

the origin coordinates of (0,0,0) for geometry construction are located at the mine floor, at the halfway point of the longwall face. The +x direction is set towards the headgate side, the +y direction towards the unmined coal, and the +z direction towards the mine roof.

4.3.2.1 Headgate, Tailgate, and Bleeder Entries

The mine entries for the headgate, tailgate and bleeder sections have identical rectangular shapes and dimensions. The height of the coal seam determines the entry height. In this model, the coal seam is 3.4 m (11 ft) high. Figure 4.5(a) shows the details of entries 1 and 2 on the headgate side. The entry width is 6.1 m (20 ft). A crosscut connects the two separated entries every 61 m (200 ft). The cross-section of the crosscut is similar to that of the mine entries; its length from one entry to another is approximately 15.2 m (50 ft). For the simulated model, there is a total of 104 crosscuts between entry 1 and entry 2.

Figure 4.5(b) shows the bleeder entries near the start-up room; these entries connect headgate to tailgate access. The first entry next to the gob is practically caved and inaccessible. Seals are constructed to limit access to this area, not necessarily serve as a ventilation control. The outer entry is considered fully open for air flow and walkable for mine personnel. Entry 5 extends from the longwall face on the tailgate side to the bleeder outlet.

4.3.2.2 Longwall Face

The model incorporates shields and a shearer to obtain a realistic pressure drop across the face. An individual shield and shearer model is provided by and used with the permission of Caterpillar, Inc., one of the largest longwall equipment manufacturers. The design sketch, as shown in Figure 4.6(a), has been positioned for a seam height of 3.4 m (11 ft). Overall size from end to end, including the top canopy of a single shield, is 8 m (26.2 ft) long and 2 m (6.5 ft) wide. There are 175 shields from headgate to tailgate in this model.

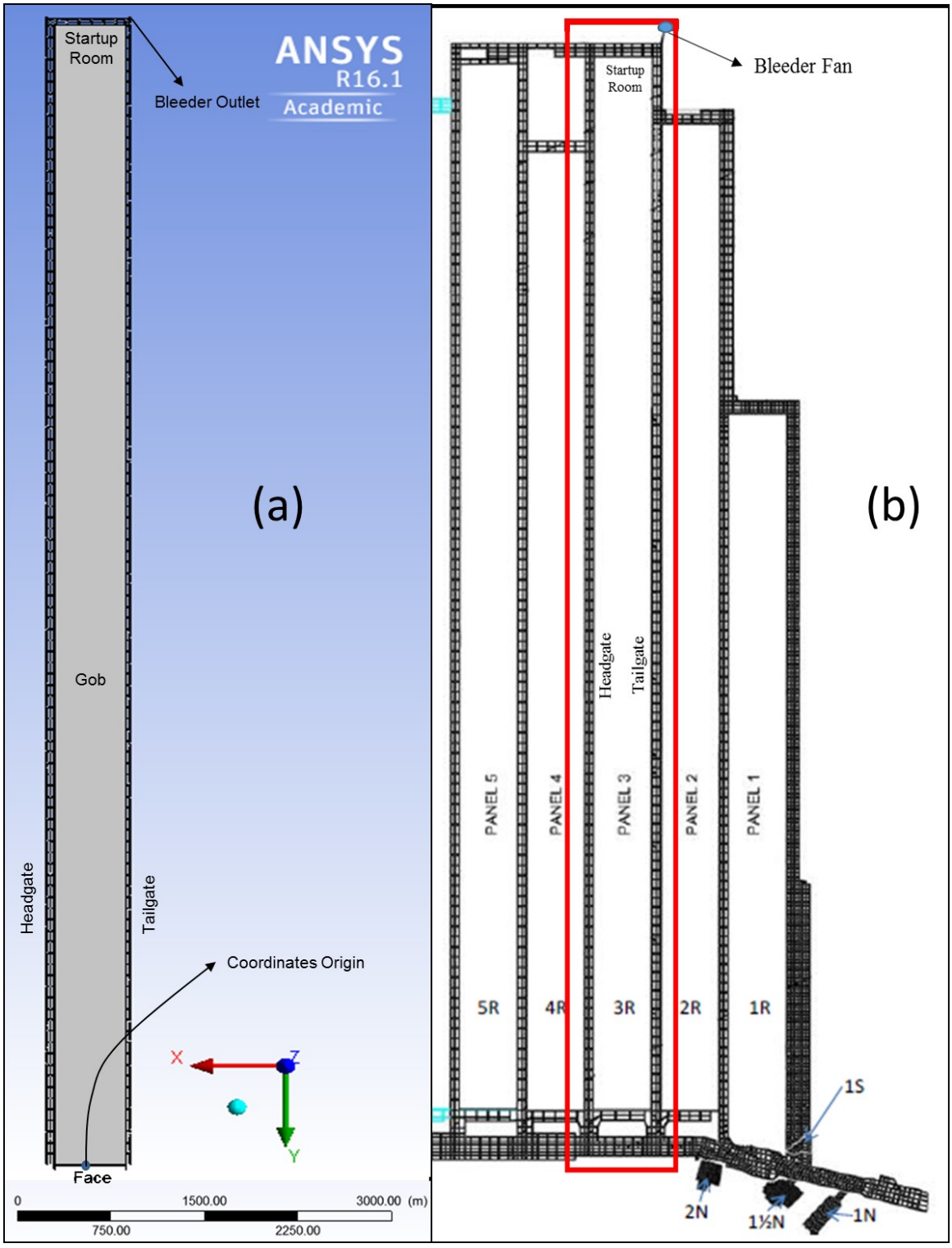

Figure 4.4: The mine layout used in this study: (a) CFD model and (b) cooperating mine

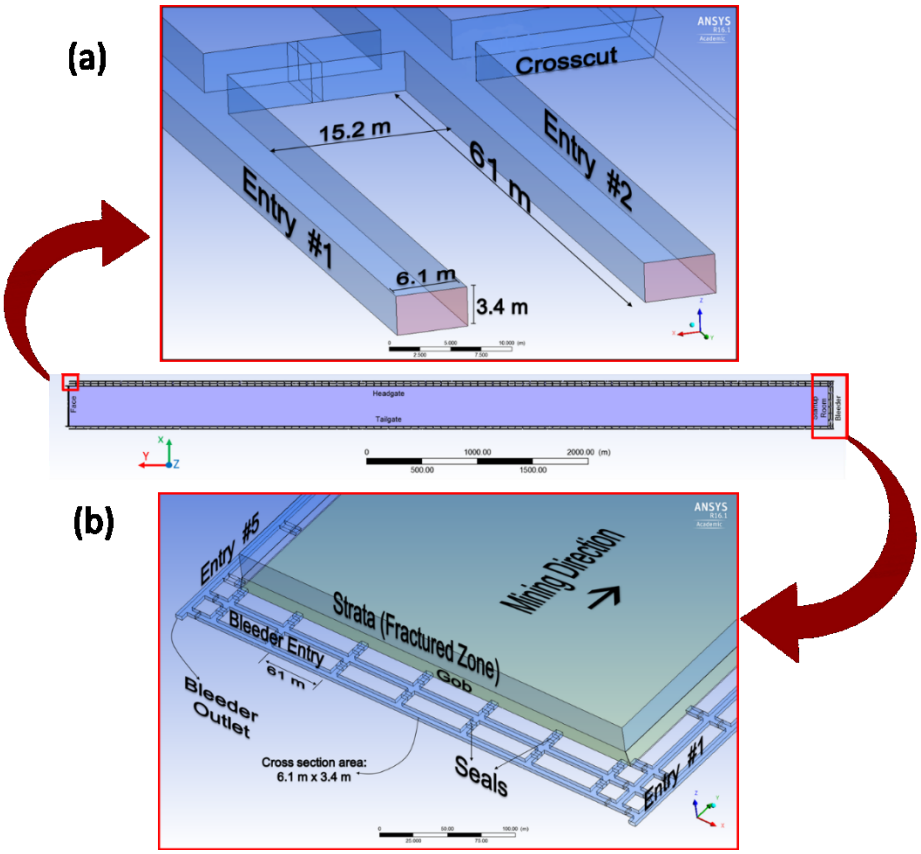

Figure 4.5: Geometry and dimension of (a) entries 1 and 2 and (b) bleeder entries

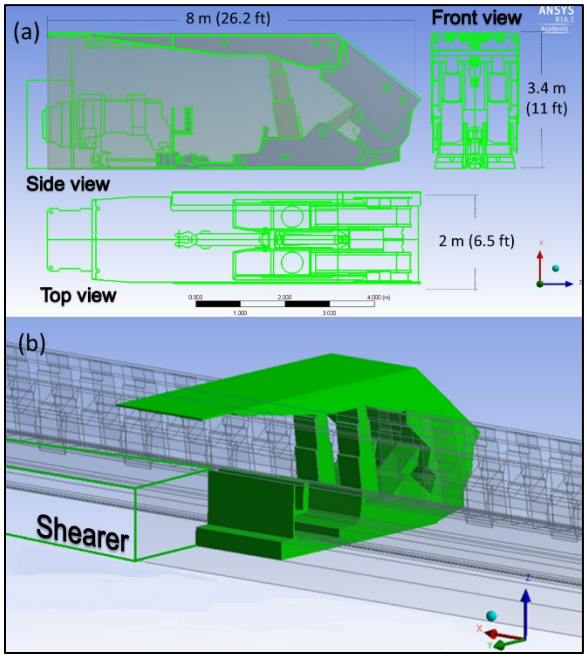

Figure 4.6: Shearer and shield model: (a) manufacturer's design and (b) ANSYS DM® output

The back end of each shield is not completely closed, leaving a square gap of 0.6 m (1.95 ft) x 0.6 m (1.95 ft) between two rear legs. This dimension is determined after converting the sketches shown in Figure 4.6(a) into a 3D model and then intersecting the tail of shield with the gob. This gap of 0.36 m^2 (3.8 ft^2) exists in every shield along the face, as shown in Figure 4.7, and becomes the open connection for fluid flow from the face to the gob. The area is significantly larger than the estimation made in previous studies (Worrall, 2012; Gilmore, 2015). The thin gap between shields is not modeled, since it is considered insignificant for leakage compared to that of the shield gaps. In addition, the construction of this thin gap can result in poor quality meshes due to high aspect ratio.

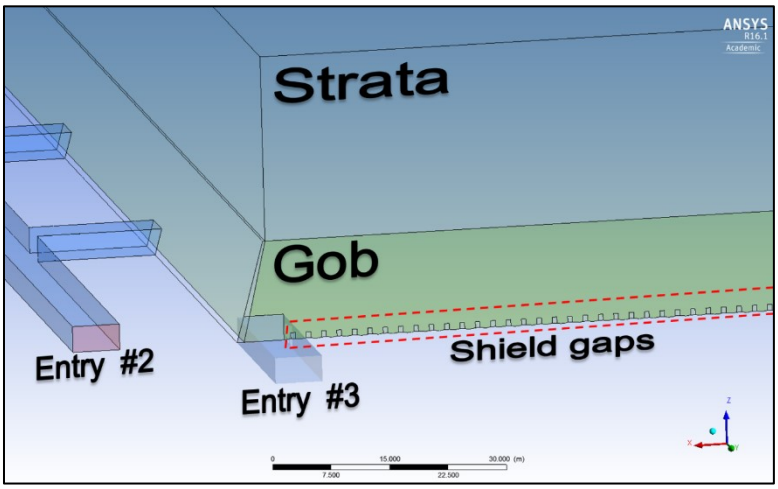

Figure 4.7: Location of shield gaps along the face

For the purpose of obtaining a realistic pressure drop across the face, the shearer model is included in the longwall face and is simplified to a rectangular box of 17 m (55.8 ft) long, 1.8 m (6 ft) wide and 1.4 m (4.5 ft) high. This model has taken into account the armored-face conveyor at the base. Other details of the shearer are ignored as they can require an extensive number of cells to capture the flow physics. The shearer is located in the middle of the longwall face length.

The base case simulation gives a pressure drop of 132 Pa (0.53-inch water gate) across the face, which falls within the range reported by several cooperating mines.

4.3.2.3 Longwall Gob

The longwall gob covers an area from the headgate to tailgate, and from the bleeder to the longwall face, which is approximately 2.4 million m^2 (26.5 million ft^2). The gob zone is created separately from the strata, as this zone represents a more porous medium with rubble and broken rocks as opposed to an intact but fractured rock strata. The porous model fit developed by Marts (2015) and Gilmore (2015), as described in Section 3.5, is applied to the gob zone. Figure 4.8 shows the geometry of the gob, a trapezoidal prism shape. The top side width is 360 m (1,180 ft) while the base is 366 m (1,200 ft). The total length of the gob is 6,840 m (22,400 ft) extending from the origin point to -y direction.

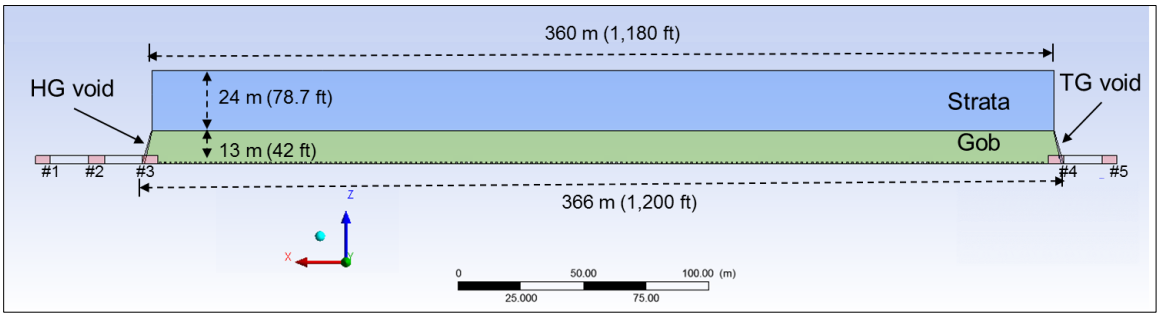

Figure 4.8: Cross-section view of gob and strata (looking into -y direction)

4.3.2.4 Gob Voids at the Headgate and Tailgate

It is understood that the equilibrium stress condition above the longwall panel will be disturbed during mining, which will be re-distributed to the gob and surrounding pillars. This new stress condition, known as side abutment stress, is greatest at the outside pillars around the gob due to bearing the redistributed stress of the gob perimeter. Reduced stress around the gob causes the gob material to be much more compacted toward the center, and voids are expected to occur along the perimeter due to uncaved roof rocks. This condition was observed during visits to three

longwall mines in the western U.S. region by Grubb and his project team (Grubb, 2008; Worrall, 2012). Figure 4.9 is a photograph taken along the gob void in one of the visited mines, juxtaposed with the team's rendering of the theoretical shape of the void.

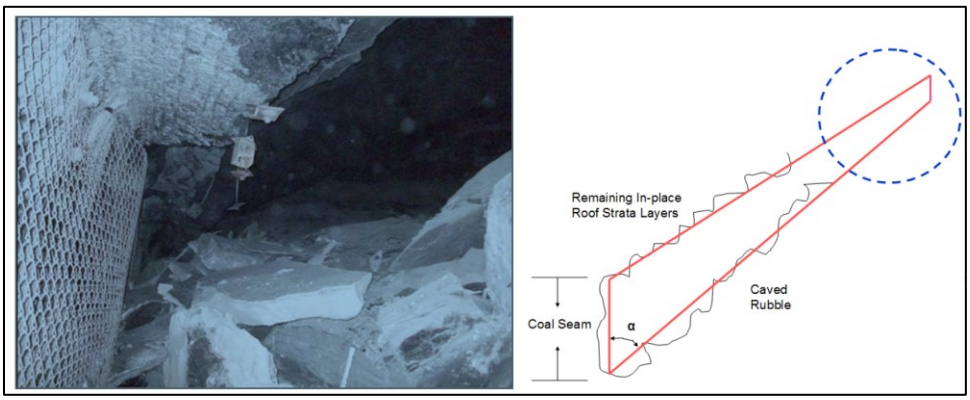

Figure 4.9: The actual gob void and its conceptual model (Worrall, 2012)

Worrall (2012) initially developed the conceptual model of the gob void, which is attached continuously around the gob in his longwall model. The void used in this study replicates the Worrall's initial concept of the gob void. The height of the void is the same as the gob height, while its width is 0.9 m (3 ft) at the base and 0.3 m (1 ft) at the top. The side facing the gob is angled from the horizontal plane at 52°. Overall, the voids are modeled as a continuously open trapezoidal prism along the headgate and tailgate sides of the gob, as shown in Figure 4.10.

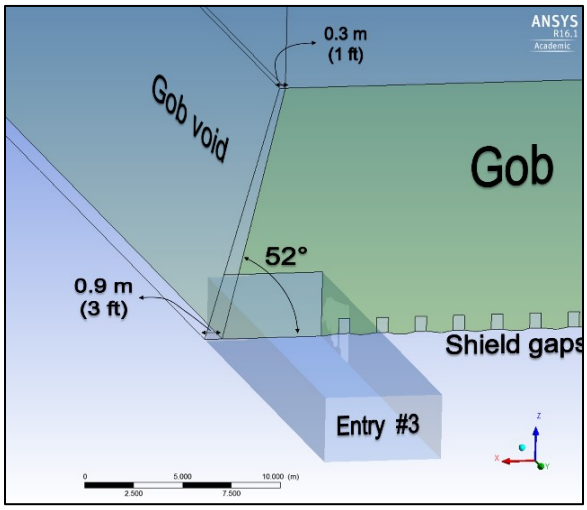

Figure 4.10: Details of the gob void on the headgate side

4.3.2.5 Overlying Strata or Fractured Zone

As shown in Figure 3.14, the strata zones above the gob will not collapse, but they are characterized by fractures and cracks. At Mine C, a rider coal seam above this zone is identified as the source of methane seepage into the gob (Worrall, 2012). Therefore, the permeability of this strata zone will determine the pressure of the methane source and the amount of methane coming into the model. To obtain a realistic methane pressure condition, the overlying strata zone is included in the model immediately above the gob, as shown in Figure 4.8. The strata's total length and width are identical to those of the gob, with a height of 24 m (78.7 ft), based on data provided by Mine C (Worrall, 2012). In the modeling, a constant pressure is simulated at the top of the fractured zone, representing the methane inlet pressure from the rider seam. Sections 4.3.4 and 4.3.5 discuss methane pressure and strata permeability.

4.3.3 Model Meshes

In general, CFD uses a finite volume method to discretize the spatial domain into small cells or grids and then solves the governing equations in each of the cells. Having a good quality mesh is extremely important, as it impacts solution accuracy and computational stability. Meshing is the most challenging stage in model preparation, particularly prior to the development of the modular meshing approach by Gilmore (2015). The modular approach involves meshing each part independently, rather than meshing the entire model at once. Each meshed portion is then imported and assembled in ANSYS Fluent® to create a full model. This modular meshing, compared to the other approach, allows better control over mesh type, size and inflation method.

The mesh must meet minimum requirements of several quality parameters to ensure high quality before proceeding further with the simulation. The higher the mesh quality, the better the accuracy and the more stable the numerical solution will be. By default, the quality parameters

include skewness, aspect ratio, element quality, orthogonal quality and smoothness. The first three parameters are the most common to check. Cell skewness is defined as the difference between the cell shape and an equilateral cell, of which ANSYS recommends a maximum of below 0.95. Depending on the cells' location, a skewness higher than 0.95 may lead to convergence issues and requires adjustment with mesh or solver controls such as the under-relaxation factor. The aspect ratio is a measure of cell stretching. Sometimes stretched cells cannot be avoided in a complicated shape, but it is best to avoid highly skewed cells in areas where the flow field exhibits large gradients. A stretched cell could be less problematic if located near the wall boundaries or in a region with low velocity flow. In general, an acceptable mesh should have an aspect ratio between 0.2 and 5.0; however, a good convergence may still be achievable with higher aspect ratio cells present in the model, depending on the mesh type, locations and the amount of the cells. The element quality provides a quality metric ranging from 0 for a poorly constructed cell to 1 for a perfect cube or square cell. ANSYS recommends that minimum cell quality be greater than 0.01 for any individual cell.

The summary of mesh type and quality for each part of the model in this study is given in Table 4.5. The full longwall model is comprised of seven parts meshed independently and imported into ANSYS Fluent® for assembly. The assembly process in ANSYS Fluent® is generated using a user-defined function given in Appendix C. The meshing parts are as follows:

1. *entry12.msh* – a meshed model of entries 1 and 2
2. *entry34.msh* – entries 3 and 4 parts, but not including the longwall face part
3. *entry5.msh* – tailgate entry from entry 5 to bleeder outlet
4. *bleeder.msh* – contains two entries in the back of the panel (bleeder area)
5. *shield.msh* – the shield and shearer model

6. *gob-full.msh* – contains meshed gob
7. *gobvoid.msh* – the headgate and tailgate gob voids
8. *strata.msh* – meshed model of overlying strata above the gob

Table 4.5: Mesh quality of the longwall model parts

Model Parts	Dominant Mesh Type	Max. cell size (ft)	Number of Cells (in 1000s)	Mesh Quality		
				Maximum Skewness < 0.95	Aspect Ratio Range 0.2 – 5.0	Minimum Cell Quality > 0.01
Headgate Entry	Hex 	2.0	1,057	0.68	1.0 – 4.7	0.34
Face	Tet 	1.0	7,483	0.84	1.1 – 10.5	0.21
Tailgate Entry	Hex 	1.0	2,883	0.32	1.0 – 4.6	0.65
Bleeder	Hex 	2.0	17	0.74	1.0 – 4.0	0.67
Gob	Hex 	4.0	6,442	0.78	1.0 – 7.72	0.32
Gob Voids	Hex 	1.0	123	0.32	1.4 – 4.0	0.45
Upper Strata	Hex 	8.0	519	1.4E-10	1.0 – 1.0	0.99

The entire model has nearly 18.6 million cells, so it is categorized as a large model by ANSYS Fluent®. Almost all meshes are dominantly constructed by hexahedron-type cells resulted from the meshing's cut-cell method. The exception of this type is the longwall face portion, which

is of the tetrahedron type. After assembly, the connections between model pieces are defined using interfaces. There are about 16 interfaces specified for the full model. Figure 4.11 shows the complete mesh of the bleeder model used in this study. The pressure inlets are shown in blue, outlets in red and wall boundaries in white.

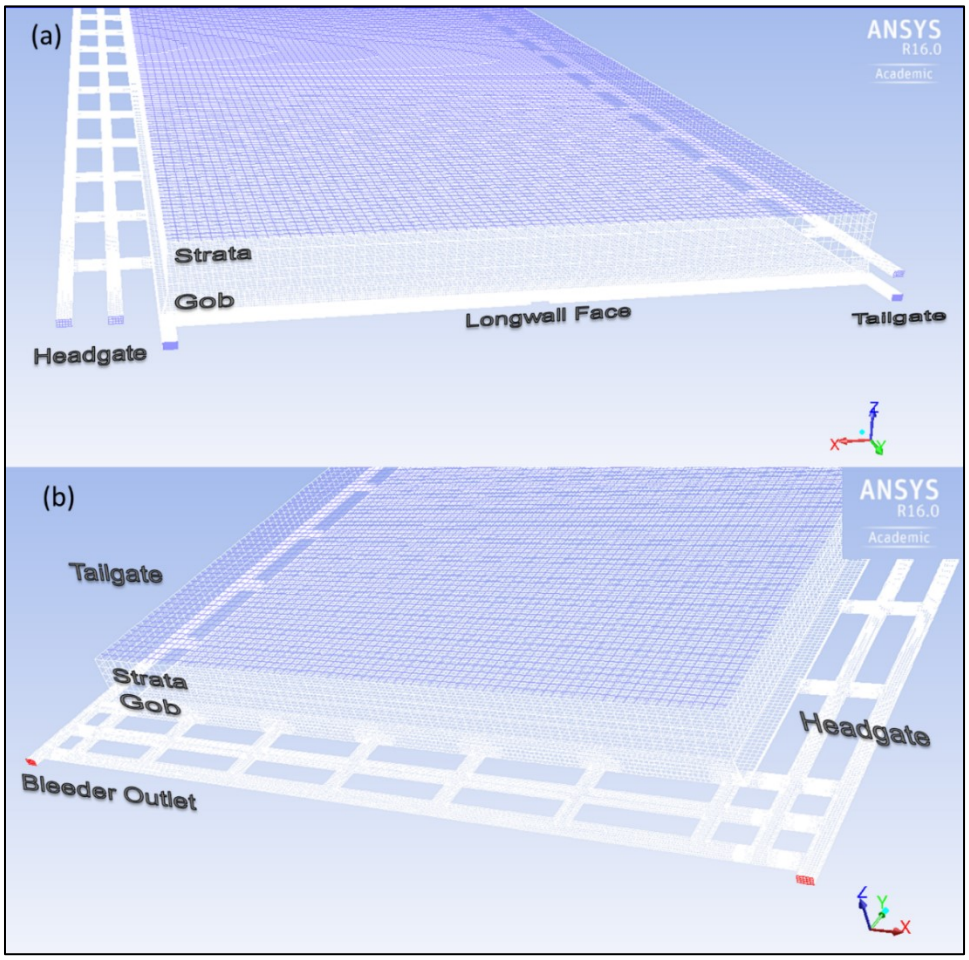

Figure 4.11: The complete meshed model (a) front view and (b) rear view

4.3.4 Boundary Conditions

There are six inlets and two outlets simulated in the model. As shown in Figure 4.3, entries 1 through 5 and the methane source are assigned as inlets, while entries 6 and 7 are the outlets. In ANSYS Fluent®, these are defined as either a Pressure-Inlet or Pressure-Outlet boundary condition. The air is supplied into the model from entries 1 through 5. Entry 3 is dedicated to

supplying air to the face, while other inlets push air around and into the gob. As the air enters the model, it mixes with methane that enters from the inlet above the fractured zone, and then exits the model through outlets 6 and 7. The pressure values for all inlets and outlets are given in Table 4.6. The hydraulic diameter of 4.3 m (14.2 ft) and a turbulence intensity of 3% are used on all inlets and outlets except the methane inlet. These values are calculated from Equations 4.16 and 4.17. Turbulence intensity represents the turbulence level of the fluid flow scheme and is determined by the Reynolds Number (N_{RE}). A turbulence intensity of 1% or less is generally considered low, and turbulence intensities greater than 10% are considered high.

Table 4.6: Pressure boundary conditions of the base case model

Location	Boundary Condition Type	Pressure Values (Pa)	Flow Rate[1]	
			(m^3/s)	(cfm)
Entry 1	Pressure-Inlet	3,332	+4.91	+10,400
Entry 2	Pressure-Inlet	3,332	+4.89	+10,350
Entry 3	Pressure-Inlet	3,467	+38.00	+80,500
Entry 4	Pressure-Inlet	3,335	+1.48	+3,100
Entry 5	Pressure-Inlet	3,328	+3.64	+7,700
Methane Inlet	Pressure-Inlet	4,630	+1.01	+2,150
Outlet 6	Pressure-Outlet	2,331	-4.51	-9,550
Outlet 7	Pressure-Outlet	2,241	-49.63	-105,150

Note: [1] Positive and negative signs represent flow entering and exiting the model, respectively

$$D_H = \frac{2\,x\,Width\,x\,Height}{(Width+Height)} \tag{4.16}$$

$$I = 0.16\,(N_{RE}D_H)^{-1/8} \tag{4.17}$$

In reality, methane may come from various sources such as mine face, rider coal seams above or below the mining level, the ribs and coals on conveyor belt. In this modeling, it is assumed that, under normal conditions, the amount of air from the ventilation system is sufficient to dilute

the methane in active working areas, and there is no inundation of methane gas from the mine floor. Methane emission from the face during the extraction process is also ignored. Investigating the air-methane mixture in the gob supplied by a rider seam above the overlying strata is the main focus of this study, based on information provided by the cooperating mine. The methane source is assumed to be infinitely available as a large reservoir. This assumption has been discussed by previous researchers (Worrall, 2012; Marts, 2015; Gilmore, 2015).

The methane inlet pressure is adjusted to supply enough methane into the gob so that the methane concentration after mixing with air at outlets 6 and 7 reaches a concentration below the statutory threshold of 2% by volume. The simulation results in a methane pressure of 4,630 Pa. This pressure is within the same order of magnitude compared to the gob borehole shut-in pressures of 1,750-3,000 Pa range measured in the Pittsburgh coalbed as reported by Diamond et al. (1999), Karacan et al. (2006) and Schatzel et al. (2008). The turbulence intensity at the inlet surface is 1% while the length scale is set at 10 m. Gilmore (2015) indicates that the solution is insensitive to the value of these turbulent parameters.

Barometric pressure fluctuations are simulated by simultaneously changing all pressures at inlet and outlet boundaries, except the methane inlet. The pressure of the methane inlet remains constant, a surmise aligned with the assumption of methane as an infinite reservoir.

The model is initialized with air comprised of 20.95% O_2 and 79.05% N_2. Analysis of the initialization method shows that the simulation results are not sensitive to the initial composition of air existing in the model. This analysis is described in Section 5.3.

4.3.5 Selected Permeability of Gob and Fractured Zones

An in-depth discussion of gob permeability and porosity was previously given in Section 3.5. For this study, gob permeability and porosity are calculated using the approach developed by

Marts (2014a). Marts calculates the final porosity based on the volumetric strain increments (VSI) output from FLAC$^{3D®}$ program using Equation 4.18.

$$n = n_o - \epsilon_v \tag{4.18}$$

where n is the calculated porosity, n_o is the initial porosity, and ϵ_v is the VSI value. VSI indicates a change from initial porosity. The FLAC$^{3D®}$ code for the VSI calculation is presented in Marts' dissertation (2015). This VSI distribution is converted into a form readable in ANSYS Fluent®. Gilmore (2015) developed piece-wise equation fits in MATLAB, as shown in Figure 4.12. The VSI values are small around the perimeter of the gob, and gets larger in the gob center. Details of these equation fits are stored in a C source file named "*gilmore-marts.c,*" which can be found in Gilmore's dissertation (2015).

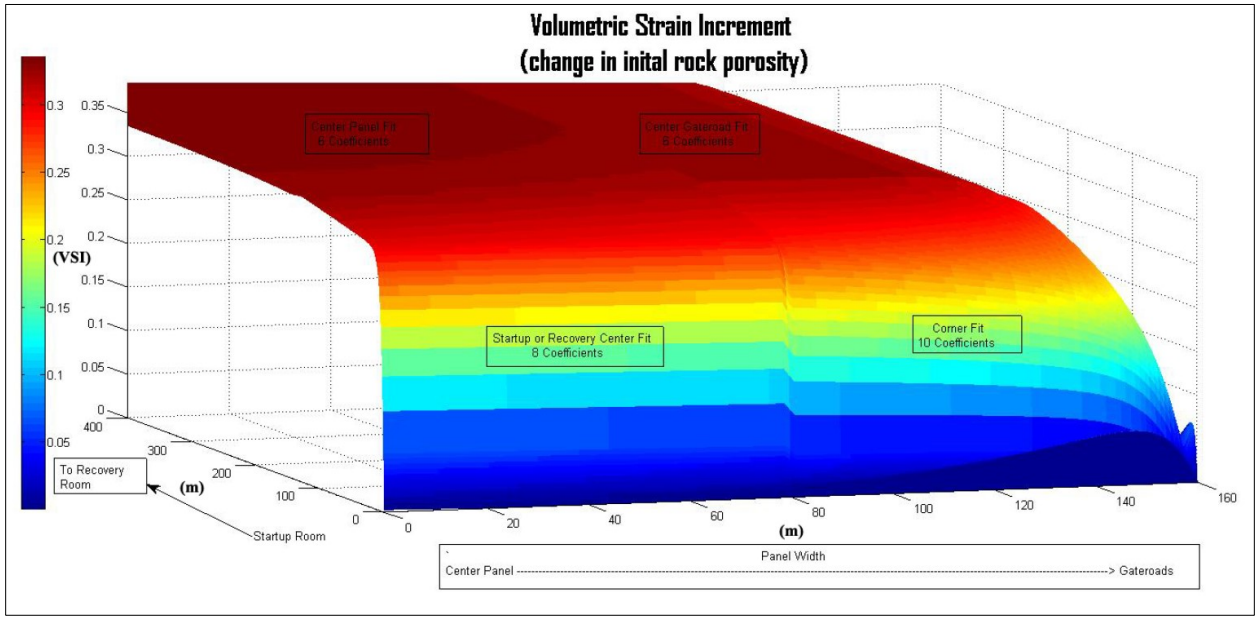

Figure 4.12: VSI curve fitting for gob (Gilmore, 2015)

The initial porosity in Equation 4.18 is assumed to be 40%. This value has been used as an initial estimation for gob porosity in Mine C by previous researchers (Gilmore, 2015; Marts, 2015). Pappas and Mark (1993b) also assumed an initial value of 40% - 50% in their gob study when

determining gob porosity. Initial porosity is derived from the void volume, which is estimated from the ratio of the extracted seam height over the caving height of the gob, and the in-situ porosity of the virgin rocks forming the gob (Pappas and Mark, 1993b).

Once the porosity value, n, is obtained from Equation 4.18, the base permeability is calculated by using the Carman-Kozeny relationship as shown in Equation 4.19:

$$K_o = \frac{n^3}{(180\ x\ (1-n)^2}\, d^2 \tag{4.19}$$

where K_o is the base permeability (m^2) of the rock, and d is the diameter of mean particles, which is assumed to be 0.2 m (Pappas and Mark, 1993a). The final permeability is calculated using Equation 3.7, which requires the value from Equation 4.19. Figure 3.21 shows the two porosity and permeability profiles used in this modeling.

ANSYS Fluent® requires a viscous resistance input to characterize a porous medium, instead of permeability. The viscous resistance is the inverse of the permeability (K) obtained from Equation 3.7. The porosity of Mine C ranges from 14% to 40%, therefore, the viscous resistance ranges from 1.45 x 10^5 m^{-2} and 5.0 x 10^6 m^{-2}.

In contrast to the gob, overlying strata are intact rock seams with cracks and fractures, but not yet collapsed. Therefore, a uniform permeability is considered sufficient for these strata. This permeability should be notably small compared to the gob permeability. Karacan (2009) reported a permeability of 9.87 x 10^{-14} m^2 based on drawdown well tests, or eight orders of magnitude smaller than the permeability of the gob; equivalent to a viscous resistance of 1.01 x 10^{13} m^{-2}.

4.3.6 Explosive Gas Zones (EGZ)

Worrall (2012) developed a color-coded diagram, as shown in Figure 3.5, to define the explosibility of the methane and air mixture in ANSYS Fluent®. In addition to identifying the

EGZ in the gob, this diagram provides convenient ways to visually investigate the effect of inertization, dilution or other ventilation adjustments to gob explosibility. The diagram is based on Coward's triangle and is visually represented with the colors: yellow, red, green and blue. Later, Gilmore (2015) modified the diagram to include the additional nitrogen included in the mixture as a result of the inertization application which is mainly implemented to replace the methane. The zone with added nitrogen is indicated by the colored-green zone below the explosive mixture in Figure 4.13. For this study, Gilmore's version of Coward's triangle is further modified by dividing the transition zones into three distinct colors to distinguish the near-explosive conditions of fuel-rich, fuel-lean, or both fuel- and oxygen-lean. The diagram shown in Figure 4.13 has incorporated this new modification. The color zone descriptions are as follows:

1. Green (GR) – a non-explosive mixture due to oxygen deficiency; can be produced by introducing more nitrogen to the mixture as in the case of nitrogen inertization.
2. Cyan (CY) – a fuel-lean, non-explosive mixture due to oxygen dominance.
3. Yellow (YE) – an inert non-explosive mixture due to excessive methane.
4. Dark Blue (DB) – a non-explosive mixture, but can become explosive with additional methane and oxygen.
5. Orange (OR) – a non-explosive mixture, but can become explosive with more methane.
6. Purple (PU) – a non-explosive mixture, but can become explosive with air dilution.
7. Red (RE) – an explosive mixture.
8. Black – a composition that is impossible to make up by methane and air.

The maximum oxygen concentration in the air is approximately 20.95%. Therefore, all possible mixture compositions with methane under normal atmospheric conditions only occur at

or less than 20.95% oxygen. Methane and air will never be found with composition in black-colored zone.

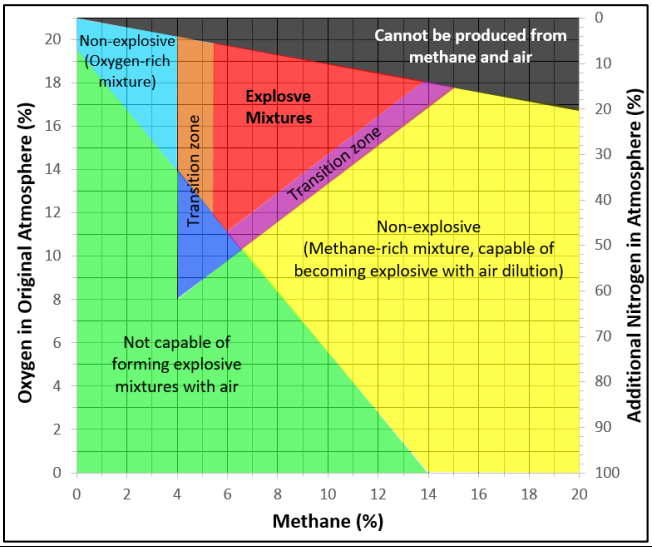

GR	CY	YE	DB	OR	PU	RE
Non-explosive			**Near-explosive**			
Methane- and oxygen-lean	Methane-lean, oxygen-rich	Methane-rich, oxygen-lean	Methane- and oxygen-lean	Methane-lean, oxygen-rich	Methane-rich, oxygen-lean	**Explosive**

Figure 4.13: Color-coded diagram used in this modeling (modified after Gilmore, 2015)

This mixture explosibility is calculated in Ansys Fluent® based on the user-defined functions (UDFs) shown in Appendix B. Each zone limit is defined by functions, as shown in Figure 4.4. These functions were originally developed by Worrall (2012) and Gilmore (2015). These UDFs are called at the end of every completed simulation run. The UDFs require Fluent® to first determine the mole fraction of methane and oxygen in a cell, then use this output to match with the appropriate zone in the explosibility diagram. The next command in the UDFs would assign a threshold value between 0 and 1 to determine which color to assign in Fluent®. The threshold value for each region are given in Appendix B. The colormap for this explosibility is pre-configured in Fluent® and consists of seven different colors.

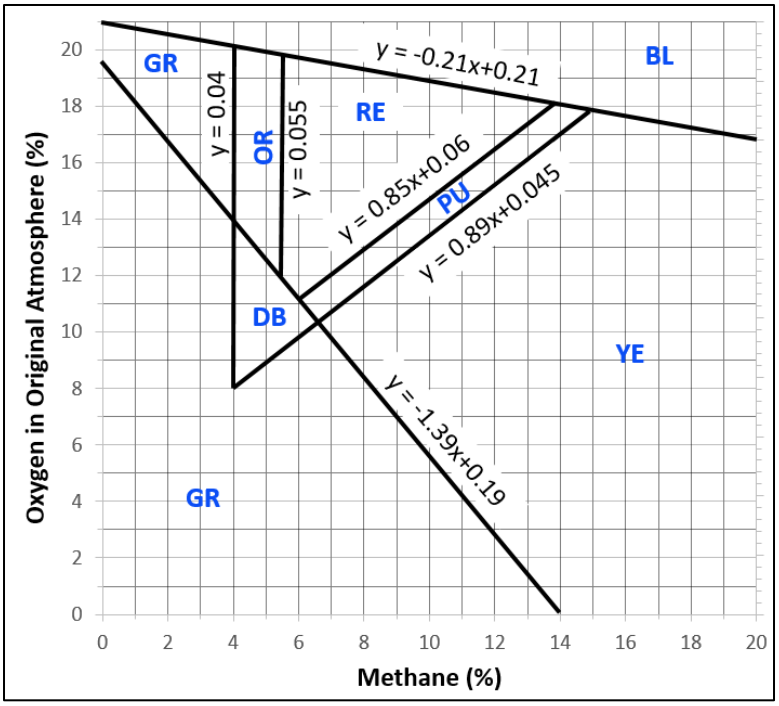

Figure 4.14: Functions used in UDFs for explosibility region limits

In this study, researcher evaluates a mixture of methane and air species, as opposed to methane, oxygen, and nitrogen gases separately as in previous modeling (Worrall, 2012; Gilmore, 2015; Marts, 2015). It is considered a more realistic scheme to model the mixture with methane-air species than methane-oxygen-nitrogen species. When using methane-air-nitrogen species, the oxygen is treated as distinct gas, and not a component of air. From the observation, having the oxygen and nitrogen as two distinct gases in the modeling causes methane which enters the fractured zone and gob from the atop inlet replaces the nitrogen more significantly than oxygen gas. This condition results in an unbalanced composition of oxygen and nitrogen as they were in air. In addition, using two species as opposed to three species in simulation noticeably reduces computational time and increases stability.

CHAPTER 5

MODEL VALIDATION AND SENSITIVITY ANALYSIS

This chapter presents the validation of the model. The model results, such as flow velocity, pressure of the methane inlet and increased methane concentration at tailgate entry after a barometric pressure drop are validated against mine measurements and reference values obtained from several actual mines. Also, findings from mesh independent study and model sensitivity analyses are presented in this chapter.

5.1 Comparison with Actual Mine Data

5.1.1 Flow Velocity in the Gob

Due to the inaccessibility and continuous caving of the gob, field measurements are impossible to conduct directly in the gob; thus, fluid flow properties such as velocity within the gob remain unknown. Without any data, it is safe to say the internal flow must be significantly slow and laminar due to gob characteristics as a porous medium. Many studies conducted to estimate the velocity and pathways of internal gob flow utilized a tracer gas. Velocity is calculated by the estimated distance of the shortest path the gas may take to a known location, and the time differential from release to first detect at this location.

Diamond et al. (1999) used sulfur hexafluoride, or SF_6, as the tracer gas in several longwall panels in the Pittsburgh coalbed. Figure 5.1 shows Panels F, G and H of the mine where a tracer gas study was conducted. The injection and sampling points are circled in red. The panels were ventilated by two bleeder fans located in the back end of panels F and G. The size of these panels were 253-305 m (830-1,000 ft) wide and 8,900 m (32,713 ft) long. The overburden depths range between 152 m (500 ft) and 274 m (900 ft).

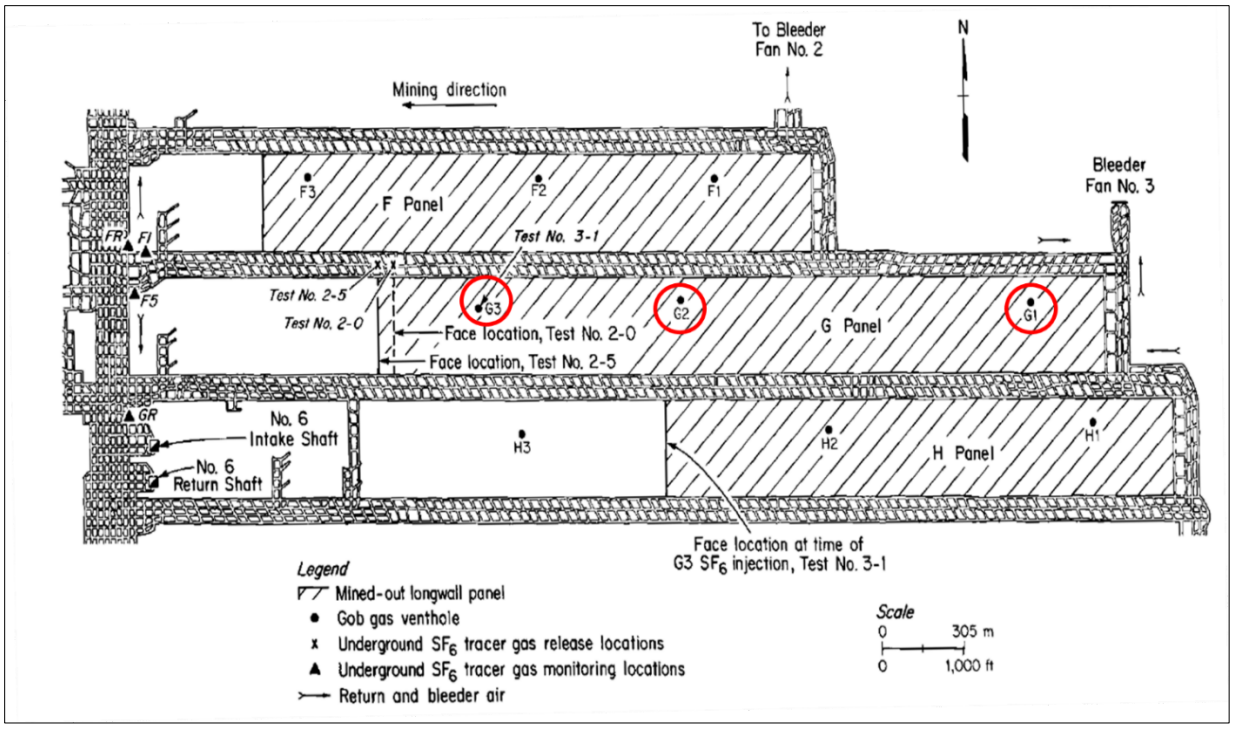

Figure 5.1: Injection and sampling points for the tracer gas study (Diamond et al., 1999)

The SF_6 was injected into the gob from the bottom of the G3 gob venthole. This venthole is located 76 m (250 ft) from the tailgate entry and 381 m (1,250 ft) from the longwall recovery room. From the automatic gas sampling (AGS) system installed at gob gas ventholes F1, G1 and G2, the pathway for the tracer gas was towards bleeder fans No. 2 and 3. Tracer gas is first detected at gob venthole G2 (the closest sampling point from G3) 27 hours after the release, giving an estimated velocity of 0.012 m/s (2.4 ft/min). The AGS system at venthole G1 detected a small concentration of the gas 367 hours after the release. The velocity was calculated to be 0.002 m/s (0.36 ft/min). It is necessary to note that the injection and sampling points are close to tailgate side, leading to an assumption that the flow velocity towards the gob center must be much lower. Using numerical modeling, Yuan et al., (2006) observed air velocity near the center of the gob of about 1×10^{-6} to 7.0×10^{-6} m/s (0.0002 to 0.0014 ft/min).

The velocity values from the gas tracer and numerical modeling above are comparable with velocities obtained in this study. Figure 5.2 shows the velocity magnitude contours in the gob of the base case model from CFD modeling. Due to wide-range values, a logarithmic scale is used and the contours are clipped to be between 0.0001 and 0.04 m/s (0.019 and 7.9 ft/min). The center of the gob is dominantly filled with methane seeping from strata, which counters the air flows coming in from the surrounding entries. As shown in Figure 5.2, the flow through the gob center is very slow, approximately 0.00015 m/s (0.029 ft/min), reflecting a similarity with values used by Yuan et al. (2006). Within 200 m (656 ft) behind the shields or three crosscuts inby, the velocities are in the range of 0.001 and 0.04 m/s (0.19 and 7.9 ft/min). At 76 m (250 ft) into the gob from the tailgate side, the approximate locations of gob ventholes G1 and G2 in tracer gas study, velocities vary between 0.01 and 0.0001 m/s (1.9 and 0.019 ft/min), comparable with magnitudes estimated in that study. The difference may be due to site-specific conditions such as gob permeability, location of bleeder fans and ventilation quantity. Given that gob permeability in the tracer gas study is unknown, the CFD modeling results are within reasonable range.

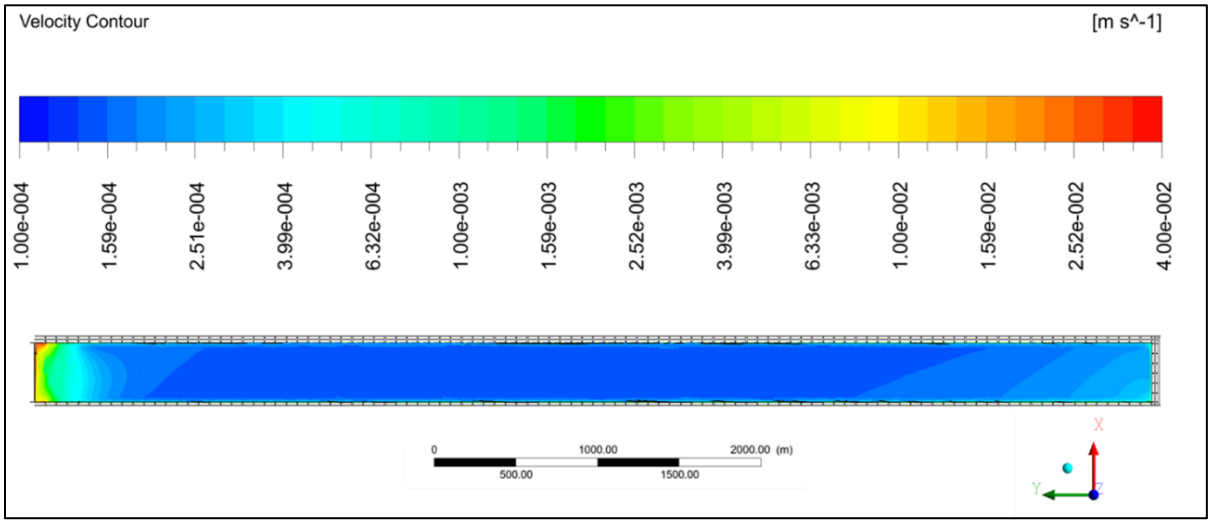

Figure 5.2: Contours of airflow velocity in the gob from the base case model

5.1.2 Methane Inlet Pressure

In this modeling, methane gas enters gob from rider seam atop the fractured zone at a constant pressure of 4,630 Pa for the base case model. At this pressure, methane inlet supplies 1.01 m^3/s (2,150 cfm) of CH_4 into the model. This pressure value is in the proximity of the gob venthole shut-in pressures reported by the Diamond et al. (1999), Karacan et al. (2006) and Schatzel et al. (2008).

Diamond et al. (1999) investigated the longwall gob gas flow paths using tracer gas SF_6 injected into an inactive gob gas venthole above the gob. In this investigation, the shut-in pressures near the bottom of two ventholes, G1 and G2, ranged between 1,750 and 2,000 Pa. Shut-in pressure was the pressure measured at a point near the bottom of the boreholes that already went off production. Schatzel et al. (2008) reported a shut-in pressure of approximately 3,000 Pa higher than the mine pressure in a borehole disturbed by the gob caving.

Other studies conducted in different coalbeds and depth measurement have reported wide range values for coalbed pressures (USEPA, 1999; Dallegge and Barker, 2000; Karacan et al., 2006; Simpson, 2008; Karacan, 2009; Erdogan et al., 2013). This strongly suggests that reservoir pressure can vary depending on many parameters such as coal permeability, overburden depth, host rock types, fractures and other geologic features.

5.1.3 Methane Concentrations on Bleeder Entries and Tailgate Returns

Regulation 30 CFR §75.323 outlines that the bleeder system must maintain methane content below 2.0% in the bleeder entries immediately before it enters another split of air. The volume of the methane entering the model through the inlet boundary at the top of the overlying strata is iterated to supply a proper amount of methane so that the methane concentration at the bleeder outlet does not exceed 2%. Figure 5.3 shows a general layout of a single bleeder-ventilated

panel taken from the MSHA (2002) ventilation specialist training textbook with measurement locations are marked by red circles. The bleeder entries must be traveled weekly and sufficient measurements must be made to determine system effectiveness.

"… at the regulators between the gob and the bleeder entries, and/or in the bleeder entries, as approved in the ventilation plan".

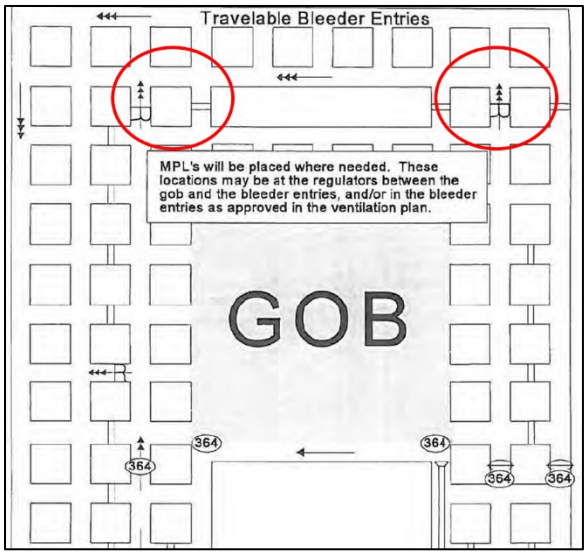

Figure 5.3: Wrap-around bleeder and recommended evaluation locations (MSHA, 2002)

In the base case model, the immediate bleeder entry adjacent to the gob (the area within the red rectangular mark in Figure 5.4) becomes a part of the gob, not travelable due to roof caving, sealed or regulated and has methane concentrations in excess of 2%. The other two bleeder entries have less than 2% methane content, mostly due to dilution by air from the headgate entries. As regulated in 30 CFR §75.323(e), methane concentration is measured at point A in walkable bleeder entry and at bleeder outlet. At the tailgate side, one entry generally remains open due to roof collapse and is connected to bleeder entries at the inby end. This entry is generally not travelable by the mine personnel. Since the tailgate crosscuts are not regulated, most of contaminated air from the gob flows toward this entry, resulting in a higher methane concentration, exceeding 2%, compared to those found in the bleeder entries.

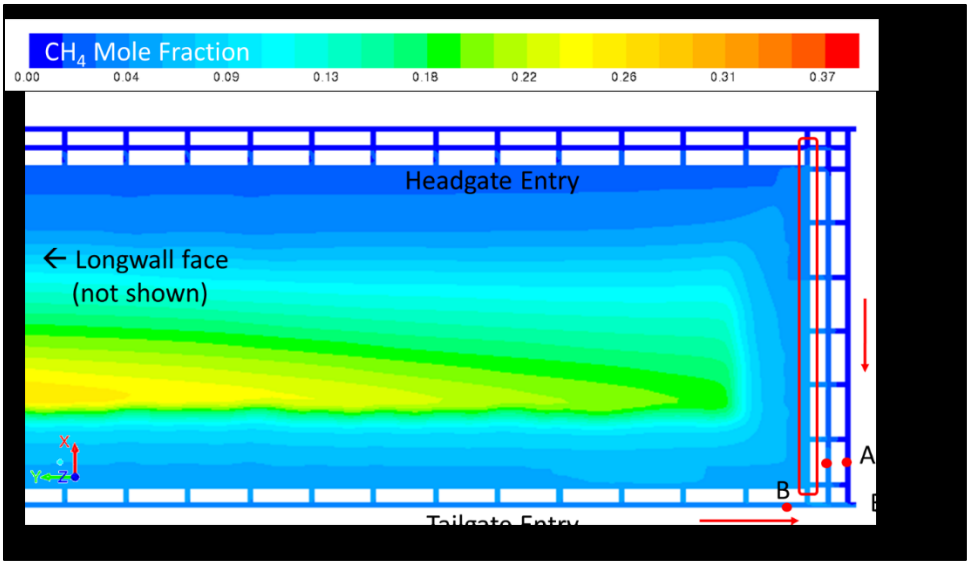

Figure 5.4: Methane concentration around the startup room for the base case

Belle (2014) conducted an extensive field investigation to examine the effect of barometric pressure changes at a highly gassy coal mine in Australia. He reported an increase of 0.5-0.94% methane content in tailgate return after a 500-Pa drop. In this study, the evaluation on the 500-Pa instantaneous drop scenario indicates an immediate methane increase at point B (Figure 5.4) by 0.8%, within the range reported from Belle's field investigation. The complete simulation results are further discussed in Chapter 6.

5.2 Gravity Effect and Buoyancy

Gravity is an important factor in this modeling for two main reasons: (1) methane and air have significantly different densities so gravity would definitely influence the layering of these two gases; and (2) gravity naturally generates pressure stratification where higher locations have less pressure than those at lower elevations. This pressure variation due to differences in elevation is clearly shown in the model. The entry 3 boundary inlet is taken as an example. Figure 5.5 shows the pressure variation at this entry boundary. The entry only supplies air and is about 3.35 m (11 ft)

high, and the pressures vary from 3,444 Pa near the roof to 3,479 Pa near the floor, giving a gradient of 35 Pa.

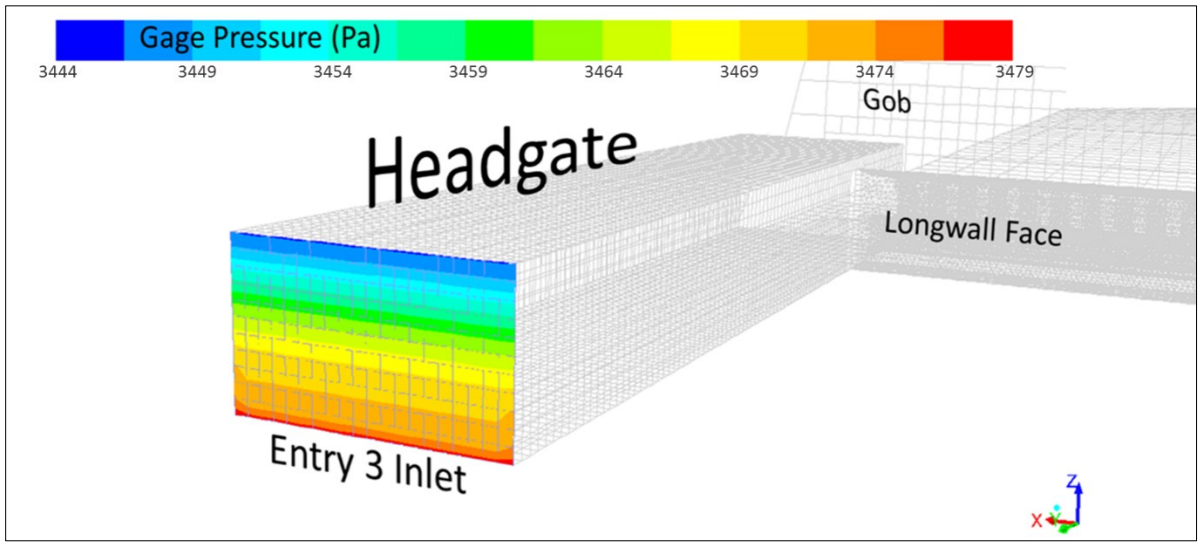

Figure 5.5: Air pressure profile at entry 3 inlet

The pressure change due to elevation variation can simply be calculated using Equation 5.1, where ρ is density of air (kg/m^3), g is gravity (m/s^2) and Δh is the elevation difference (m).

$$\Delta P = -\rho g \Delta h \tag{5.1}$$

With an average density of 1.11 kg/m^3 (adjusted to the cooperating mine elevation of 1,000 m above sea level), and a 3.35-m elevation difference, Equation 5.1 gives 36 Pa, in approximation with the pressure gradient shown in Figure 5.5.

In the gob, gravity is known to produce a buoyancy effect in the form of a separation between methane and air under conditions that methane and air are not mixed and both exist in extremely low velocities. This may only occur if the methane is released from relatively higher locations than the ventilation air stream, such as from the mine roof, the upper section of the coal face or ribs, or from rider seam above the gob. In this study, methane stratification due to the buoyancy effect was clearly observed in the gob. Figure 5.6 shows methane stratification in the gob and overlying strata from various view planes. This stratification became diminished behind

the shields (section A-A'), in the startup room (B-B'), around the gob perimeter (C-C') and in the center of the gob. The high pressure from the ventilation air and the development of a highly turbulent flow overcame the layering of methane around the perimeter of the gob. In the center of gob, as shown in the top plan view of Figure 5.6, very little air could penetrate, causing this area became a methane-rich zone, and thus no stratification was expected.

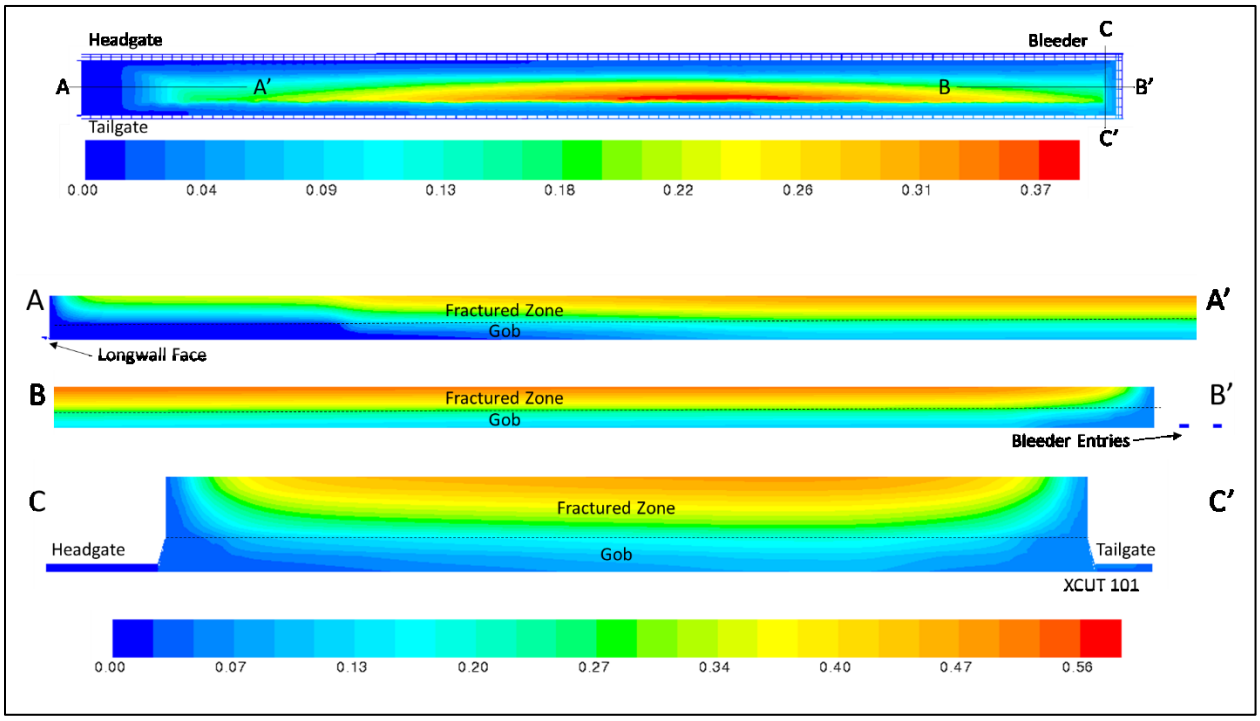

Figure 5.6: Methane mole fraction profile in various section views

5.3 Model Sensitivity

A sensitivity analysis was conducted to examine the significance of solution changes with the alteration of initialization method, gob permeability inputs and mesh size.

5.3.1 Initialization Method

The ANSYS Fluent® program requires an initial "guess" for the solution flow field. A user must provide the initial values before the program can start the iteration. This procedure is called initialization. Providing each cell with a "guess" value close to the final solution means less

computational time the program needs to reach converged results. A *hybrid* initialization is used in all cases in this modeling based on ANSYS Fluent® recommendations for a pressure-based simulation setup. With hybrid initialization, the program considers the values set at boundary conditions and uses a collection of boundary interpolation methods available in the program to obtain initial values. Users do not need to provide additional inputs for initial values, which in many cases can improve the robustness of the convergence (ANSYS, 2013).

The initial condition of the methane-air mixture in the overlying strata and gob is thought to be one of the major assumptions in this modeling. Initial conditions of mixture composition in the model may affect the final condition of the explosive mixture. To evaluate the significance of the initial condition to the final results, three cases of different methane-air compositions for initialization were simulated: pure air, a 50%CH_4 - 50%H_2O composition, and pure methane. Table 5.1 shows the comparison of EGZ volumes and methane content from converged simulations.

Table 5.1 Comparison of results of CFD initialization condition

Initial Condition for CH4	CH4 Mole Fraction (%)			EGZ Volume Fraction (%)			Methane Inlet Flowrate (m^3/s)	CH4 Conc. at Bleeder Outlet (%)
	Overlying Strata	Gob	TG Entry*	Overlying Strata	Gob	TG Entry*		
0	34.346	13.750	1.754	18.044	35.379	15.971	1.0160	1.909
50%	34.372	13.743	1.754	18.036	35.369	15.568	1.0156	1.907
100%	34.391	13.814	1.806	18.031	35.347	15.661	1.0150	1.905
Std Dev. (RSD)	0.07%	0.28%	1.69%	0.04%	0.05%	1.34%	0.05%	0.10%

*Include tailgate crosscuts

From Table 5.1, the results from three different initial conditions are relatively comparable. From these results, it is worth noting that slightly more methane would be found in the model when it was initialized with pure methane than pure air. In contrast, EGZ volumes seemed to be inversely proportional to the methane mole fraction. A greater EGZ volume was found in the model with less methane or initialized with pure air. Since EGZ is a result of methane and air mixing, more air in the dominantly methane-filled gob allows more forming of the EGZ. In this study, all models were initialized with a mixture of 50% CH_4 - 50% O_2.

5.3.2 Gob Permeability Input

Gob permeability is one of the major uncertainties in this study. The EGZ occurs in the gob, and thus is strongly controlled by permeability. In CFD modeling, permeability input sensitivity to the resulting EGZ volume is investigated by varying the base permeability and analyzing the EGZ volume that forms. Gob permeability varied by 10% - 50%. The contour plots of these permeability variations are presented in Figure 5.7.

Figure 5.7: Contours of the gob permeability variation used for sensitivity analysis

Only the gob area near the face is shown in the figure since the farthest part of the gob is mirrored from this area in respect to permeability. Gob permeability does not vary with height, so

the plots represent values at any elevation within the gob. The base permeability of the model ranges between 2.0 x 10^{-7} and 5.1 x 10^{-6} m^2, which replicates the condition of the Mine C gob (Marts et al., 2014a). Modifications in the gob permeability result in observable changes in the EGZ volumes, as shown in Figure 5.8 through 5.10. Figure 5.8 indicates a larger yellow area (methane-rich zone) formed with decreasing gob permeability, pushing the explosive range outward and thus reducing the red EGZ regions. The colors refer to the Coward's triangle in Figure 4.13. It is important to note that Figure 5.8 shows the condition at two-dimensional slice located 3 m above the mine floor and may not necessarily represents the trend in entire model volume. The three-dimensional shape of EGZ in the base permeability scenario is shown in Figure 5.9.

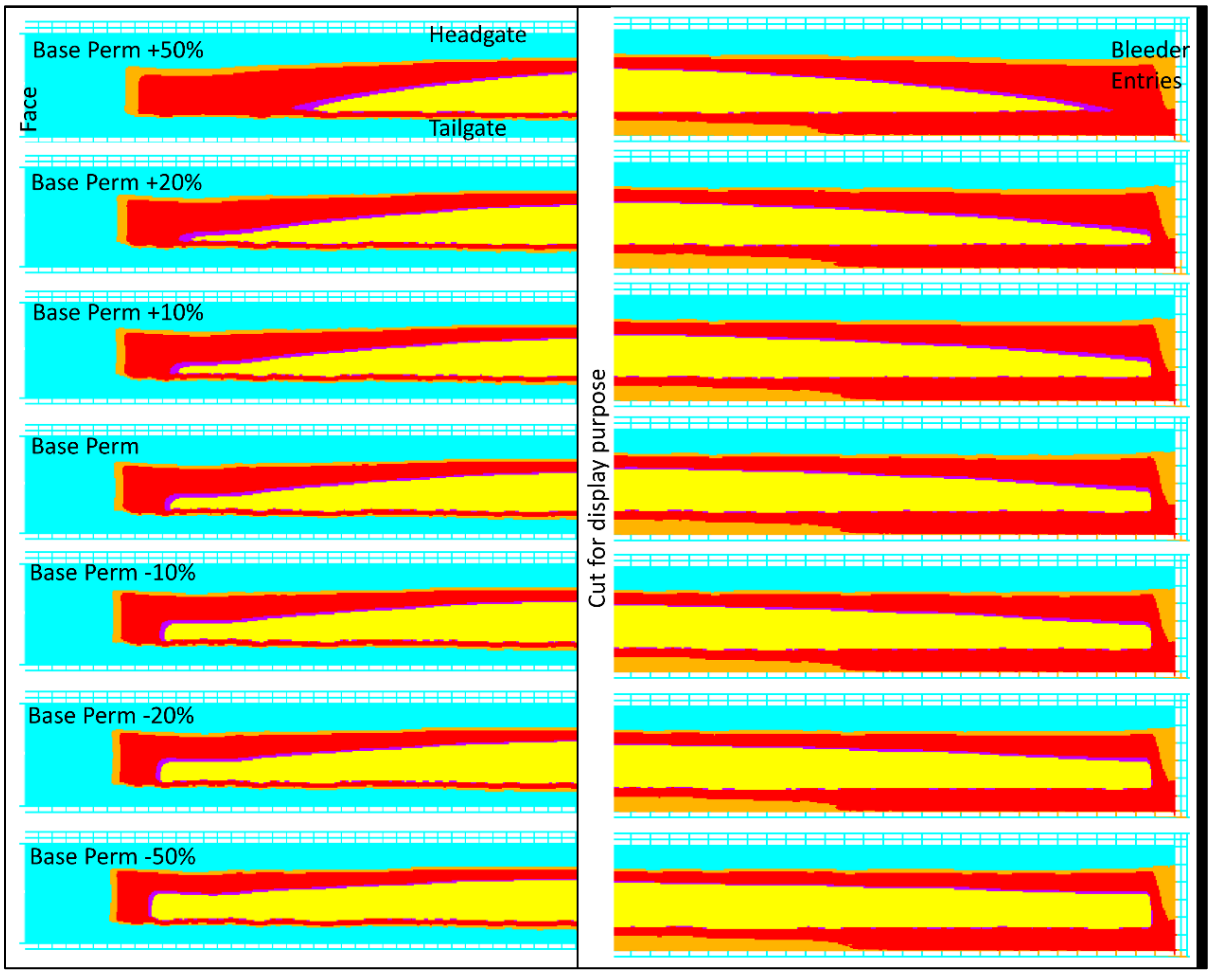

Figure 5.8: EGZ condition at 3 m above the mine floor with permeability variation

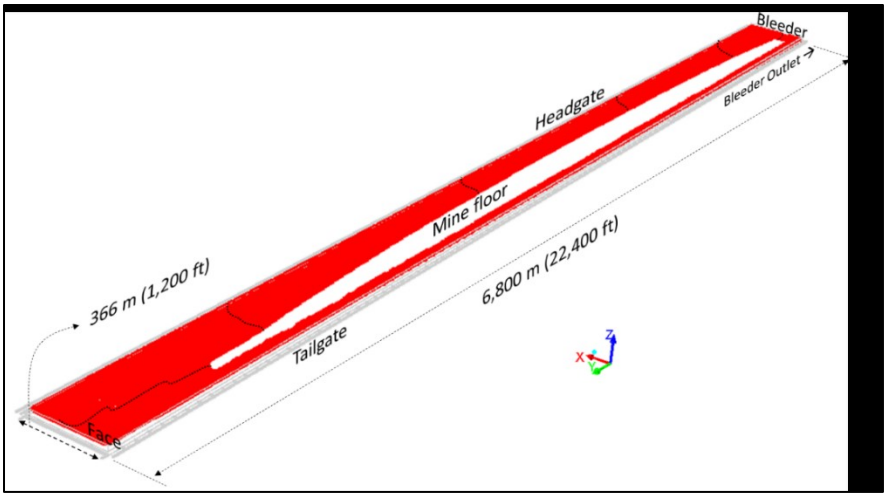

Figure 5.9: A 3-dimensional formation of EGZ in the gob with base perm scenario

This phenomenon is also illustrated by the graph in Figure 5.10. The EGZ volume in the gob increases with higher permeability. A 50% increase in the permeability results in a 1.5% increase in the EGZ volume, while a 50% decrease results in a 2.4% decrease in the EGZ volume.

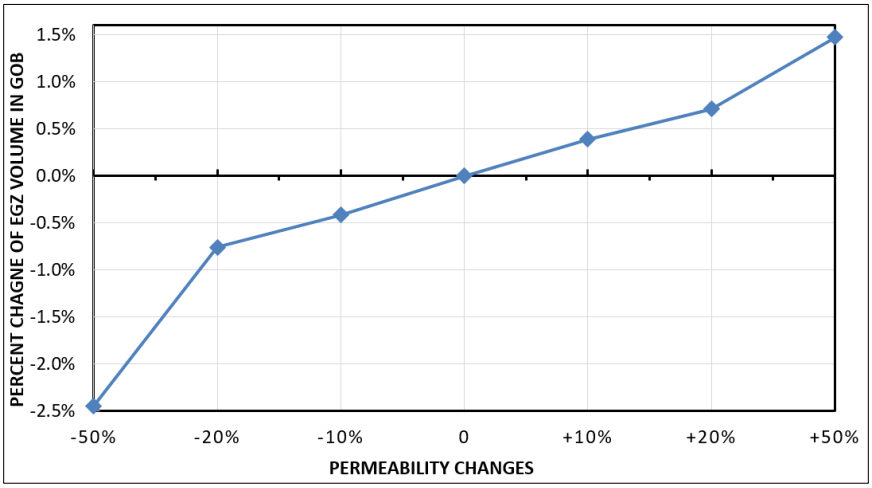

Figure 5.10: Change in gob EGZ volume with permeability variation

Figure 5.11 reveals that at the same inlet pressure, methane inflow from the simulated rider seam above the overlying strata slightly decreases permeability increases, as indicated by the blue line. The larger EGZ and reduced methane inflow with higher permeability are potentially caused by the amount of air in the gob and smaller pressure drop. As indicated by the red line in Figure

5.11, the oxygen mole fraction increases in the higher permeability gob. This shows that an increasing permeability allows more oxygen ingress into the gob, pressurizing it and slowing down the methane inflow from above. More oxygen in the gob also creates a condition more susceptible to forming a larger EGZ, confirming the condition observed in Figure 5.8.

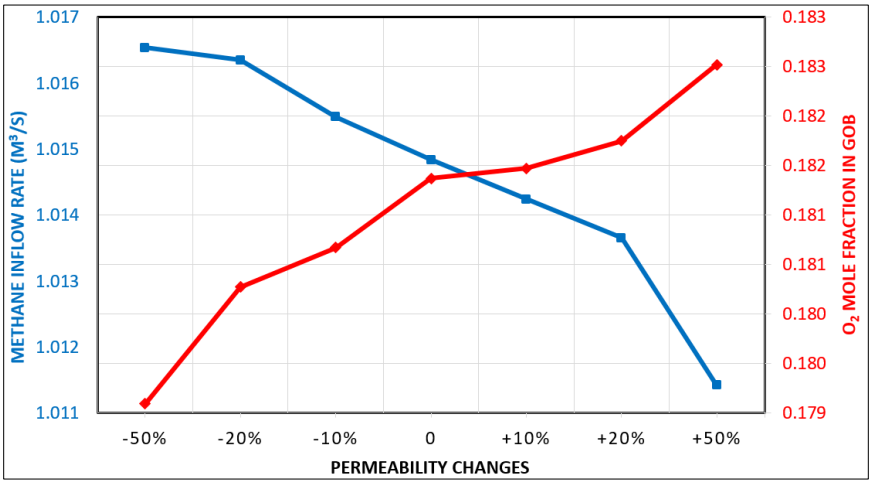

Figure 5.11: Change in methane inflow rate from the rider seam with permeability variation

5.3.3 Mesh Independence

In a converged model, solutions must be independent from the mesh and no longer change as mesh sizes decrease. Therefore, a mesh-independent study was conducted to analyze the mesh sensitivity and ensure true solutions are achieved. Due to limited computational resources, the study only focused on the gob and tailgate entry parts where most EGZ changes and leakages were observed to occur. The maximum mesh sizes of these parts were refined as shown in Figure 5.12, and corresponding EGZ volumes in the model were analyzed. The original meshes of gob and tailgate return were a 8- and 4-inch size, respectively. A two-step refinement was conducted by cutting the mesh size by half twice, resulting in two refined models named Model 2X and Model 4X. All other parts of the models remain unchanged (original size). The second refinement of the entire gob and tailgate return resulted in substantially large number of cells that caused the computer to crash. Therefore, the refinement in Model 4X was only applied to the rear half of the

longwall gob, starting from crosscuts XC 61. The other half of model closer to face was only refined once, replicating the Model 2X. Figure 5.2 shows the mesh of the gob from headgate (HG) to tailgate (TG) entry in the vertical section along the crosscut XC 100. The location of XC 100 refers to section C-C' in Figure 5.6.

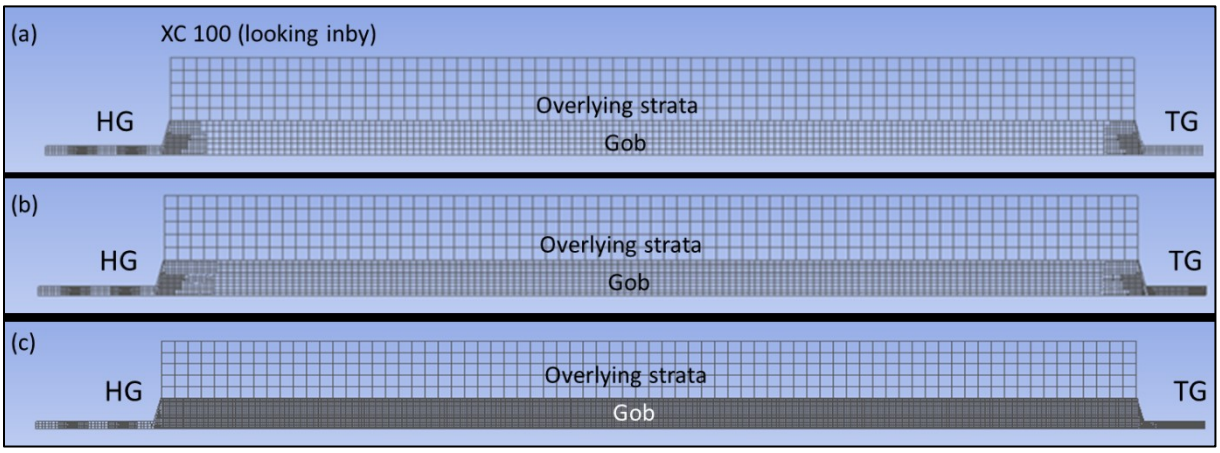

Figure 5.12: Comparison of (a) original mesh, (b) Model 2X and (c) Model 4X

Table 5.2 shows the details of mesh control, total number of cells and resulting EGZ volumes found in each model. In all simulations, the pressure boundary conditions shown in Table 4.6 were used. Table 5.2 indicates an increase in EGZ volumes by more than 3% at tailgate return from original model to Model 2X. With further refinement, the EGZ volume, methane inflow rate and concentration at bleeder outlet in Model 4X are relatively the same as in Model 2X with changes less than 1%. This insignificant difference confirms the mesh independence of Model 2X, which was therefore selected as the base case model in this study.

Table 5.2: Results of mesh independent study

Model	Largest Mesh Size (ft)		Total No. of Grids/Cells (in million)	EGZ Volume Fraction (%)			Methane Inlet Flowrate (m^3/s)	CH4 Conc. at Bleeder Outlet (%)
	Gob	TG Entry		Overlying Strata	Gob	TG Entry		
Original, 1X	8	2	11.2	18.036	35.369	15.568	1.0156	1.907
2X	4	1	17.8	18.085	35.138	15.955	1.0152	1.883
4X*	2	0.5	35.7	18.085	35.162	15.956	1.0155	1.889
Std. Dev. (RSD)				0.16%	0.36%	1.41%	0.02%	0.66%

*only rear half of gob and tailgate entry were further refined, the other half remained as in Model 2X

CHAPTER 6

MODELING RESULTS AND DISCUSSION

This chapter presents modeling results and discussion regarding the impact of external pressure changes. Pressure conditions in the simulated mine before and after barometric pressure changes are evaluated and compared. The changes in internal EGZ formation, the outgassing phenomenon and methane concentration changes in surrounding entries after different scenarios of instantaneous and gradual pressure changes are also discussed.

6.1 Methane Concentration, EGZ Formation and Airflow Condition

The base case scenario simulates conditions of a bleeder-ventilated longwall panel. The pressure conditions and airflow requirements at all inlets and outlets are listed in Table 4.6. Since the geometry and ventilation data used in all simulations are obtained from the cooperating mines, the resulting EGZ and airflow are expected to show a general direction of what would happen in a real situation. In addition, modeling outputs such as airflow velocity in the gob, methane concentrations at the tailgate return and pressure conditions have been verified and validated against field data.

Figure 6.1 shows the methane concentration output in the gob at a steady-state condition. The horizontal view is located 3 m above the mine floor, while the vertical views are along sections A-A' through C-C'. The CH_4 concentration is 1.9% at the bleeder outlet which is one of designated bleeder evaluation points (BEPs) around the panel. As the bleeder system allows air from headgate entries and face to enter the gob and exit through tailgate crosscuts, the methane within the gob is diluted and pushed away toward the tailgate side. The air from face leakage is able to sweep the methane behind the shields and in a higher zone above the gob (section A-A'). The general "tub"

shape of methane profile in the gob is shown in sections A-A' through C-C'. The overlying strata or fractured zones and the mid-section of the gob are mostly filled with a methane-rich mixture. The maximum concentration of methane in the gob at 3 m above mine floor, as shown in Figure 6.1, is 38%.

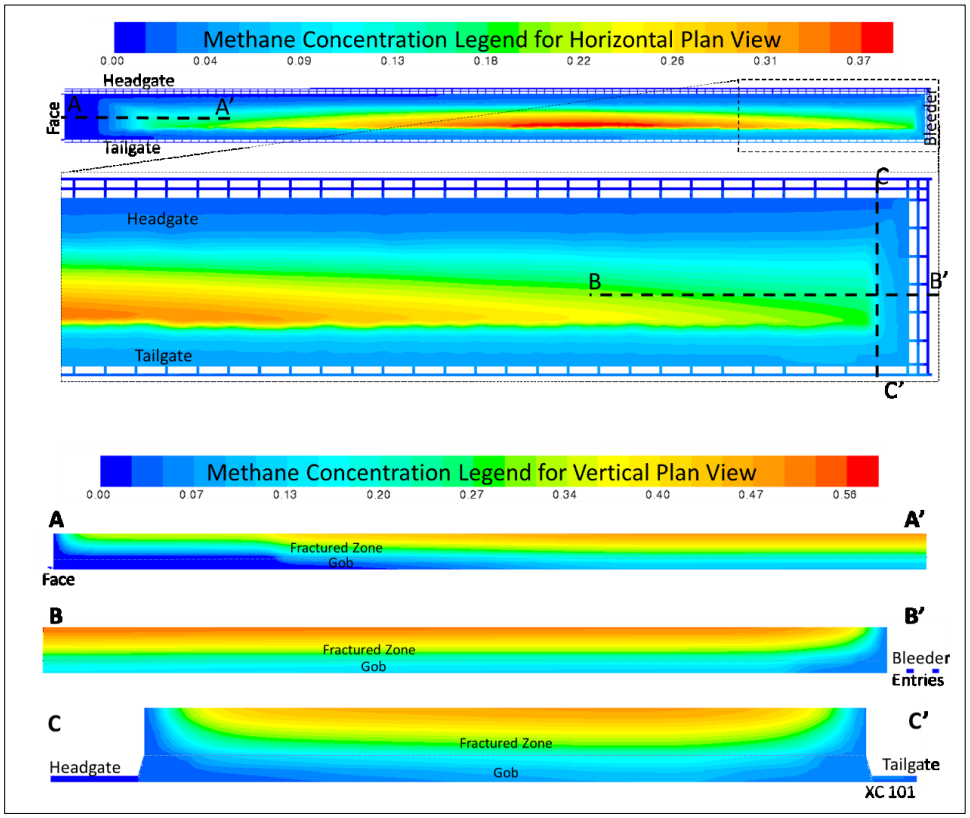

Figure 6.1: Initial condition of methane concentration in the gob

Figure 6.2 shows the explosibility of methane-air mixture within the gob. Explosibility is defined by the color-coded diagram shown in Figure 4.13. The red color indicates an explosive mixture or EGZ which is proportional to the 5.5-14% CH_4 in Figure 6.1. The top profile in Figure 6.2 indicates a large fringe of EGZ formed within the gob, a finding also reported by other researchers to be associated with bleeder ventilation system (Brune, 2013; Gilmore, 2015; Krog, 2016). In a 3-D view, the EGZ fringe will have a "tub" shape, as shown in Figure 6.3.

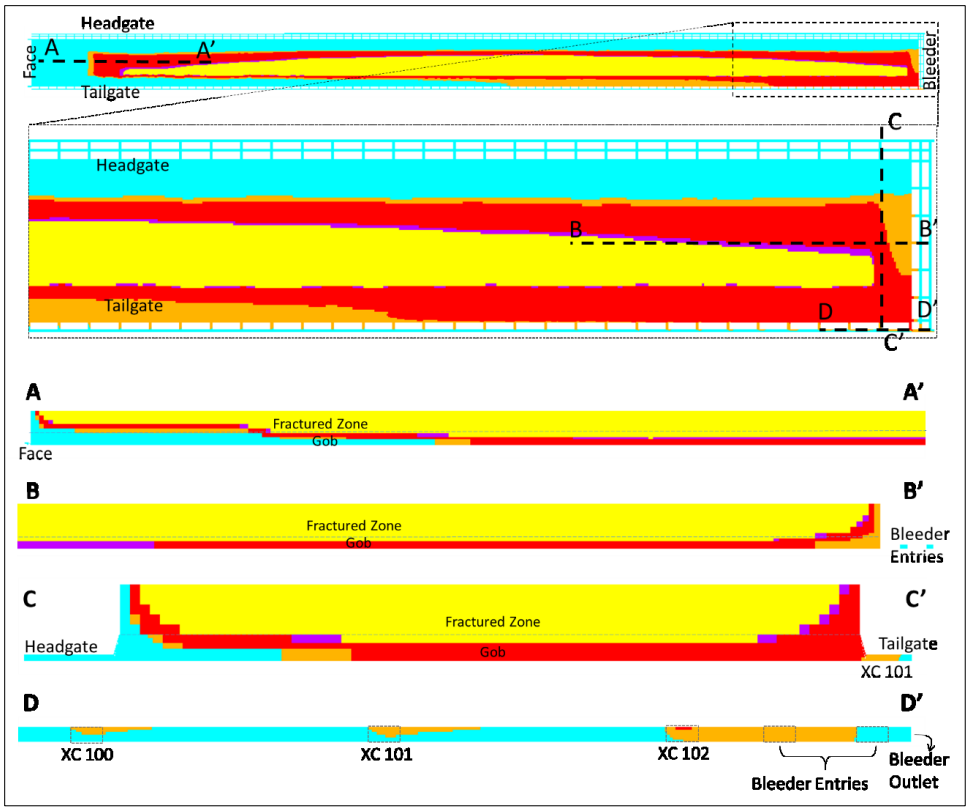

Figure 6.2: Initial condition of EGZ formation in the gob and tailgate return

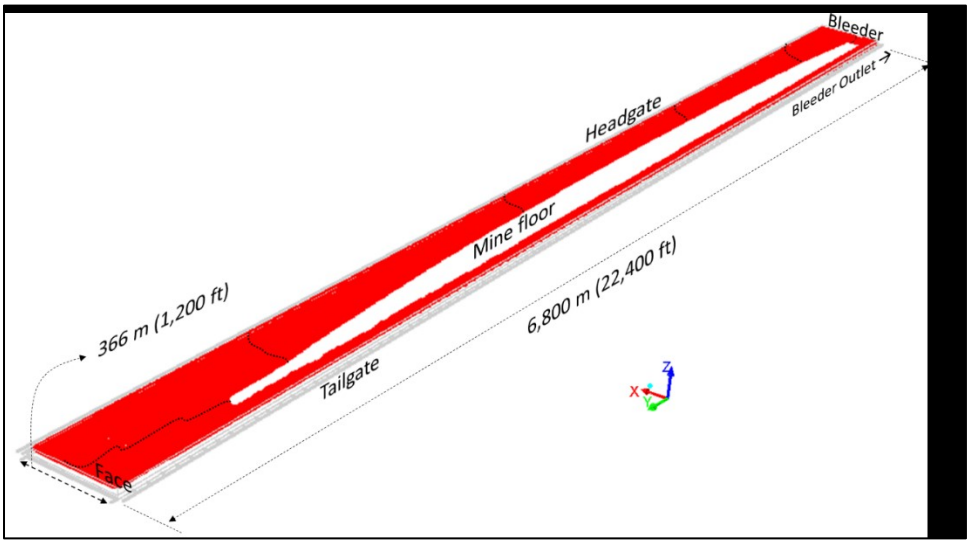

Figure 6.3: A 3-dimensional view of initial EGZ profile in the gob

Per the bleeder ventilation system design, some ventilation air enters the gob from gaps on the back of shields along the face and through headgate crosscuts. The courses of ventilation air

across the gob are depicted by streamlines shown in Figure 6.4. The contaminated air would then exit the gob through tailgate crosscuts, heading toward the bleeder outlet. Because of this leakage, the EGZ is observed to accumulate in the corner of tailgate-bleeder returns, which represents the location within the gob possessing the lowest pressure. Behind the shields, the gob area is dominated by oxygen, which pushes the EGZ away from the face to the sixth crosscut (section A-A' in Figure 6.2). About 50 m (164 ft) into the gob along headgate side is also clear from the EGZ (section C-C').

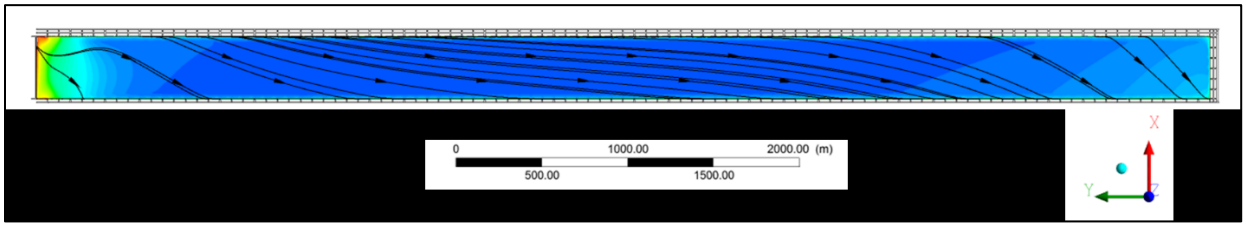

Figure 6.4: Direction of airflow in the bleeder-ventilated gob

Moreover, section D-D' in Figure 6.2 shows the vertical view along the back end of tailgate return looking into the gob. A near-explosive mixture, the orange-colored zone, exists in several tailgate crosscuts. The EGZ is observed to flow out from crosscut XC 102. This condition emphasizes that a methane concentration of 1.9% at the BEP (bleeder outlet) does not provide accurate information on the mixture in the tailgate return. Krog (2016) also indicates the possibility of having high methane exiting the tailgate returns before reaching the monitoring locations. The EGZ outgassing at the tailgate return is concerning because the EGZ could rapidly disperse given the turbulent disruptive nature of air movement in the tailgate entry and if ignited, the explosion can constitute imminent danger due to its proximity to miners' working areas.

6.2 General Response of Mine and Gob Pressure to Barometric Pressure Changes

It is known that pressures in surrounding mine entries and within the gob respond differently to barometric fluctuation. The pressure in mine entries changes almost instantaneously,

approximately at the speed of sound, following a barometric pressure fluctuation (Stevenson, 1968; Wasilewski, 2014), whereas gob pressures change after certain delays mainly due to flow obstruction by the porous medium. The following modeling is conducted to further investigate these different responses of pressures in mine areas and the gob.

The base case model uses pressure boundary conditions as listed in Table 4.6. To simulate the variation in barometric or mine pressures, all boundaries except the methane inlet are concurrently dropped by 1,000 Pa using a UDF (shown in Appendix A). The pressure change at several locations inside and outside the gob are monitored after the drop. Figure 6.5 shows six pressure evaluation points inside the gob, A through F, and three outside the gob at the tailgate return and crosscuts G through I. Most of these points are not physically accessible, but serve as markers in the CFD model. All points are located 3 m (9.8 ft) above the mine floor. Points A through F are 1,000 to 6,000 m away, inby the face. Points G and I are placed in the tailgate entry or return, while point H is in crosscut XC 099.

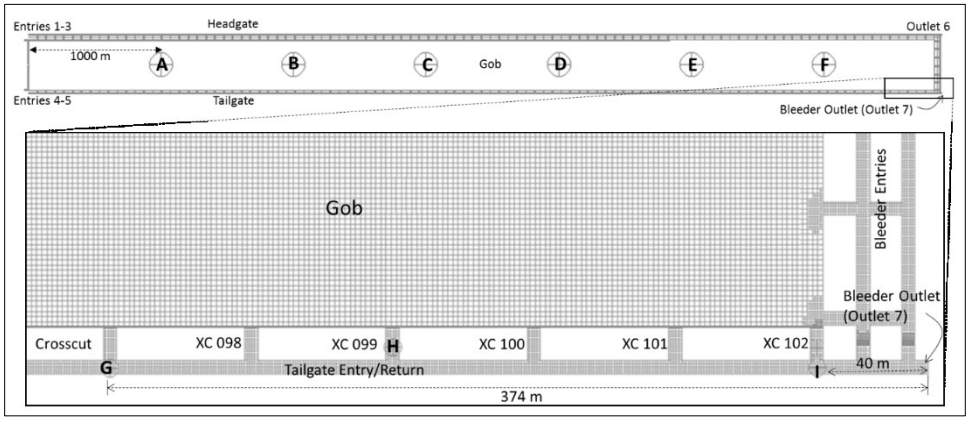

Figure 6.5: Locations of evaluation points A-F in the gob and G-J outside the gob

Figure 6.6 shows the pressure profiles at 0.5-second increments monitored at points A through I after the external pressure is instantaneously dropped at t=0 second. A flat profile in the beginning of the external pressure drop was observed on points located in the mid-section of gob,

B through E. These flat profiles indicate a duration when these particular evaluation points have not "sensed" the pressure changes that already occurred outside. Figure 6.6 (b) shows that points C and D, located in the gob center, start to decrease after t=15 seconds. Both points are approximately 3,000 m away from any inlets or outlets, indicating that the pressure waves from inlet or outlets outside the gob travel at roughly 200 m/s, substantially slower than the speed of sound (~340 m/s). Pressures at points B and E decrease after nine seconds, and points A and F after a three-second delay. These delays point out the effect of gob materials and distance from the pressure source of inlets and outlets.

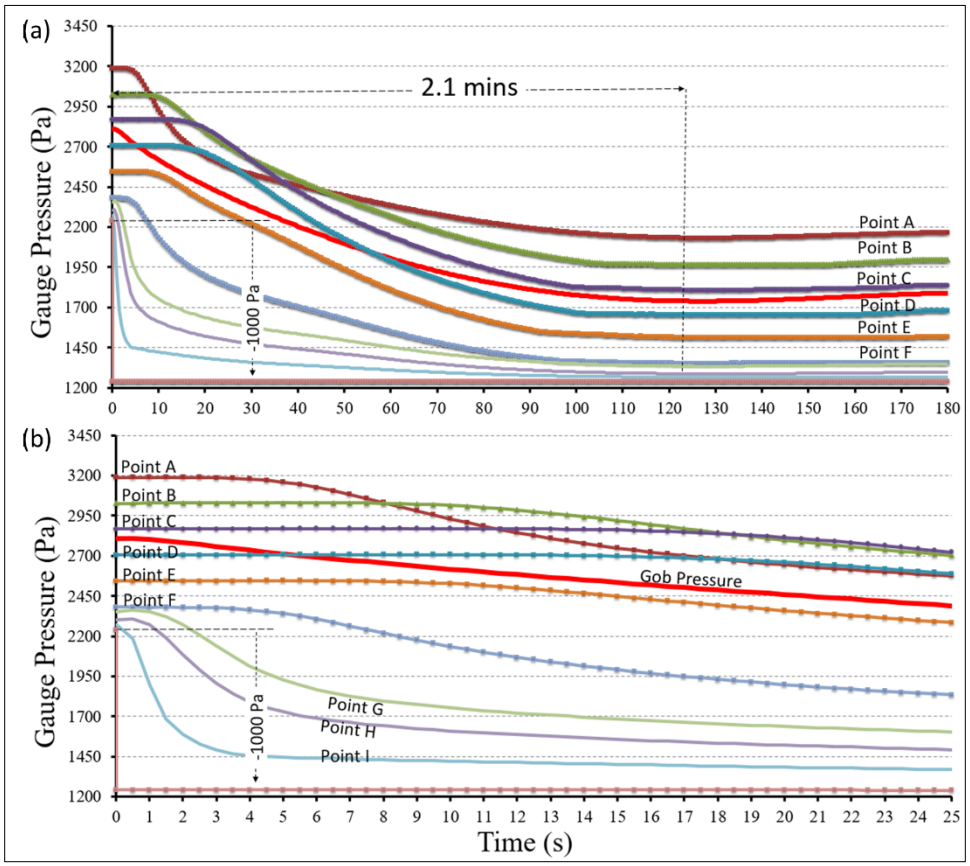

Figure 6.6: Pressure changes within the gob during an instantaneous 1,000 Pa drop

Conversely when considering the above observation, the pressures in mine entries and active working areas are found to change much more quickly. In Figure 6.6 (b), the pressure at

point G starts decreasing at about one second. Point G is 374 m away from the bleeder outlet, roughly the distance sound can travel per second. This result confirms studies by Stevenson (1968) and Wasilewski (2014) that barometric pressure changes would impact the underground mine entries or working areas almost instantaneously. Points H and I, which are located closer to the bleeder outlet, start decreasing much earlier than point G (in less than one second). The rate of change eventually slows for all locations and goes flat as it achieves equilibrium, as in the initial condition. The average gob pressure reaches this equilibrium after 2.1 minutes which is estimated when the change is less than 0.1%, this is defined as the time lag in this research. It is noted that the pressures near the end of the time lag shows a curving profile, which goes below the equilibrium condition (between t=110 and 170s). This condition is caused by the imbalance rate of mass influx and outflux across the gob due to different gob and fractured zone permeabilities. The permeability of the fractured zone above the gob is about eight times smaller than the gob's; as pressure decreases, this causes mass outflowing from the gob to the surrounding entries faster than methane inflow from the fractured zone to the gob.

In the pressure rise scenario, the same finding of time lag is also obtained. The immediate response of mine pressure and the delayed change of gob pressure indicate the occurring time lag is independent from whether the outside pressure increases or decreases.

6.3 Effect of Different Magnitude of Pressure Changes on EGZ

While barometric pressures fluctuate fairly regularly in good weather, it can change abruptly and to a greater magnitude during stormy weather, as explained in Chapter 3. Most studies have reported barometric pressure changes in major mine explosions within a range of 100 to 1,000 Pa (Hosler, 1948; Fauconnier, 1992; Hemp, 1994; Wasilewski, 2014; Belle, 2014). Figure 3.6 shows a recent 2,000-Pa drop in a western coal mine during a storm (Lolon et al., 2015). Zipf

et al. (2010) reported a much higher pressure change in the 3,400 – 6,800 Pa range during severe storms and as high as 16,600 Pa during the hurricane season. Instantaneous pressure fluctuations can also occur during major events like a mine fan stall or a roof fall. In this modeling, instantaneous pressure changes were simulated at various magnitudes ranging from 100 to 2,000 Pa, and the results of EGZ alteration, outgassing and methane concentration changes were examined.

6.3.1 Scenario 1: Instantaneous Drop of External or Barometric Pressure

In this scenario, the pressure boundary conditions at all inlets and outlets, with an exception for the methane inlet above the overlying strata, were decreased simultaneously by 100, 500, 1000, and 2000 Pa. Pressures at evaluation points A through F (Figure 6.5) were monitored.

The pressure trends in Figure 6.7 denote time lags of 1.2, 1.8, 2.1, and 2.8 minutes, respectively for 100-, 500-, 1000-, and 2000-Pa drops, highlighting the proportion of time lags against the magnitude of the pressure drops. The time lag is determined to begin when the outside pressure stops changing, and lasts until the gob pressure is no longer fluctuating (<0.1% change). The gob pressure is the volume-weighted-average pressure of the entire gob, and the additional pressure differential, ΔP_b, is generated during the time lag. This is represented by the green-colored area under the gob pressure curves. Before t=0s, gob outgassing already occurs as a result of the bleeder ventilation system. The outgassing is driven by the bleeder system's pressure differential, ΔP_s (yellow-colored area). The outgassing increases instantly at t=0s due to the addition of ΔP_b to the system. Outgassing during the time lag is driven by the total of $\Delta P_b + \Delta P_s$. The magnitude of ΔP_b decreases over time, causing the outgassing to taper off gradually and eventually reach equilibrium, which mimics the initial conditions where $\Delta P_b=0$ and only ΔP_s exists.

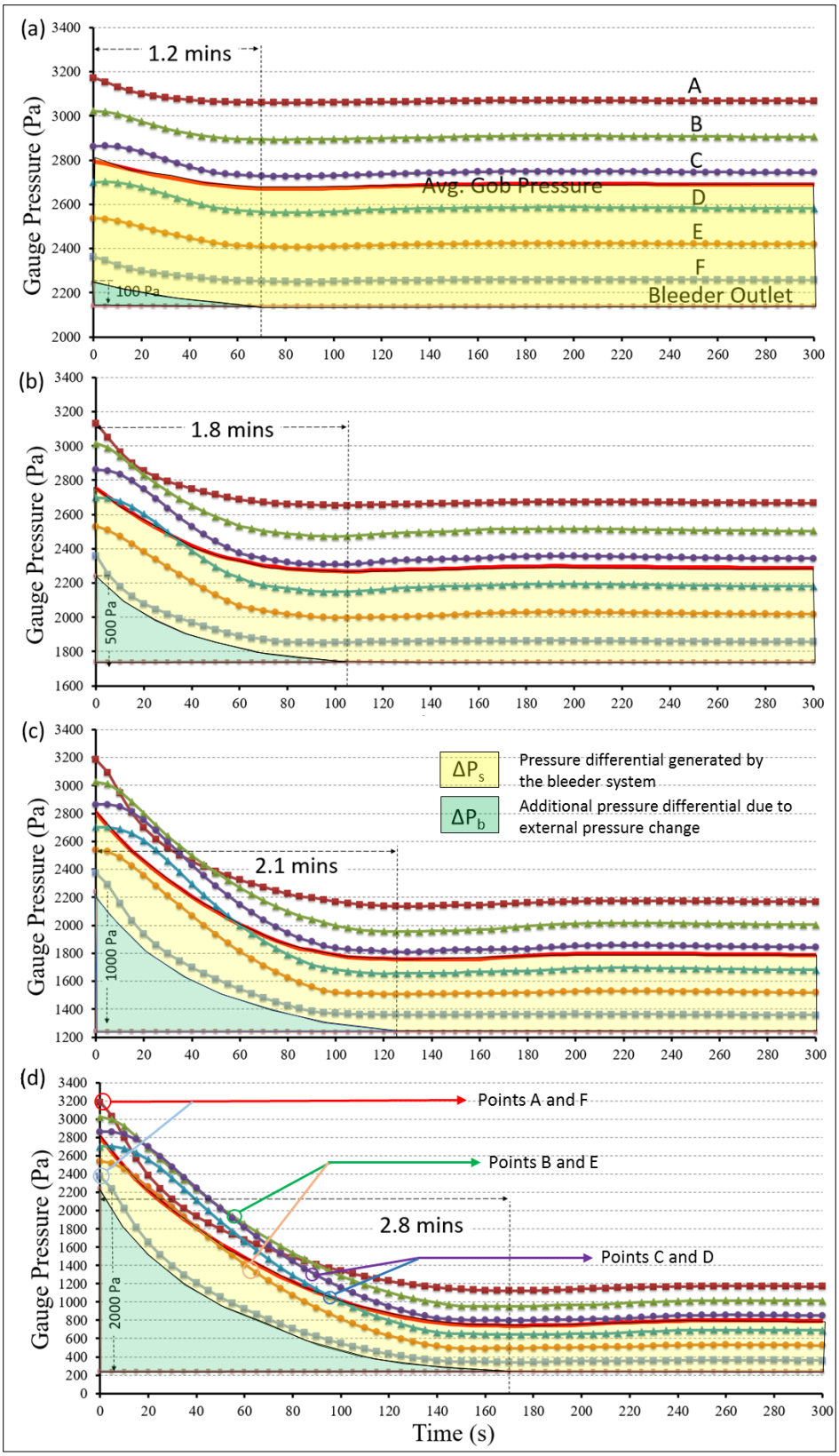

Figure 6.7: Pressure changes within the gob during various pressure drops

The internal gob pressure field tends to organize into three distinct pairs, as discussed in Section 6.2, most clearly visible in Figure 6.7(c); A-F, B-E, and C-D each exhibit similar delay trends based on their distance from the inlets and outlets as the pressure change source. It is also noticeable from Figure 6.7 that gob pressures decline slightly below the steady-state condition near the end of the time lag. This is caused by the different EGZ rate and methane gas outflow from the gob and the rate of methane influx into the gob from the rider seam. The much smaller permeability of the fractured zone than that of the gob causes slow inflow of methane back into the gob.

Figure 6.8 to 6.10 show the EGZ conditions during the time lag for all cases at t=300s, when steady-state equilibrium is reached. In all cases, decreasing outside pressure induces an expansion of the near-explosive mixture and EGZ within the gob on the tailgate and bleeder sides, marked by dotted rectangular in Figure 6.8(d).

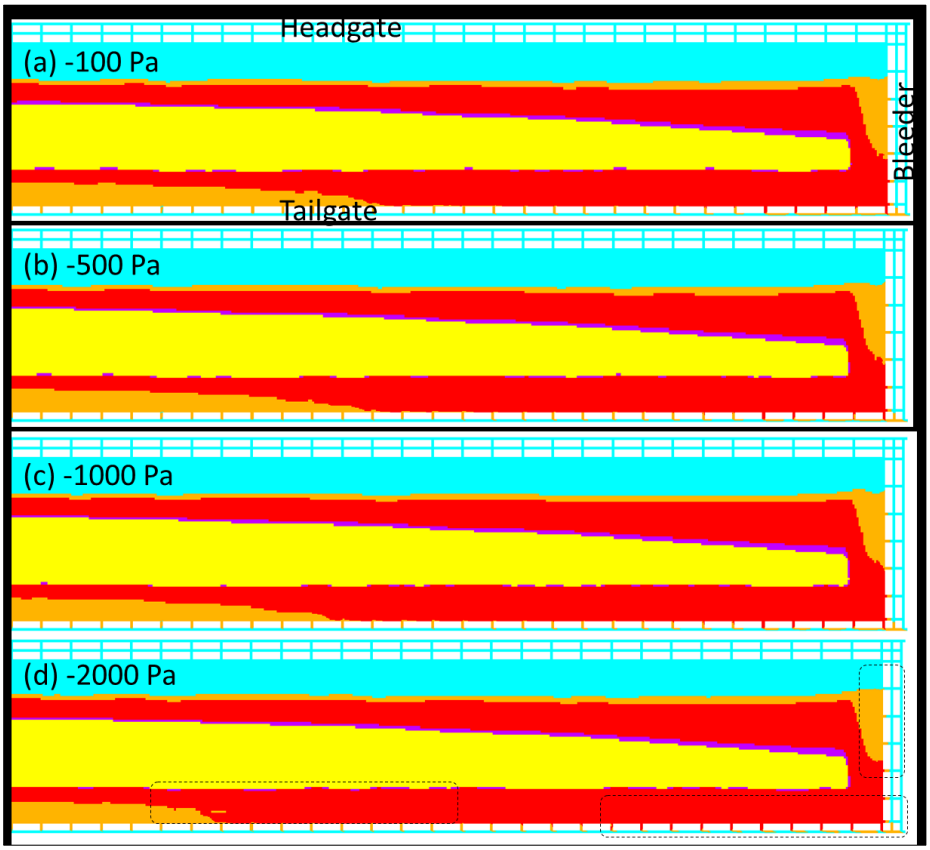

Figure 6.8: EGZ profile along the horizontal plane view at t=300s of pressure drop

In Figure 6.9 and 6.10, more EGZ in the tailgate crosscuts and return are observed to be associated with greater pressure drops. The EGZ is found to seep mostly along the crosscut and tailgate entry roof, pointing out the buoyancy effect on the methane-air mixture.

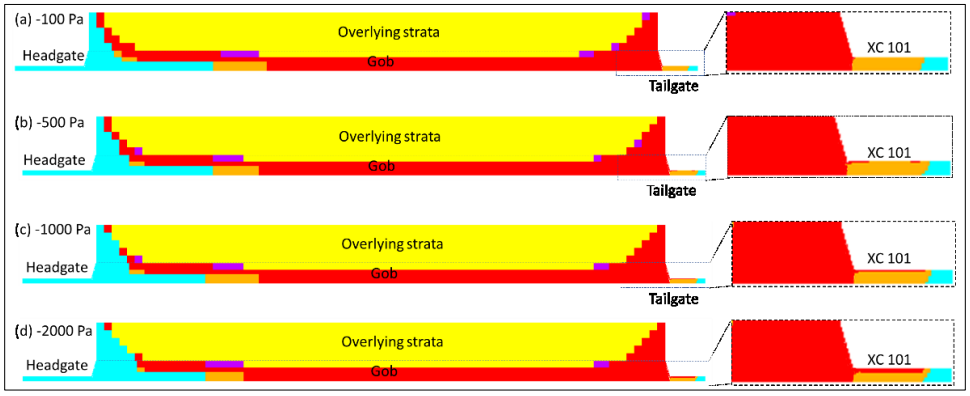

Figure 6.9: EGZ profile in the vertical section along XC 101 at t=300s of pressure drop

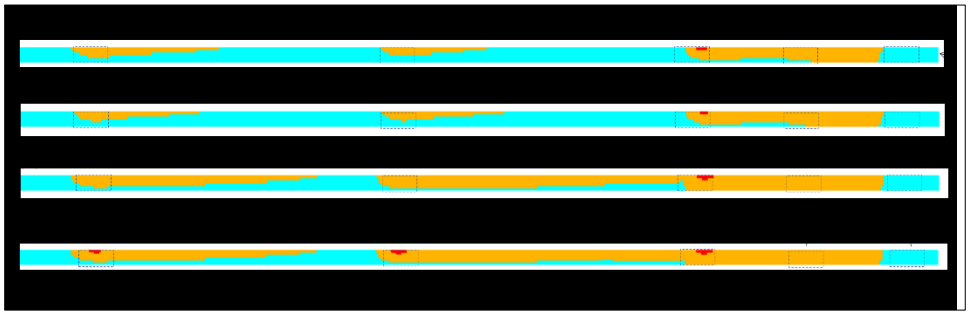

Figure 6.10: EGZ profile along the tailgate return at t=300s of pressure drop

Figure 6.11 shows the normalized EGZ volume within the fractured zone and gob over two hours following the pressure drop. The 0 and 1 ranks are associated with the minimum (x_{min}) and maximum (x_{max}) values in the dataset, respectively. The difference between the minimum and maximum values is approximately 2% of the initial EGZ volume in the gob. The other values (x) in between these ranks are normalized using the unity-based normalization method as follows:

$$Normalized\ x' = \frac{x - x_{min}}{x_{max} - x_{min}} \tag{6.1}$$

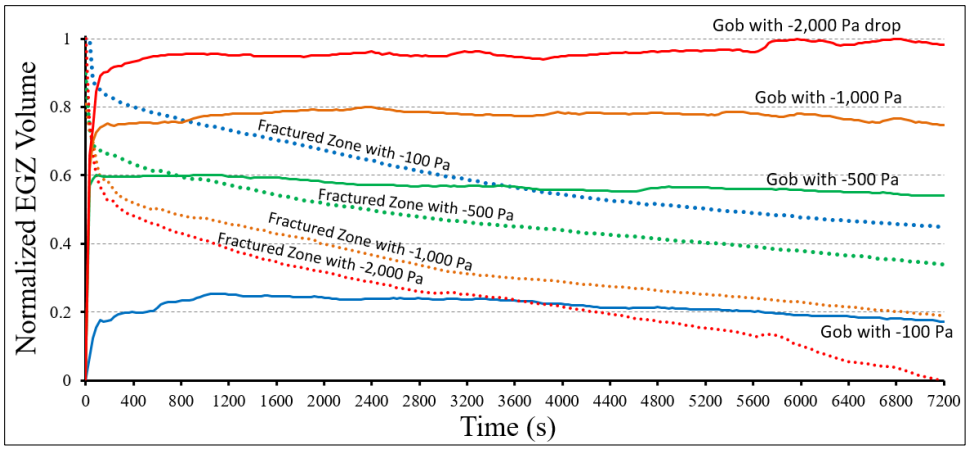

Figure 6.11: Normalized EGZ volume in the fractured zone and within the gob

Figure 6.11 further indicates that, when barometric pressure is falling, the EGZ volume increases in the gob but decreases within the fractured zone. Though the volume change is relatively small compared to the total EGZ volume, this condition emphasizes the movement of the EGZ from the fractured zone to the gob. The pressure drop also increases the methane influx from the rider seam, which pushes the EGZ in the fractured zone to the gob. The greatest EGZ volume increase or decrease is associated with the highest pressure drop of 2,000 Pa. In all scenarios, the most significant EGZ changes are observed to occur between t=0s and 200s, or during the time lag described in Figure 6.7. During the lag, the additional pressure differential, ΔP_b, occurs in the system, at its peak in early seconds before gradually decreasing.

Due to its proximity to the bleeder tap, most EGZ outflow is observed to happen through XCs 94 through 102. XC 102, the last tailgate crosscut connected to the gob (see Figure 6.5), is taken as an example to analyze the EGZ volume change during the pressure drops. Figure 6.12 shows the change in EGZ volume in XC 102. Initially, in the base case scenario, EGZ constitutes 70% of XC 102 volume (see Figure 6.2). This EGZ volume increases by 6.2% with a 2,000-Pa drop approximately within 200 seconds, shortly after the end of the time lag. As shown in Figure 6.7(d), the time lag for the 2,000-Pa drop scenario is estimated to be 2.8 minutes or 168 seconds.

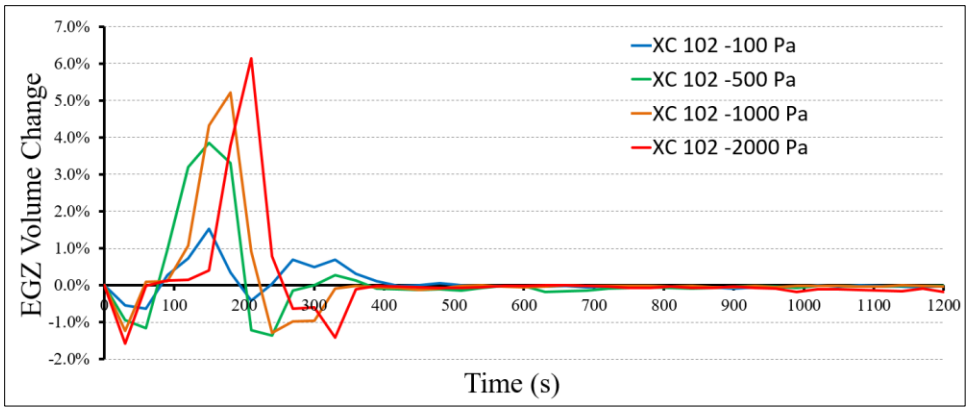

Figure 6.12: EGZ volume change in XC 102 as a function of external pressure drop

Interestingly in all cases, XC 102 did not see any increase in EGZ volume until after approximately t=80s. Figure 6.12 shows a negative change during the initial 80 seconds. The explanation for this is that, since XC 102 is obstruction-free and closer to the bleeder tap than the fractured zone is to the bleeder tap, the pressure drops would "draw" out the EGZ in XC 102 more quickly than the EGZ from the fractured zone or gob. In addition, the low permeability of gob and fractured strata result in a delayed response of methane inlet to add more methane. The EGZ increase at tailgate return within the first t=50s, as shown in Figure 6.13, is attributed to this immediate outgassing of the existing EGZ in the crosscuts, and probably in the gob perimeter. The declining trend that follows is because the volume of this EGZ is limited and being drawn out faster than the rate of outgassing from the gob.

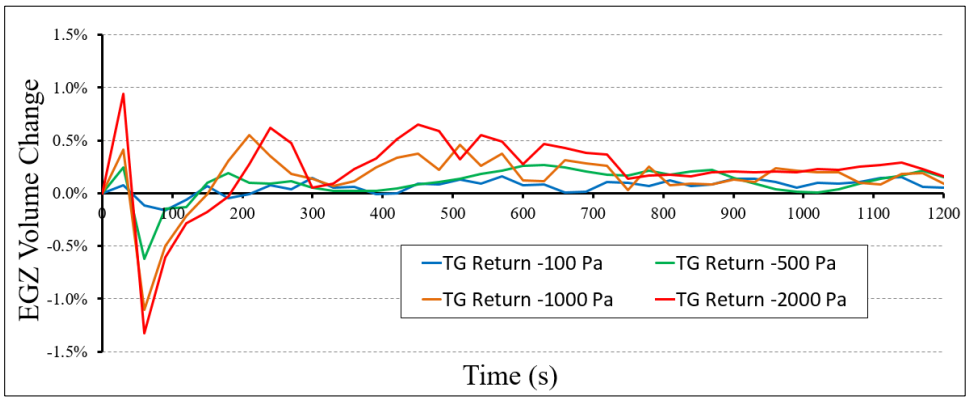

Figure 6.13: EGZ volume change in tailgate return as a function of external pressure drop

The total EGZ outgassing after two hours is shown in Figure 6.14. The simulation reported an overall increase at the tailgate return from the initial condition by 13%, 15%, 21%, and 32% for respective 100-, 500-, 1000-, and 2000-Pa drop scenarios. It is clearly shown that a greater magnitude of drop generates greater a pressure differential, ΔP_b, which drives more outflow of the EGZ from the gob to the surrounding tailgate entries.

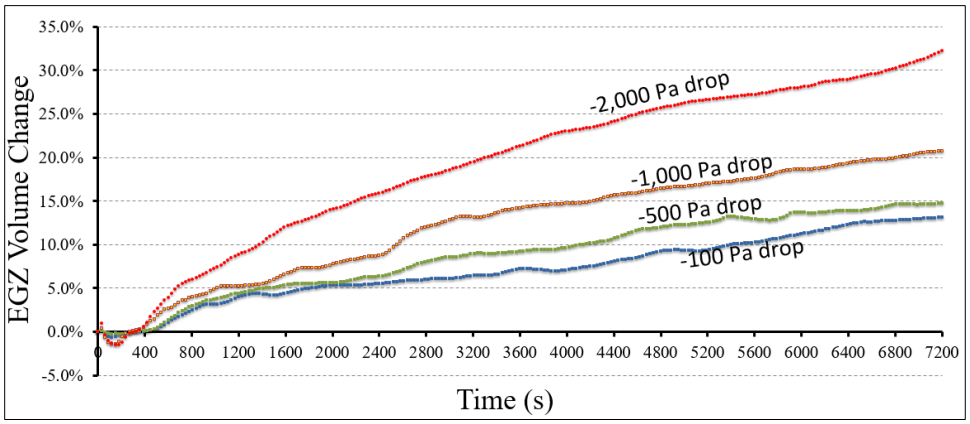

Figure 6.14: Total volume of EGZ outgassing at the tailgate return after two hours

6.3.2 Scenario 2: Instantaneous Rise of External Barometric Pressure

The sudden rises of 500 and 1,000 Pa were simulated to analyze the changes in EGZ formation and gob ingassing. Figure 6.15: Pressure changes within the gob during various pressure rises shows the pressure changes in the gob as a result of these increases. The pressure trends indicate time lags of 1.8 and 2.1 minutes, respectively for 500- and 1,000-Pa increases, identical to the results from pressure decrease scenarios in Figure 6.7. The location pairs of similar delay and rising rates, A-F, B-E and C-D, are also in agreement with findings from the pressure drop scenario. This finding conclusively shows that the pressure lag is independent from the pressure change direction, rising or falling pressures, but is dependently influenced by the gob permeability and distance from the inlets or outlets.

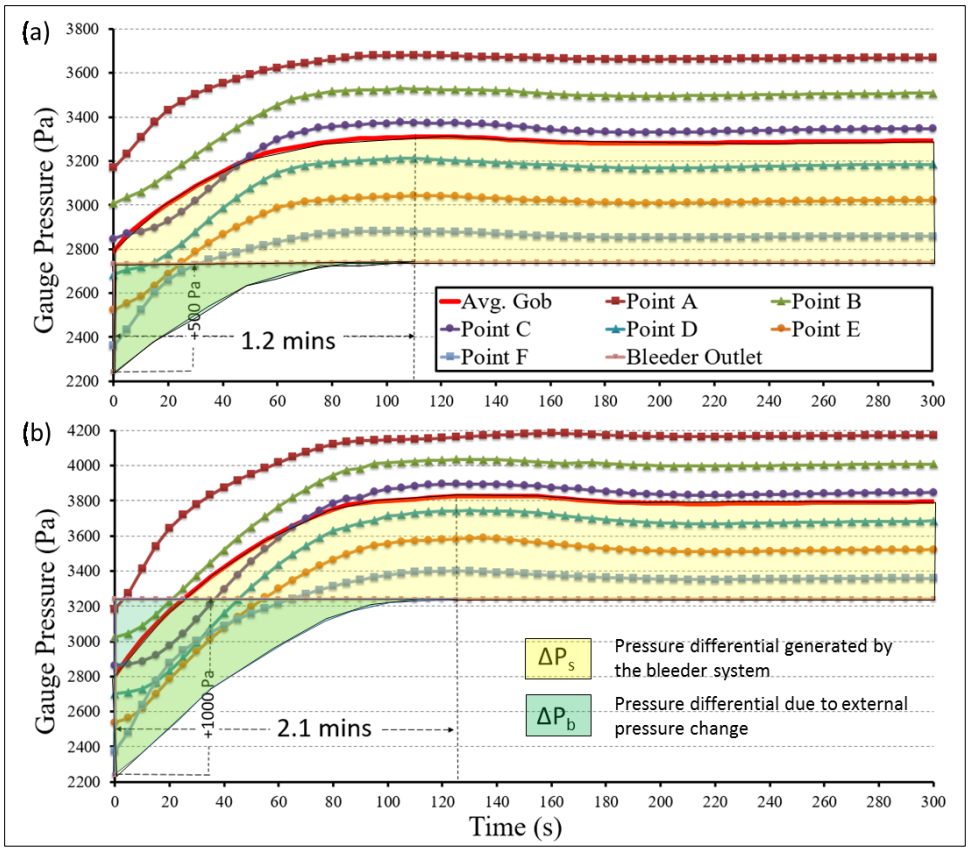

Figure 6.15: Pressure changes within the gob during various pressure rises

Figure 6.15 shows that the pressure changes overshoot the steady-state profile near the end of the time lag. This can be explained by the "fluid hammer" effect (Ponnuswami, 2005). This pressure surge occurs with momentum change when the gas flow in motion suddenly stops, slows down or changes direction due to the instantaneous rise of outside pressure. As the outside mine pressure instantaneously rises above the gob pressure, the outgassing toward the bleeder return suddenly stops and reverses direction, causing transitory pressure buildup from shockwave within the gob, especially at the mine floor level.

As shown in Figure 6.16, the EGZ formation within the gob at the view plane is slightly smaller at 500-Pa than in the 1,000-Pa scenario. Comparing to the initial condition, both scenarios show a smaller EGZ than the initial condition shown in Figure 6.2. This change is attributed to increasing air ingress into the gob. With a higher magnitude of rise, the air can be seen to sweep

the EGZ in the setup room, as well as reducing a near-explosive mixture from the tailgate crosscuts (orange-colored zone in Figure 6.17).

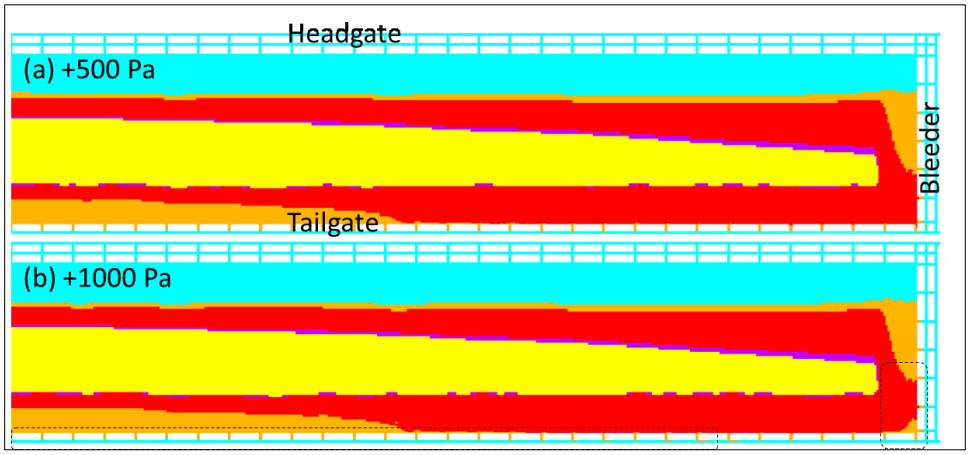

Figure 6.16: EGZ profile along the horizontal plane view at t=300s of pressure rise

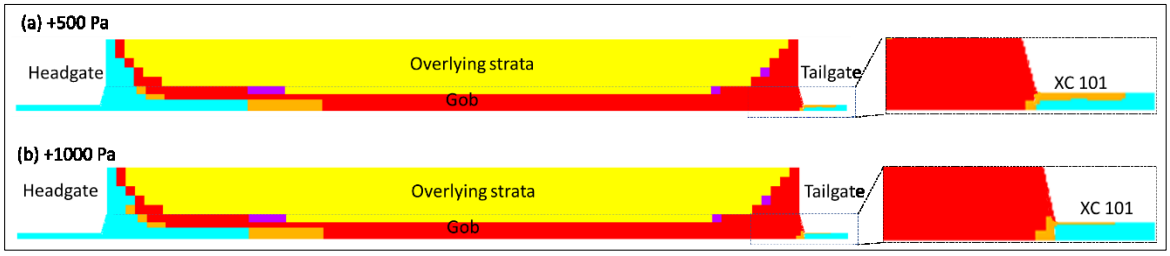

Figure 6.17: EGZ profile in the vertical section along XC 101 at t=300s of pressure rise

In contrast to the falling pressure scenario, EGZ volumes in both the overlying strata and the gob decline in this scenario. Figure 6.18 shows that, after two hours, the remaining EGZ in the gob due to a 1,000-Pa rise is 0.5, in normalized scale, less than that in the 500-Pa rise, or is equivalent to 0.4% of the initial EGZ volume. Furthermore, the reduction of EGZ volume in the fractured zone is slower in the 500-Pa case. For the fractured zone, the drop from the maximum normalized volume of 1 to the minimum 0 is equivalent to 1% of the EGZ volume initially exists in the zone, which is insignificant. The fractured zone is pressurized by the methane pressure of 4,630 Pa over the top of strata, which makes either the 500- and 1,000-Pa increases externally cause little impact to the total volume.

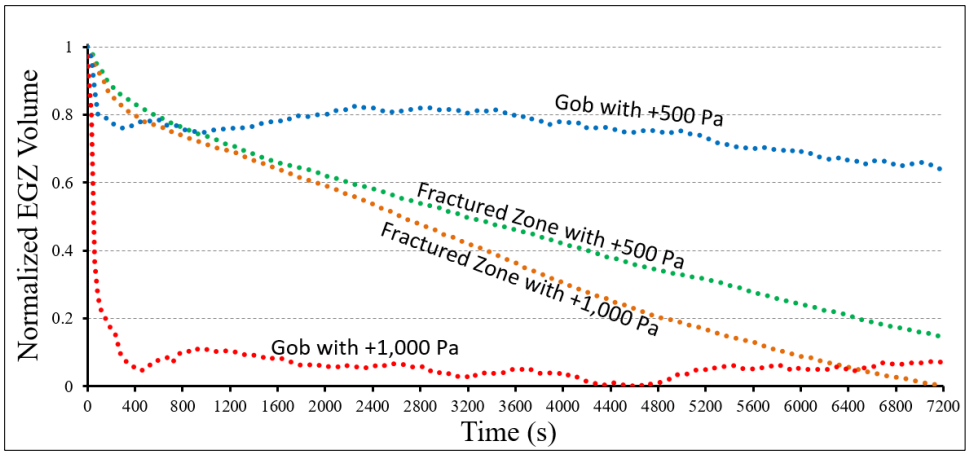

Figure 6.18: Normalized EGZ volume in the fractured zone and within the gob

Against conventional wisdom, the finding shows a declining EGZ in the gob and the fractured zone when external pressure increases. It has long been believed that increasing barometric pressure would induce more air ingress to the gob, which leads to more mixing of methane and air for a larger EGZ. This notion is partially true, as increased air is observed to enter the gob during the simulation. However, this does not necessarily generate a larger EGZ. This can be explained by the Coward's diagram shown in Figure 6.19. The EGZ (red-colored zone) separates the fresh air zone (A) from the yellow zone of high methane concentration (E). The transition from A to E must pass through explosive zone C and near-explosive regions B and D. The air ingress to the gob would dilute and move the mixture toward the lean-methane mixtures. In Coward's triangle, dilution can shift some portion of E mixture to D, D to C, C to B and so on. Since the EGZ fringe has a tub shape, this shifting is actually moving the fringe inward away from longwall work area, which reduces the volume.

From this finding, a rising external pressure is fundamentally favorable for mining operations, as it reduces the EGZ volume in the gob and no outgassing is observed in surrounding entries. This condition, however, should be considered as a warning because rising pressure is usually followed by a falling pressure trend.

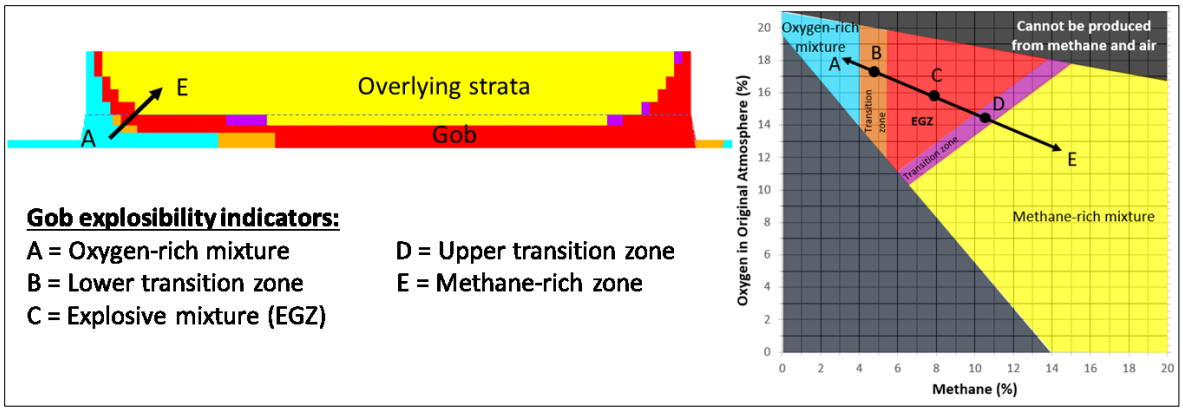

Figure 6.19: Gob explosibility shifts due to increasing external pressure

6.4 Effect of Different Rates of Pressure Changes on the EGZ

Rapid atmospheric pressure fluctuation changes over 203 Pa/hour (NWS, 2015). Severe storms can result in much higher fluctuations of 3,400 - 6,800 Pa over the course of two to 10 hours (Zipf and Mohamed, 2010); even a powerful thunderstorm can change the pressure as much as 3,660 Pa/hour (Francart and Beiter, 1997). Other studies reported an average 270 Pa/hour fluctuation in South African mines (Fauconnier, 1992), between 70 and 148 Pa/hour in Australian mines (Belle, 2014), and as high as 3,000 Pa over the course of 30 hours in a Polish mine (Wasilewski, 2014). Based on this information, the researcher selected various rates between 50 and 1,000 Pa/hour to analyze the rate effect on EGZ outgassing.

6.4.1 Scenario 3: Gradual Decrease of 100 Pa

In this scenario, the pressure condition was simulated to drop by 100 Pa at two different rates, 50 and 100 Pa/hour. Figure 6.20 shows the pressure profiles at six monitoring points within the gob, A through F, as a function of 50-Pa/hour drop, represented by dotted lines, and 100-Pa/hour drop, marked by solid lines. The case with the 50-Pa/hour rate took twice as long as the 100-Pa/hour scenario to drop by 100 Pa.

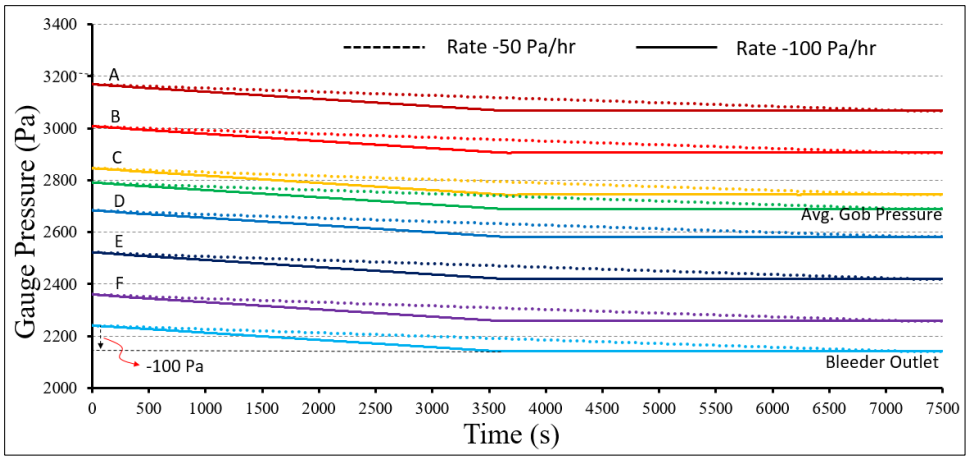

Figure 6.20: Pressure changes within the gob during gradual pressure drops

Figure 6.21 shows the EGZ condition within the gob after two hours, at which a steady condition is reached in both cases. The EGZ profiles appear identical in both cases, noting the insignificance of the rate decrease in overall outgassing condition.

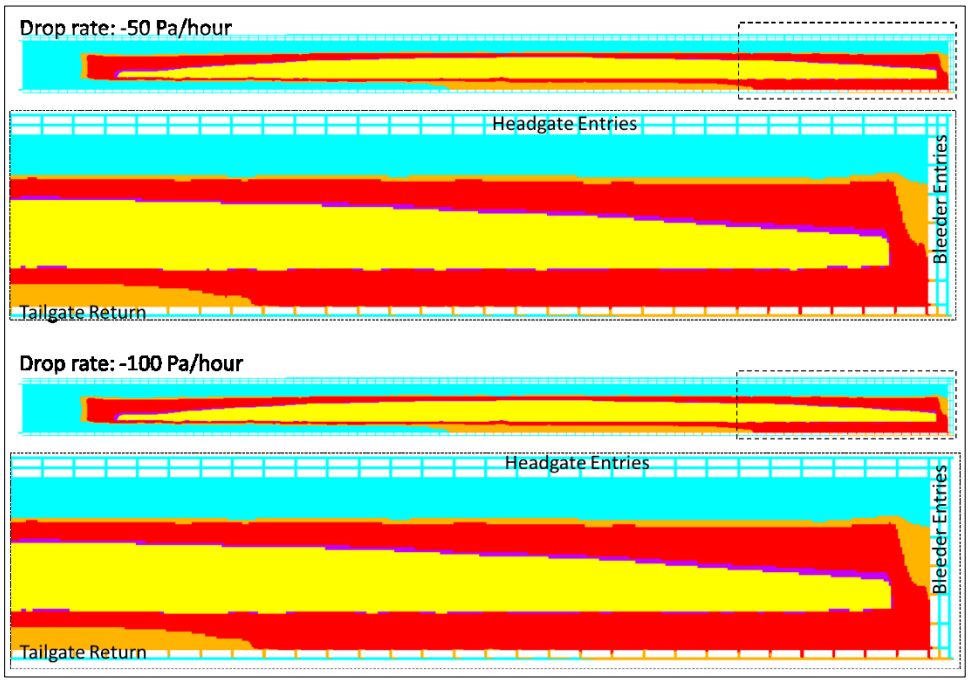

Figure 6.21: EGZ profile along the horizontal plane view at t=7200s of pressure drop

The above finding is also noted from the normalized volume trends shown in Figure 6.22. The blue and red lines represent two scenarios showing distinct trends of EGZ volume change, but

eventually (after two hours when both scenarios reach steady pressure condition) the EGZ volume within the gob is found to be comparable. Further, the EGZ increase in the gob is concurrent with the EGZ reduction in the fractured zone – a similar condition observed in instantaneous drop scenarios (Scenario 1 in Section 6.3.1). The minimum to maximum normalized EGZ volume in the gob shown in Figure 6.22 is equivalent to slightly over 0.4% of total EGZ volume. This reduction translates to 13% increase in EGZ outgassing monitored at tailgate return (Figure 6.23). The methane concentration at the bleeder tap increases to 2.1% after two hours.

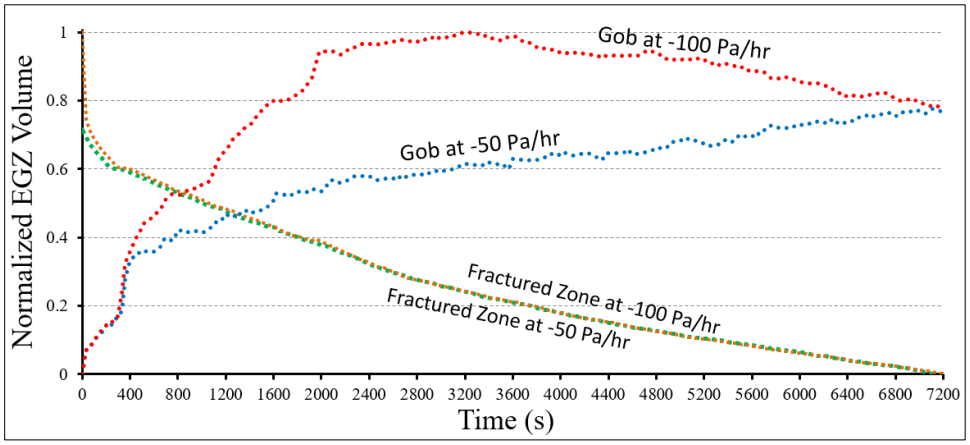

Figure 6.22: Normalized EGZ volume in the fractured zone and within the gob

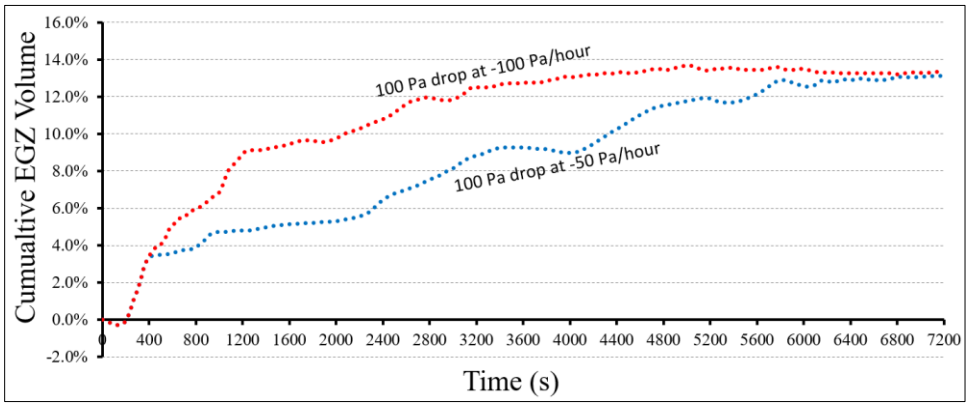

Figure 6.23: Total volume of EGZ outgassing at tailgate return after two hours

6.4.2 Scenario 4: Gradual Decrease of 1,000 Pa

In this scenario, the modeling simulates a falling pressure of 1,000 Pa at two different rates, 500 and 1000 Pa/hour. Figure 6.24 shows the pressure changes monitored at points A through F within the gob associated with this falling pressure. The 500-Pa/hour case reaches a 1,000-Pa drop in two hours, and the 1,000-Pa/hour case reaches it in 1 hour.

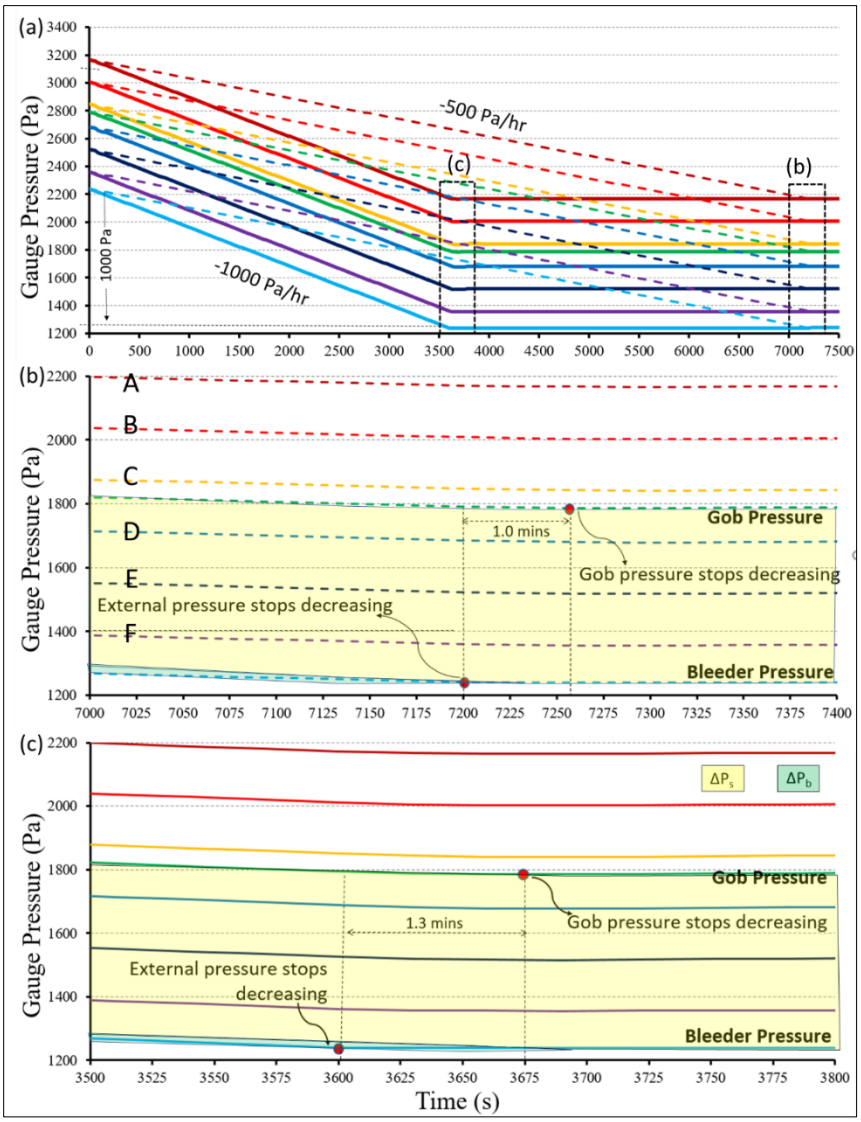

Figure 6.24: Pressure changes within the gob during gradual pressure drops

Figure 6.24(b) and (c) are insets to show the pressure condition near equilibrium. In Figure 6.24(b), the external pressure stops decreasing at t=7200s, but the gob pressure continues dropping

until t=7260s. Figure 6.24(c) shows a similar but longer delay for the 1,000-Pa/hour case. The gob lags 1-1.3 minutes behind the external pressure, which are much shorter than those in instantaneous drop scenarios, suggesting its dependency on the drop rate.

As learned in Scenario 3, the EGZ formation would be comparable for two cases with the same magnitude of pressure drop, though the change rates are different. This is also observed in this scenario. Figure 6.25 shows that the contours of the EGZ in the horizontal view within the gob and crosscuts show a similarity. In both cases, the EGZ is largely found within the last eight tailgate crosscuts from the back end, and along the roof as a result of buoyancy (Figure 6.26).

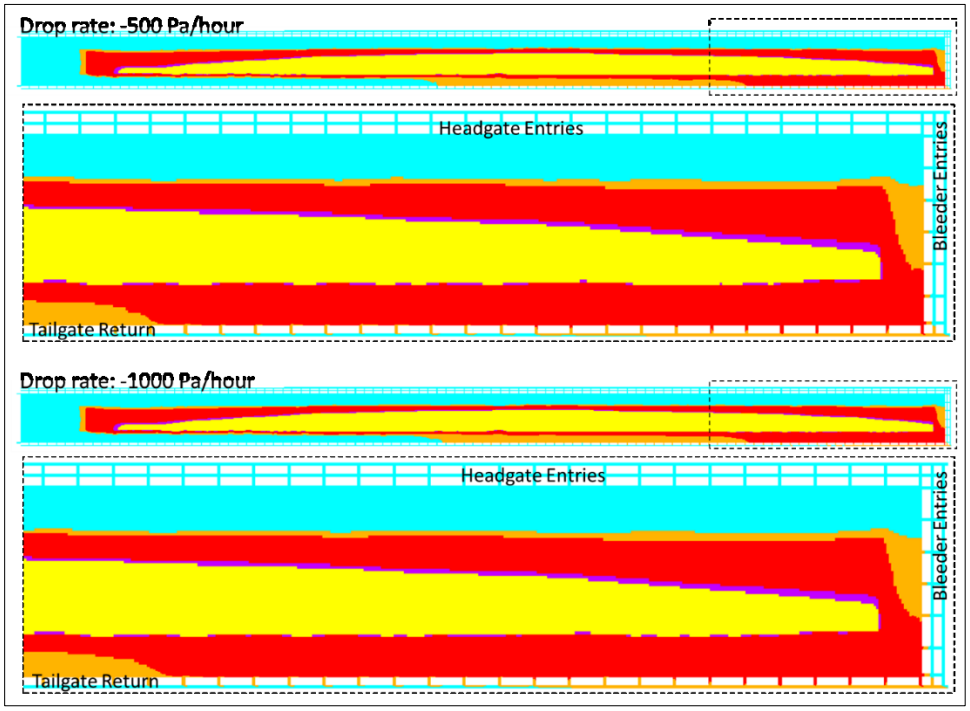

Figure 6.25: EGZ profile along the horizontal plane view at t=7200s of pressure drop

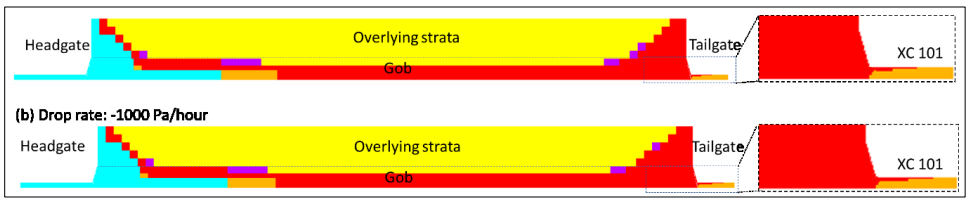

Figure 6.26: EGZ profile in the vertical section along XC 101 at t=7200s of pressure drop

Figure 6.27 shows that, in both cases, the EGZ volume within the gob increases while decreasing in the fractured zone. This reflects the condition observed in the instantaneous pressure drop (Section 6.3.1). The decrease in external pressure induces a higher methane influx from above the fractured zone, which forces the EGZ in the fractured zone to flow down to the gob. The pressure in the fractured zone is relatively maintained by the constant pressure of the methane inlet and thus, the outside fluctuation rate may have little impact on the EGZ in the fractured zone. As a result, the green and orange trends appear to be alike. The increase from 0 to 1 rank in normalized scale is equivalent to 2% of the total EGZ volume in the gob.

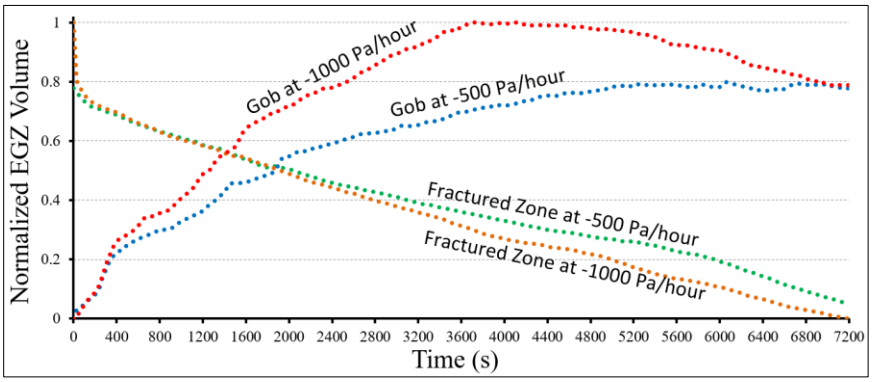

Figure 6.27: Normalized EGZ volume in the fractured zone and within the gob

In both cases, the EGZ outgassing from the gob to the tailgate return increases by 21% after two hours (Figure 6.28). This outgassing volume equals an approximate 1.6% reduction of the EGZ from within the gob. The red and blue lines reflect two different rates; one reaches maximum value at around t=3600s while the other reaches it around t=7200s. At the end of two hours, both lines approximately reach the same total outgassing volume. It leads to a conclusion that the total outgassing volume primarily depends on the magnitude, not the rate, of pressure drop.

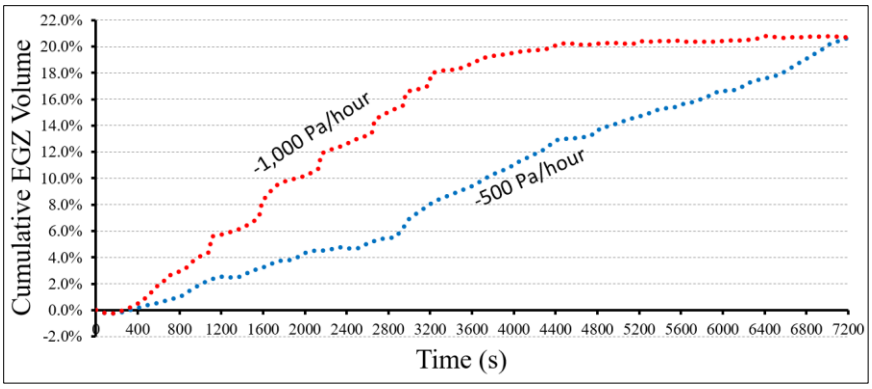

Figure 6.28: Total volume of EGZ outgassing at the tailgate return after two hours

6.5 Summary of the Effect of Pressure Change on the EGZ

There are four scenarios simulated to analyze the effect of external pressure changes on the EGZ in the gob. Table 6.1 shows the results of each simulation. The lag of the gob response to the external pressure changes depends on the gob's porous medium characteristics, distance from the surface, the magnitude and the rate of external pressure changes. A prolonged time lag is observed in the very low permeability gob located far from the inlets or outlets after great and sudden pressure changes.

Table 6.1 also indicates that total outgassing volume is a function of the magnitude of pressure changes. The volume of EGZ outflow from the gob is relatively comparable for scenarios with the same magnitude of changes, regardless of the change rates. The rate of pressure changes determines the rate of outgassing; therefore, a sudden change causing an abrupt outgassing in the beginning which would slow down after certain period of time. In contrast, a gradual pressure fall causes a more consistent, steadier outgassing over time. In all cases, outflow primarily occurs through the last 10 tailgate crosscuts near the bleeder tap, a combination of methane expanding and mixing with outside air and the increasing methane influx from the source above the fractured zone. The increasing methane influx (in m^3/s) is also shown in Table 6.1.

Table 6.1: Summary of simulation results

Simulated Condition	Magnitude of Pressure Change (Pa)	Rate of Pressure Changes	Time Lag (mins)	After Two Hours of BP Changes				
				Total EGZ Outgassing in TG Return (m^3)	Total EGZ Outgassing (%)	Methane Inflow (m^3/s)	CH_4 Conc. at Bleeder Outlet (%)	Potential Location of EGZ Outgassing
Scenario 1: Instantaneous Pressure Drop	-100	Instantaneous	1.2	700	13.2	1.10	2.0	Tailgate return, bleeder entry
	-500		1.8	790	14.7	1.30	2.1	Tailgate return, bleeder entry
	-1,000		2.1	1,110	20.7	1.50	2.2	Tailgate return, bleeder entry
	-2,000		2.8	1,730	32.3	2.10	2.4	Tailgate return, bleeder entry
Scenario 2: Instantaneous Pressure Rise	+500	Instantaneous	1.2	-110	-2.1	0.80	1.0	No outgassing observed
	+1,000		2.1	-120	-2.2	0.80	1.0	No outgassing observed
Scenario 3: Gradual Pressure Decrease of 100 Pa	-100	-50 Pa/hour	< 0.5	700	13.2	1.10	2.0	Tailgate return, bleeder entry
	-100	-100 Pa/hour	< 0.5	710	13.4	1.10	2.0	Tailgate return, bleeder entry
Scenario 4: Gradual Pressure Decrease of 1,000 Pa	-1,000	-500 Pa/hour	1.0	1,110	20.7	1.50	2.2	Tailgate return, bleeder entry
	-1,000	-1000 Pa/hour	1.3	1,110	20.8	1.50	2.2	Tailgate return, bleeder entry

CHAPTER 7

EVALUATION OF MITIGATION MEASURES

This chapter includes a high-level evaluation of recommendations for prevention and mitigation measures on EGZ outgassing. The main goals of this evaluation are to prevent EGZ outflow during barometric pressure fluctuations, but if it eventually occurs there are early warning and plans in place to mitigate the issue. The discussed methods include the development of a risk matrix, best practices in monitoring techniques, and the application of GVBs.

7.1 Risk Matrix for EGZ Outgassing

The results obtained from the modeling demonstrate the influence of gob permeability characteristics, longwall panel dimensions, pressure conditions, methane sources and other mine specific parameters. Though the EGZ outgassing location and trends from various rates and magnitudes of barometric or external pressure changes are considered to be similar from one mine to another, quantitative indicators such as outgassing volume and absolute methane concentration can be different. Therefore, each mine operator should conduct their own analysis on the impact of barometric pressure fluctuations. Understanding the effects of barometric pressure fluctuations on gob breathing does not itself prevent EGZ outgassing from occurring, particularly due to the fact that the bleeder system is designed to leak contaminated gas from the gob. However, such understanding accommodates any effort of determining a response plan to prevent EGZ outgassing from becoming a disastrous mine explosion.

The response plan can be developed in the form of a risk matrix similar to the one shown in Table 7.1. The risks are ranked based on the likelihood and consequence criteria. The likelihood can be defined from historical data, and is categorized from “Rare” to “Likely.” The consequence

consists of "Insignificant" to "Severe," which are determined by the magnitude and rate of drop, and the measured methane concentration at the tailgate return. Tables 7.2 through 7.3 are represented only as an example to illustrate rating criteria. This should be tailored to accommodate the parameters that are of interest of the mine.

Table 7.1: Example of a risk matrix for EGZ outgassing due to barometric pressure changes

Likelihood	Consequence			
	Severe	Moderate	Minor	Insignificant
Likely	Extreme	High	Medium	Medium
Possible	High	Medium	Medium	Low
Unlikely	Medium	Medium	Low	Low
Rare	Medium	Medium	Low	Low

Table 7.2: Example of likelihood criteria

Rating	Definition
Rare	Frequency of occurrence expected to be less than 2 times in a year Occurs in summer season
Unlikely	Frequency of occurrence expected to be 2-5 times in a year Occurs in summer season
Possible	Frequency of occurrence expected to be 5-10 times in a year May occur in fall and spring seasons
Likely	Frequency of occurrence expected to be 20 times or more in a year Will most likely occur in hurricane and winter seasons

Table 7.3: Example of consequence criteria

Rating	Definition
Insignificant	Magnitude of drop ≤ 50 Pa Instantaneous or gradual Negligible outgassing
Minor	Magnitude of drop between 50 – 100 Pa Instantaneous drop Gradually decreases < 50 Pa/hour Methane concentration at tailgate BEP reaches 2%
Moderate	Magnitude of drop between 100 – 1000 Pa Instantaneous drop Gradually decreases > 50 Pa/hour Methane concentration at tailgate BEP reaches 2-5.5%
Severe	Magnitude of drop > 1,000 Pa Instantaneous drop Gradually decreases > 50 Pa/hour Methane concentration at tailgate BEP reaches 5.5% and higher

The recommended mitigation plan should be developed based on the pre-determined risk matrix rank. For a low-risk rank, the mine operation may only need to take more frequent methane readings at the tailgate return and BEPs, and potentially adjust ventilation to ensure outgassing is well diluted. In the most extreme cases, the miner may need to temporarily stop the operation and start evacuation while a ventilation adjustment is ongoing. Table 7.4 shows an example of a recommended mitigation plan.

Table 7.4: Example of mitigation plan for the risk matrix

Rating	Recommended Mitigation Plan
Extreme	Operation halt, power equipment deenergized, miners should be evacuated from the active panel, continuous atmospheric monitoring, ventilation adjustment
High	Operation halt, power equipment deenergized, more frequent monitoring, ventilation adjustment
Medium	Power equipment deenergized, more frequent monitoring, ventilation adjustment
Low	More frequent monitoring, ventilation adjustment

The risk matrix and mitigation plan above are shown for guideline purposes. As EGZ outgassing is found to be a mine-specific phenomenon, the risk criteria and mitigation plan should be developed exclusively and specifically for each mine. Since barometric pressure fluctuation is strongly affected by the weather, this plan may need to be developed differently for each season.

7.2 Real Time Monitoring System and Location

In most underground longwall operations, bleeder systems must be monitored once a week at the BEPs using a handheld gas detector (MSHA, 2008). Monitoring methane concentration and the EGZ within the gob is difficult, but the ability to measure them outside in the immediate surrounding entries will give an indication of how well the bleeder system is functioning. Handheld gas detectors are one of the real-time detection systems available to measure mine atmosphere, however, a detector also requires a miner or ventilation specialist to be directly exposed to the

methane-air mixture it is measuring. A real-time or telemetric monitoring system is considered better for this situation. The system is strategically placed where gas measurements are needed, and then sends that measurement to the surface without having any mine personnel in contact with the mixture. The disadvantage of this system is that each individual sensor in this system must be calibrated regularly (Brady, 2008) so it is more suitable for short-term monitoring in the accessible areas, such as in walkable bleeder entries.

Tube bundle and gas chromatography techniques are suited for long-term monitoring in the tailgate return without needing to re-access the end sampling point. This technique is best for monitoring explosibility in the gob perimeter (Brady, 2008; Zipf et al., 2013a, 2013b), though results availability is not immediate. Due to the nature of constantly changing barometric pressures, a continuous monitoring system is the ideal method to measure methane concentrations in surrounding entries as result of gob breathing.

The simulation outputs indicate that fringes of explosive mixtures form around the perimeter of the gob. The bleeder system appears to have been the most effective behind the shields, pushing EGZ further inby six crosscuts or approximately 400 m (~1,300 ft) from the longwall face. The system also has effectively diluted the 50-m (164-ft) area of the gob along the headgate side as well as the setup room corner on the headgate side. However, this does not mean the explosive mixtures are rendered. It only pushes the fringe of the EGZ further into the gob towards the bleeder entries. The worst conditions with a high concentration of methane are found to be in the tailgate return near the setup room and in the immediate bleeder entry adjacent to the gob. Therefore, it is recommended mines install continuous monitoring sensors, such as tube bundle, in the tailgate return downstream of the last crosscut that connects to the gob. Other short-term monitoring system like telemetric sensors can be placed along the walkable bleeder entries

or at other accessible BEPs with an alarm placed in the control room and throughout the mine. The alarm would occur for a magnitude and rate of change over prescribed period per methane concentration requirement and specifications of the mine.

7.3 Gob Ventilation Borehole Application

Bessinger et al. (2005), Karacan (2008) and Saki et al. *(*2015) demonstrated the effectiveness of the Gob Ventilation Borehole (GVB) application to reduce EGZ formation in the gob and prevent methane emission to the active working areas. Though GVBs are normally used in a bleederless system with a sealed gob, the function of this application is practically feasible in reducing or even preventing barometric pressure-induced outgassing to the surrounding entries.

Using the same concept as in a bleederless system, a GVB is placed where the accumulation of methane or the EGZ occurs. From the modeling output, the gob area on the tailgate-bleeder corner, which is previously a part of the setup room, is considered the best location for this GVB. In this area, the accumulation of the EGZ is observed; a single or multiple GVBs can be set up from the surface down to this location (Figure 7.1). Due to its proximity to the bleeder tap, this location will continually have the lowest pressure across the entire gob during mining, and thus this GVB can be used over the life of the panel if it is maintained open over time. The GVB can also be operated from the mine surface as the EGZ begins to accumulate in the area or when the barometric pressures start decreasing.

Depending upon the effectiveness of this application, multiple GVBs may be required for better coverage of pulling force or replacement of dysfunctional GVBs. If multiple GVBS are to be used, it is suggested to have these GVBs placed within the gob along the tailgate side, 18-35 m into the gob and between crosscuts XCs 85-102, where the base case simulation shows accumulation of the EGZ (Figure 6.2). Saki et al. (2015) found that GVB flow is maximized at

approximately 18 m (60 ft) from the tailgate side. Due to its practicability and promising result shown in other studies, further research is suggested to determine the optimized location of this application for a bleeder-ventilated panel.

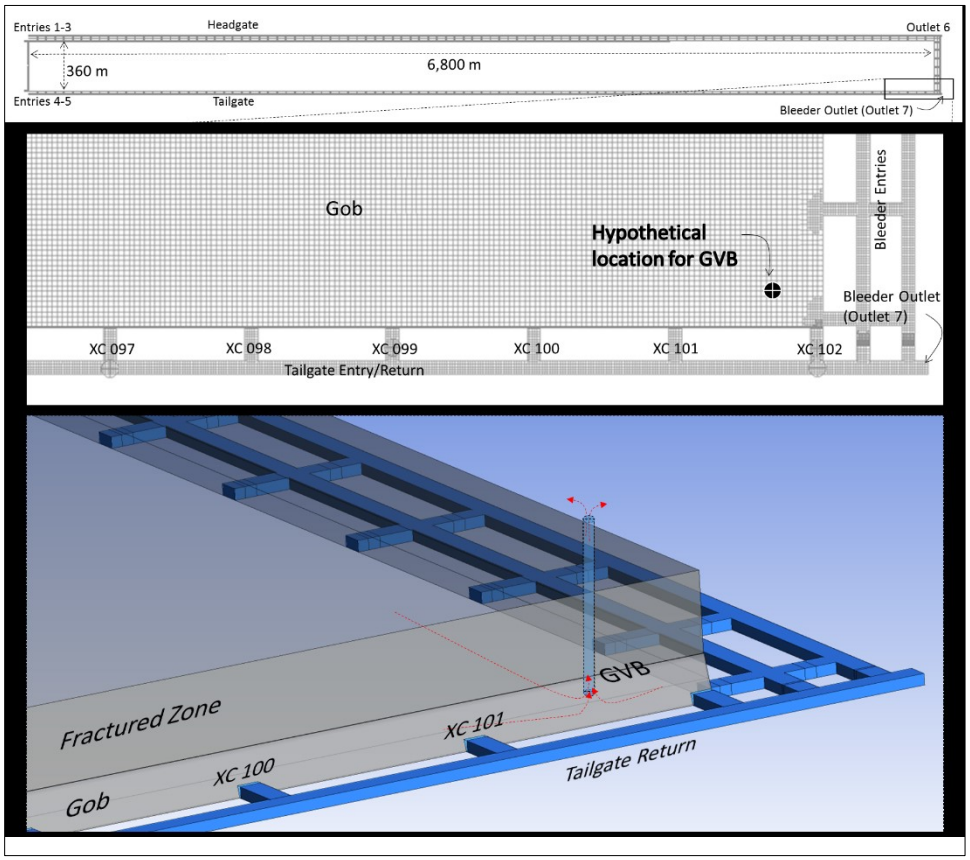

Figure 7.1: Hypothetical location for GVB application

CHAPTER 8

CONCLUSIONS

External barometric pressure fluctuations have been widely known to cause gob breathing in longwall mines. However, the detailed cause-effect relationship between the fluctuations and gob breathing is not well understood. Most past studies focused on a statistical review of coal mine explosions during intense fluctuations of barometric pressure in an effort to understand this connection. This research presents a new approach of using a CFD model to analyze the gob breathing phenomenon and its correlation with external pressure changes. The following section summarizes the findings based on trends observed from CFD modeling outputs.

- Throughout the modeling, fringes of EGZ are shown to exist within the caved gob before, during and after external pressure changes. This finding is in agreement with other studies and observations made from a number of bleeder-ventilated mine fire and explosions (Kissell, 2006; Brune, 2013; Gilmore, 2015).
- Outside the gob, the EGZ presents in several crosscuts along the tailgate return and the bleeder entries in the back end of a panel (setup room). These are also the most likely locations for EGZ outgassing during pressure drops, which is concerning due to their proximity to miners' activities.
- When the external pressure changes, the air pressure in mine workings and entries changes almost instantaneously, a finding in agreement with experimental studies conducted by Stevenson (1968) and Wasilewski (2014). In this study, pressure waves propagate at the speed of sound in mine entries, but they experience delays when propagating within the gob zone. This delay or time lag varies by gob permeability, the distance to surface above ground

and the magnitude and rate of pressure change. For example, a low-permeability gob located deep underground would have a longer time lag.

- CFD simulations report that gob pressures lag between 0-3 minutes when barometric pressures change by 100-2,000 Pa. The greater the magnitude and rate of pressure change, the longer the resulting time lag. The lag causes a pressure differential between the gob and surrounding entries that is greater in a falling pressure scenario, and smaller in a rising pressure scenario. A greater pressure differential induces more EGZ outgassing, whereas the other case reduces the outgassing and potentially causes air ingress.
- Against conventional wisdom, CFD simulations show that rising outside pressure propels more oxygen into the gob, but it does not necessarily cause the EGZ volume to increase within the gob. The ingressing air dilutes the outer EGZ fringes and "squeezes" them further into the gob. The rising barometric pressure appears to negate the effectiveness of a bleeder system by preventing gob leakage toward the tailgate return, which on one hand is actually favorable as it eliminates EGZ outgassing to the surrounding entries.
- A sudden, abrupt fall of barometric pressure is more concerning than a gradual decrease. A sudden fall immediately generates a large pressure differential, which potentially induces a high amount of EGZ outgassing to the tailgate return in a short time. If this area is not well diluted, this EGZ inundation poses a serious explosion threat. In contrast, a slow pressure drop causes a steady, constant outgassing over time, which should be swept out quickly by the ventilation air.
- Total EGZ outgassing volumes depend on the magnitude of a pressure drop, regardless of the rate of change. Both an instantaneous and a gradual decrease scenarios would result in relatively the same EGZ outgassing volume after pressure falling by the same magnitude.

Overall, CFD modeling reports a 13% to 32% increase of EGZ volume in the tailgate return due to 100-2,000 Pa pressure drops. In addition, pressure drops of less than 100 Pa cause negligible EGZ outgassing. For comparison, Belle's (2014) experiments in Australian mines indicated that a significant increase of methane in tailgate return was attributed to barometric pressure decreases greater than 500 Pa, while Fauconnier (1992) suggested a potential danger for the studied South African mines if pressure drops in excess of 270 Pa.

- The methane inflow from the inlet above the fractured zone slightly increases with decreasing external pressures. Thus, methane concentrations recorded at the bleeder tap are higher for greater pressure drops.
- Though this study has primarily concentrated on methane outflow from the gob during failing barometric pressure, the oxygen concentration is also monitored in work areas and bleeder entries as it can affect the continuation of the mine operation if below 19.5% as per regulation 30 CFR §75.321. In all scenarios simulated in this study, the minimum 19.5% of oxygen concentration is recorded in active working area and bleeder entries, showing the sufficient fresh air in the areas outside of the gob.
- EGZ outgassing is strongly influenced by the mine condition. Since it is a mine-specific issue, a mine operator can implement CFD modeling to conduct in-house analyses and develop a response plan in the event of barometric pressure fluctuations. The plan should include preventive and mitigation measures such as developing a risk register for EGZ outgassing based on likelihood and consequence, placing GVBs around the bleeder-tailgate corner where EGZ accumulates, and placing continuous monitoring systems (e.g., tube bundle system, gas chromatography and other telemetric sensors) in strategic locations.

- Per the modeling trend of the EGZ outgassing locations and the fact that barometric pressures are constantly changing, continuous monitoring systems should be placed primarily in the tailgate return at the back end of the panel and along the bleeder entries because EGZ outgassing mostly occurs through the last 10 crosscuts on the tailgate side near the bleeder tap. Other short-term monitoring system like telemetric sensors can be placed along the walkable bleeder entries or at other accessible BEPs with an alarm placed in the control room and throughout the mine. The alarm would occur for a magnitude and rate of change over prescribed period per methane concentration requirement and specifications of the mine.

CHAPTER 9

SUGGESTIONS FOR FUTURE WORK

The implications of this research for future work and model improvement are detailed in the following chapter, including model geometry, modeling parameters and the explosive mixture definition.

9.1 Improvements to Longwall Face Mesh

The face model includes a total of 175 shields with a square gap of 0.6 m (1.95 ft) x 0.6 m (1.95 ft) in the back section of each shield for face leakage airway. In actual condition, the gaps between shields may also provide significant channel for fluid flow from the face to the gob and should be included. This gap was not modeled in this research as it potentially creates a very high aspect ratio mesh due to the thin shape of the gap.

9.2 Improvements to Modeling Parameters

The unknown conditions of the methane inlet and gob characteristics are the largest sources of error in this modeling. The following are some suggested improvements:

- The only methane source considered in this modeling is the rider seam at the top of overlying strata or fractured zone. Other emission sources such as a lower seam, face, ribs, coal on the belt conveyor and coal within the gob should also be included in the model.
- Methane gas enters the model from a surface above the fractured zone or overlying strata at a constant pressure which is assumed to be an infinite reservoir. Future work must consider a depleting methane source as opposed to an infinite reservoir. In addition, the

methane gas is pushed uniformly from a large surface, which is arguably a major assumption when considering the dynamic of a longwall mine.

- The gob permeability has a tub-like shape on a horizontal plane but no variation with height has been considered thus far. Esterhuizen and Karacan (2007) recognized a variation of gob material packing during gob compaction in vertical direction, thus, the additional profile in vertical direction, i.e., higher permeability values as the height increases would be more appropriate. However, such variations are difficult to model as the gob is inaccessible for validation.
- Due to the modeling condition for ideal gas that requires a non-negative and non-zero pressures as boundary conditions, the modeling is conducted in a positive pressure system. It is necessary to carry out the modeling under the scheme of exhaust ventilation system for comparison.

9.3 Definition of Explosive Mixture

The Coward's diagram used in this research for the explosibility indicator is based on Coward and Jones' laboratory experiments (Coward and Jones, 1952). The results were attributed to the temperature, pressure, humidity and other laboratory conditions during the experiments. The diagram may shift or change for the gob, especially if spontaneous combustion exists. The presence of other flammable gases, such as carbon monoxide and hydrogen in the gob, can also change the explosibility of a methane-air mixture. This variation is not considered in this modeling, as the researcher assumed only methane and air components were present in the gob and that no spontaneous combustion event was taking place. The inclusion of other common gases found in the gob in the modeling may give a better prediction of EGZs in an actual mine condition.

9.4 Further Investigation on Study Recommendations

The application of Gob Ventilation Borehole (GVB) has been commonly used in longwall mines for methane drainage and is considered practicable for preventing outgassing from occurring toward the tailgate return. Further study is required to determine the effectiveness of this GVB based on specific mining conditions. In addition, a variable speed mine fan is technically capable of countering the effect of barometric pressure fluctuation on mine atmosphere. Currently, this type of fan is not considered legally and economically viable due to regulation restriction of using variable fan pressure in coal mines. The fact that barometric pressures continuously change may also negate the effectiveness of this mechanically-adjusted fan, calling for further research on automation system.

9.5 Ultimate Validation of Simulation Results

The modeling parameters are collected and validated against actual mine measurements, and the simulation results are also verified with published data and common practices in the mine. The availability of mine data modeled in this research is very limited for validation. This is due to the sensitivity of such data and the difficulties of getting data within the gob and tailgate return, areas which may be inaccessible. The ultimate validation of this research, which is not possible in this research, is comparing the modeling results against the actual measurement of EGZ outgassing volumes or methane concentration variations at different barometric pressure conditions in the modeled mine.

REFERENCES CITED

Alpha Natural Resources, Inc. "Alpha Natural Resources to permanently close Upper Big Branch Mine. Company Release, April 4, 2012." Accessed online on September 24, 2015: http://ir.alphanr.com/Mobile/file.aspx?IID=4100842&FID=13080816.

ANSYS, Inc., *Ansys Fluent Theory Guide.* Release 15.0. SAS IP, Inc.: Canonsburg, PA, 2013.

Balusu, R., Rent, T.X., and Humphries, P. "Proactive Inertisation Strategies and Technology Development." In ACARP Project C12020. CSIRO Exploration and Mining, Australia, 2005.

Balusu, R., Xue, S., Wendt, W., Mallet, C., Robertson, S.B., Holland, R., Moreby, R., Mclean, D., and Deguchi, G. "An Investigation of the Gas Flow Mechanics in Longwall Goafs." In *Proceedings of the North American/9th US Mine Ventilation Symposium*, edited by E. D. Souza. 443-450. Kingston, Canada: Taylor & Francis, 2002.

Bear, J. *Dynamics of Fluid in Porous Media*. American Elsevier Publishing Company, Inc.: New York, USA, 1972.

Belle, B. "Evaluation of Barometric Pressure (BP) and Cage Effect on Longwall Tailgate Gas Levels." In *Proceedings of the 10th International Mine Ventilation Congress,* 501-511. Sun City, South Africa: MVSSA, 2014.

Bessinger, S.L., Abrahamse, J.F., Bahe, K.A., McCluskey, G.E., and Palm, T.A. "Nitrogen Inertization at San Juan Coal Company's Longwall Operation." *Preprint of the Society for Mining, Metallurgy and Exploration Annual Meeting* (2005): 05-032.

Boyer, R.F. "Coal Mine Disaster: Frequency by Month." *Science* 19 Vol. 144 No. 3625 (1964): 1447-1449.

Boxho, J., Stassen, P., Mücke, G. Noack, K., Jeger, C., Lescher, L., Browning, E., Dunmore, R., Moris, L. *Firedamp Drainage: Handbook for the coal mining industry*. Verlag Glückauf GmbH: Essen, 1980.

Brady, D. "The Role of Gas Monitoring in the Prevention and Treatment of Mine Fires." In *Proceedings of the Coal Operators' Conference*, edited by Naj Aziz, 202-208. University of Wollongong, Wollongong: AusIMM, 2008.

Brier, G.W. "Diurnal and Semidiurnal Atmospheric Tides in Relation to Precipitation Variations." *Monthly Weather Review* Vol. 93 No.2 (1965): 93-100.

Brune, J.F. "Methane-Air Explosion Hazard within Coal Mine Gobs." *Trans. Soc. Min., Metall., and Explor.* Vol. 334 (2013): 376-390.

Brune, J.F., Grubb, J.W., Bogin Jr., G.E. Marts, J.A., Gilmore, R.C., and Saki, S.A. "Lessons Learned from Research about Methane Explosive Gas Zones in Coal Mine Gobs." *International Journal of Mining and Mineral Engineering* Vol. 7 No. 2 (2015):155-169.

Brunner, D.J. "Ventilation Models for Longwall Leakage Simulation." In *Proceedings of the 2nd U.S. Mine Ventilation Symposium*, edited by P. Mousset-Jones, Reno, NV: AIME, 1985.

Calizaya, F., Duckworth, I.J., and Wallace, K.G. "Studies of Air Leakage in Underground Mines using Computational Fluid Dynamics." In *Proceedings of the 10th US/North American Mine Ventilation Symposium*, edited by S. Bandopadhyay and R. Ganguli, 417-424. Anchorage, AK: SME, 2004.

Carico, A.D. "Report of Investigation Methane Ignition/Explosion/Mine Fire Accident, February 14, 2015 at Buchanan Mine #1, Consolidation Coal Company. ID No. 44-04856." U.S. Department of Labor, MSHA, 2006.

Carman, P.C. *Flow of Gases through Porous Media*. Academic Press: New York, 1956.

Carter, W.H.N., and Durst, C.S. "The Influence of Barometric Changes on the Emission of Firedamp." *Trans. Inst. Min. Eng*. 115 (1955):3-29.

Cervik, J. "Behavior of Coal-Gas Reservoirs." In *Technical Progress Report 10 Bureau of Mines Methane Control Program.* U.S. Department of the Interior, 1969.

Chapman, S. and Malin, S.R.C. "Atmospheric Tides, Thermal, and Gravitational: Nomenclature, Notation and New Results*." Journal of the Atmospheric Sciences* Vol. 27 No. 5 (1970): 707-710.

Cliff, D. and Bofinger, C. "Dissemination of Information on Spontaneous Combustion." In *Australian Coal Association Research Program* No. C600, Safety in Mines Testing and Research Station (SIMTARS), 1998.

Colinet, J.F., Rider, J.P., Listak, J.M., Organiscak, J.A., and Wolfe, A.L. "Best Practices for Dust Control in Coal Mining." *Information Circular* 9517. Centers for Disease Control and Prevention. National Institute for Occupational Safety and Health, 2010.

Coward, H.F., and Jones, G.W. "Limits of Flammability of Gases and Vapors." *Bulletin* 503. U.S. Bureau of Mines, 1952.

Dai, A. and Deser, C. "Diurnal and Semidiurnal Variations in Global Surface Wind and Divergence Fields." *Journal of Geophysical Research* Vol. 104, No. D24 (1999): 31109-31125.

Dallegge, T.A., and Barker, C.E. "Coal-Bed Methane Gas-in-Place Resource Estimates using Sorption Isotherms and Burial History Reconstruction: An Example from the Ferron Sandstone Member of the Mancos Shale, Utah." In *Geological Assessment of Coal in the Colorado Plateau: Arizona, Colorado, New Mexico, and Utah* PP 1625-B. U.S. Geological Survey, 2000.

Dershowitz, W., LaPointe, P., Eiben, T., and Wei, L. “Integration of Discrete Feature Network Methods with Conventional Simulator Approaches.” In *SPE* 49069. Society of Petroleum Engineers, 1998.

Diamond, W.P., Ulery, J.P., and Kravits, S.J. “Determining the Source of Longwall Gob Gas: Lower Kittaning Coalbed, Cambria County, PA.” In *Report of Investigations* No. 9430. U.S. Bureau of Mines, 1992.

Diamond, W.P., Schatzel, S.J., Garcia, F., LaScola, J.C., McCall, F.E., Jeran, P.W., and Mucho, T.P. “Characterization of Gas Flow in Longwall Gobs: Pittsburgh Coalbed.” In *Proceedings of the International Coalbed Methane Symposium*, 233-244. Tuscaloosa, AL: University of Alabama, 1999.

Dougherty, H., Karacan. C., and Goodman, G. “Reservoir Diagnosis of Longwall Gobs through Drawdown Tests and Decline Survey Analyses of Gob Gas Venthole Productions.” *International Journal of Rock Mechanics and Mining Sciences* 47-5 (2010): 851-857.

Dubaniewicz, Jr. T.H., and Chilton, J.E. “Remote Fiber-Optic Methane Monitor.” In *Report of Investigations* No. 9407. U.S. Bureau of Mines, 1992.

Dziurzynski, W., and Wasilewski, S. “Model and Experimental Studies in the Longwall Goaf under Methane Inflow Conditions.” In *Proceedings of the 14th US/North American Mine Ventilation Symposium,* edited by F. Calizaya and M. Nelson, 111-118. University of Utah, Salt Lake City, UT: SME, 2012.

Edwards, J.C. “CFD Analysis of Mine Fire Smoke Spread and Reserve Flow Conditions.” In *Proceedings of the 8th US Mine Ventilation Symposium*, edited by J.C. Tien, 417-422. Rolla, MO: SME, 1999.

Elkins, D.W., Luzik, S.J., and Lemon, J.O.D. “Report of Investigation Underground Coal Mine Fire, November 25, 1998, Willow Creek Mine, Cyprus Plateau Mining Corporation, Helper, Carbon County, Utah, ID No. 42-02113.” U.S. Department of Labor, MSHA, 2001.

Energy and Minerals Field Institute (EMFI). *Coal Mining Methods – EMFI Summary.* Colorado School of Mines: Golden, 2010.

Erdogan, S.S., Karacan, C.Ö., Okandan, E. “Use of Reservoir Simulation and In-Mine Ventilation Measurements to Estimate Coal Seam Properties.” *International Journal of Rock Mechanics and Mining Sciences* 63 (2013): 148-158.

Esterhuizen, G.S., and Karacan, C.Ö. “Development of Numerical Models to Investigate Permeability Changes and Gas Emission around Longwall Mining Panel.” In *Proceedings of Alaska Rocks, 40th US Symposium on Rock Mechanics*, 13-26, Anchorage, AK: AMRA, 2005.

Esterhuizen, G., and Karacan, C. “A methodology for determining gob permeability distributions and its application to reservoir modeling of coal mine longwalls.” *Preprint of the Society for Mining, Metallurgy and Exploration Annual Meeting* (2007): 07-078.

Esterhuizen, G., Mark, C., and Murphy, M.M. "Numerical model calibration for simulating coal pillars, gob and overburden response." In *Proceedings of the 29th International Conference on Ground Control in Mining,* 46-57. Morgantown, WV: ICGCM, 2010.

Fauconnier, C.J. "Fluctuations in Barometric Pressure as a Contributory Factor to Gas Explosions in South African Mines." *Journal of the South African Institute of Mining and Metallurgy* Vol. 92 No. 5 (1992): 131-147.

Fig, M.K., Bogin, Jr. G.E., Brune, J.F., and Grubb, J.W. "Experimental and Numerical Investigation of Methane Ignition and Flame Propagation in Cylindrical Tubes Ranging from 5 to 71 cm – Part 1: Effects of Scaling from Laboratory to Large-Scale Field Studies." *Journal of Prevention in the Process Industries* Vol. 41 (2016): 241-251.

Fiscor, S. "U.S. Longwall Operators Scale Back Production, U.S. Longwall Census." *Coal Age* Vol. 121 No. 2 (2016): 18-22.

Fleagle, R.G. and Businger, J.A. "An Introduction to Atmospheric Physics." *International Geophysics Series 2nd Ed.* Vol. 25. Academic Press: London, UK, 1988.

Foster-Miller, Inc. "Improved Ventilation of Sealed Mine Gob." *A Mining Research Contract Report* J0308029. U.S. Bureau of Mines, 1988.

Francart, W.J., and Beiter, D.A. "Barometric Pressure Influence in Mine Fire Sealing." In *Proceedings of the 6th International Mine Ventilation Congress*, edited by R. Ramani, 1-2. Pittsburgh, PA: SME, 1997.

Frette, V., Feder, J., Jossang, T., and Meakin, P. "Buoyancy-Driven Fluid Migration in Porous Media." *Physical Review Letters* Vol. 68. No. 21 (1992): 3164-3167.

Gates, R.A., Phillips, R.L., Urosek, J.E., Stephan, C.R., Stoltz, R.T., Swentosky, D.J., Harris, G.W., O'Donnel Jr., J.R., and Dresch, R.A. "Report of Investigation Fatal Underground Coal Mine Explosion, Sago Mine, Wolf Run Mining Company, ID No. 46-08791." U.S. Department of Labor, MSHA, 2007.

Gilmore, R.C., Marts, J.A., Brune, J.F., Worrall, D.M., Bogin Jr., G.E., and Grubb, J.W. "Control of Explosive Gas Zones in Longwall Gobs through Nitrogen Injection." In *Proceedings of the 23rd World Mining Congress*, Montreal, Canada: CIM, 2013.

Gilmore, R.C. "Computational Fluid Dynamics Modeling of Underground Coal Longwall Gob Ventilation Systems using a Developed Meshing Approach." Ph.D. diss., Colorado School of Mines, 2015.

Griffin, K.R. "Utilization and Implementation of Atmospheric Monitoring Systems in United States Underground Coal Mines and Application of Risk Assessment." Ph.D. diss., Virginia Polytechnic Institute and State University, 2013.

Grubb, J.W. "Preventive Measures for Spontaneous Combustion in Underground Coal Mines." Ph.D. diss., Colorado School of Mines, 2008.

Harris, M.F. “Pressure-Change Theory and the Daily Barometric Wave.” *Journal of Meteorology* Vol.12 (1954): 394-404.

Hartman, H.L., Mutmansky, J.M., Ramani, R.V., and Wang, Y.J. *Mine Ventilation and Air Conditioning 3rd Ed.* John Wiley & Sons, Inc.: Hoboken, NJ., 1997.

Hemp, R. “The Effect of Changes in Barometric Pressure on Mines in the Highveld of South Africa.” *The Journal of the South African Institute of Mining and Metallurgy* (1994): 13-146.

Ho, C.K., and Webb, S.W. *Gas Transport in Porous Media: Theory and Applications of Transport in Porous Media* Vol. 20. Springer: Netherlands, 2006.

Hoek, E., and Bray, J.W. *Rock Slope Engineering. Revised 3rd Ed.* Institute Mining and Metallurgy: London, UK., 1981.

Hosler, C.L. “Atmospheric Surface Pressure related to Coal Mine Explosions.” *Trans. Amer. Geophys*. Union, Vol. 29 No. 5 (1948): 607-612.

Hoover, H.C. and Hoover, L.H. *De Re Metallica (by Gregorius Agricola*). English translation. Dover Publications, Inc.: New York, USA, 1950.

Itasca, C.G. *Fast Lagrangian Analysis of Continua in 3-Dimension (FLAC 3D v. 5.0)*. Itasca Consulting Group: Minnesota, 2013.

Jell, S. “Electricity from natural gas surpasses coal for first time, but just for one month”. In *Today in Energy*. Energy Information Administration, 2015.

Joy Global. *Longwall Systems Product Overview*. Warrendale, PA, 2014.

Karacan, C.Ö., Diamond, W.P., Schatzel, S.J., and Garcia, F. “Development of Application of Reservoir Models for the Evaluation and Optimization of Longwall Methane Control System.” In *Proceedings of the 11th U.S./North American Mine Ventilation Symposium,* edited by J.M. Mutmansky and R.V. Ramani, 425-432. University Park, PA: Taylor & Francis, 2006.

Karacan, C.Ö. “Degasification system selection for US Longwall Mines using an Expert Classification System.” *Computers & Geosciences* 35 (2008): 515-526.

Karacan, C.Ö. 2009. “Reconciling Longwall Gob Gas Reservoirs and Venthole Production Performances using Multiple Rate Drawdown Well Test Analysis*.” International Journal of Coal Geology* No. 80 3-4 (2009): 181-195.

Karacan, C.Ö. “Prediction of Porosity and Permeability of Caved Zone in Longwall Gobs.” *Transport in Porous Media* Vol. 72 No. 2 (2010): 413-439.

Karacan, C.Ö. and Yuan, L. “Effect of Discrete Fracture Network Representation of Gob on Airflow Distribution near the Longwall Face.” In *Proceedings of the 15th North American*

Mine Ventilation Symposium, edited by E. Jong, E. Sarver, S. Schafrik, and K. Luxbacher, 15-59. Virginia Polytechnic Institute and State University, Blacksburg, VA: SME, 2015.

Kissell, F.N. *Methane Migration Characteristics of the Pocahontas No.3 Coalbed*. RI 7649. Bureau of Mines Report of Investigations: Pittsburgh, PA, 1972.

Kissell, F.N. *Handbook for Methane Control in Mining IC 9486*. National Institute for Occupational Safety and Health. Centers for Disease Control and Prevention: Pittsburgh, PA, 2006.

Kissel, F.N., Nagel, A.E., and Zabetakis, M.G. "Coal Mine Explosions: Seasonal Trends." *Science* Vol. 179 (1973):891-2.

Köppen, W. and Wegener, A. *The Climates of the Geological Past*. English Translation of "Die Klimate der Geologischen Vorzeit." Borntraeger Science Publishers: Berlin, Stuttgart, 1924.

Krog, R.B. "Critical Analysis of Longwall Ventilation Systems and Removal of Methane." Ph.D. diss., West Virginia University, 2016.

Krog, R.B., and Bise, C.J. 2009. "Investigation into the Practical Use of Belt Air at U.S. Longwall Operations." *Preprint of the Society for Mining, Metallurgy and Exploration Annual Meeting* (2009): 09-105.

Light, T.E., Herndon, R.C., Guley Jr., and Pruitt, M.E. "Report of Investigation Fatal Underground Coal Mine Explosion Darby No. 1 Mine, ID No. 15-18185." U.S. Department of Labor, MSHA, 2007.

Lindzen, R.S. "On the Theory of the Diurnal Tide." *Nature* 213 (1966): 1260-1261.

Lindzen, R.S. and Chapman, S. "Atmospheric Tides." *Space Science Reviews* 10 (1969): 3-188.

Loane, E.N., Bulloch, R.D., Carthew, J., Marshall, E., and Rowlands, D. "Report on an Accident at Kianga No. 1 Underground Mine." Warden's Inquiry, Queensland, Australia. 1975.

Lolon, S., and Calizaya, F. "Computational Fluid Dynamics Study on Hot Spot Location in Longwall Gob." *Mining Engineering* Vol. 61 No. 8 (2009): 36-41. Littleton, CO: SME, 2009.

Lolon, S.A., Gilmore, R.C., Brune, J.F., Bogin, G.E., Grubb, J.W., Zipf, R.K., Juganda, A., and Saki, S.A. "Effect of Decreasing Barometric Pressure on Explosive Gas Zones in Bleeder Ventilated Longwall Gobs." In *Proceedings of the 15th North American Mine Ventilation Symposium,* edited by E. Jong, E. Sarver, S. Schafrik, and K. Luxbacher, 439-444. Virginia Polytechnic Institute and State University, Blacksburg, VA: SME, 2015

Lolon, S.A., Brune, J.F., Bogin, Jr., G.E., Grubb, J.W., Saki, S.A., Juganda, A. "Computational Fluid Dynamics Simulation on the Longwall Gob Breathing." *International Journal of Mining Science and Technology* Vol. 27 Issue 2 (2017a):1-5.

Lolon, S., Brune, J., Bogin Jr., G., Grubb, J., Juganda, A. "Understanding Gob Outgassing Associated with Pressure Disturbances in Longwall Mine." In *Proceedings of the 16th North American Mine Ventilation Symposium*, edited by J. Brune, Colorado School of Mines, Golden, CO: SME, 2017b.

Lovoll, G., Meheust, Y., Maloy, K.J., Aker, E., Schmittbuhl, J. "Competition of Gravity, Capillary and Viscous Forces during Drainage in A Two-Dimensional Porous Medium, A Pore Scale Study." *Energy* 30 (2005): 861-872.

Lowndes, I.S., Silvester, S.A., Giddings, D., Pickering, S., and Hassan, A. "The Computational Modelling of Conveyor Belt Fires in Mine Galleries." In *Proceedings of the 8th International Mine Ventilation Congress*, 299-308. Brisbane, Australia: AusIMM, 2005.

Lynn, K.P., Maitland, J., Jones, H., Ross, K., and Kathage, B.A. "Report on an Accident at Moura No. 4 Underground Mine on Wednesday, 16th July 1986." Warden's Inquiry, Queensland, Australia, 1986.

Marts, J.A. "Nitrogen Injection in Progressively Sealed Longwall Gobs and the Formation of a Complete and Dynamic Seal." Ph.D. diss., Colorado School of Mines, 2015.

Marts, J.A., Gilmore, R.C., Brune, J.F., Bogin, Jr., G.E., Grubb, J.W., and Saki, S.A. "Dynamic Gob Response and Reservoir Properties for Active Longwall Coal Mines." *Mining Engineering* Vol. 66 No.12: 41-48. Littleton, CO: SME, 2014a.

Marts, J.A., Gilmore, R.C., Brune, J.F., Bogin Jr., G.E., Grubb, J.W., and Saki, S.A. "Accumulations of Explosive Gases in Longwall Gobs and Mitigation through Nitrogen Injection and Face Ventilation Method." In *Proceedings of the 6th Aachen International Mining Symposia*, 347-358. RWTH Aachen University, Aachen, Germany: 2014b.

McKinney, R., Crocco, W., Tortorea, J.S., Wirth, G.J., Weaver, C.A., Urosek, J.E., Beiter, D.A., and Stephen, C.R. "Report of Investigation, Underground Coal Mine Explosions, Creek Mine, Cyprus Plateau Mining Corporation, Helper, Carbon County, Utah. ID No. 42-02113." U.S. Department of Labor, MSHA, 2001.

McPherson, M.J. *Subsurface Ventilation and Environmental Engineering 1st Ed*. Chapman & Hall: New York, 1993.

Mine Safety and Health Administration (MSHA). *Historical Summary of Mine Disasters in the United States, Vol. II – Coal Mines*. U.S. Department of Labor, Coal Mine Safety and Health. Reprinted 2001: 1998.

Mine Safety and Health Administration (MSHA). *Bleeder and Gob Ventilation Systems*. Ventilation Specialist Training: Course Text. U.S. Department of Labor: 2002.

Mine Safety and Health Administration (MSHA). *Atmospheric Monitoring Systems Operator's Training Guide* 3188. U.S Department of Labor: 2008.

Mine Safety and Health Administration (MSHA). *Code of Federal Regulations Title 30 Mineral Resources, Parts 1 to 199.* The Office of the Federal Register National Archives and Records Administration. Washington, DC.: 2014.

Mine Safety and Health Administration (MSHA). *Fatality Statistics.* Accessed online from September 2014 through May 2015: http://www.msha.gov/ACCINJ/accinj.htm.

Mitchell, D.W. *Mine Fires: Prevention, Detection, Fighting*. Intertec Publishing, Inc.: Chicago, IL, 1996.

Mucho, T.P., Diamond, W.P., Garcia, F., Byars, J.D., and Cario, S.L. "Implications of Recent NIOSH Tracer Gas Studies on Bleeder and Gob Gas Ventilation Design." *Preprint of the Society for Mining, Metallurgy and Exploration Annual Meeting* (2010): 00-008.

National Institute for Occupational Safety and Health. *Coal Mining Disasters: 1839 to Present.* Accessed online from September 2014 through March 2016: www.cdc.gov/niosh/mining/statistics/content/coaldisasters.html.

National Climatic Data Center (NCDC). *Barometric Pressure Data by National Oceanic and Atmospheric Administration (NOAA)*. Accessed online from November 2014 through January 2015: http://cdo.ncdc.noaa.gov/qclcd/.

National Weather Services (NWS). *Jetstream: An Online School for Weather*. Accessed online from August through September 2015: http://www.srh.noaa.gov/jetstream/global/climate_max.htm.

Page, N.G., Caudill, S.D., Godsey, J.F., Moore, A.D., Phillipson, S.E., Steffey, D.A., Stoltz, R.T., Watkins, T.R., Cripps, D.R., Maggard, C.J., Morley, T.A., Sherer, H.E., Stephan, C.R., Vance, J.W., Brown, A.L. "Report of Investigation Fatal Underground Mine Explosion, April 5, 2010. Upper Big Branch Mine-South, Performance Coal Company. ID No. 46-08436." U.S. Department of Labor, MSHA, 2011.

Pappas, M.D., and Mark, C. "Behavior of Simulated Longwall Gob Material." In *Report of Investigations* No. 9458. U.S. Bureau of Mines, 1993a.

Pappas, M.D., and Mark, C. "Load Deformation Behavior of Simulated Longwall Gob Material." In *Proceedings of the 12th International Conference on Ground Control in Mining*, 184-193. West Virginia University, Morgantown, WV: SME, 1993b.

Peng, S.S. *Longwall Mining 2nd Ed.* Department of Mining Engineering, West Virginia University: Morgantown, WV, 2006.

Peng, S.S., Ma, W., Zhong, W. *Surface Subsidence Engineering*. Society for Mining, Metallurgy, and Exploration: Littleton, CO, 1992.

Phillips, C.A. "Report of Investigation into the Mine Explosion at the Upper Big Branch Mine." West Virginia Office of Miners' Health, Safety and Training. 2012.

Pidwirny, M. *The Mid-Latitude Cyclone - Fundamentals of Physical Geography 2nd Ed*. Online eBook. 2006. Accessed online in November 2014: http://www.physicalgeography.net/fundamentals/7s.html.

Ponnuswami, R. "Water Hammer: Quantitative Causes and Effects." *Water Encyclopedia* 1 (2005): 891-892. John Wiley & Sons.

Ren, T., and Balusu, R. "The use of CFD modelling as a tool for solving mining health and safety problems." *Underground Coal Operators' Conference* (2010): 339-349.

Ren, T., Balusu, R., and Claassen, C. "Computational Fluid Dynamics Modeling of Gas Flow Dynamics in Large Longwall Goaf Areas." In *Proceedings of the 35th Application of Computers and Operations Research in the Minerals Industry Symposium*, edited by E.Y. Baffi, 603-613. Wollongong, Australia: AusIMM, 2011.

Ren, T.X., Balusu, R., and Humphries, P. "Development of Innovative Goaf Inertization Practices to Improve Coal Mine Safety." In *Proceedings of the Coal Operator's Conference*, edited by N. Aziz, 315-322. University of Wollongong, Wollongong, Australia: AusIMM, 2005.

Ren, T.X., and Edwards, J.S. "Goaf Gas Modeling Techniques to Maximize Methane Capture from Surface Gob Wells." In *Proceedings of the North American/Ninth U.S. Mine Ventilation Symposium*, edited by E.D. Souza, 279-286. Kingston, Ontario: A.A. Balkema Publishers, 2002.

Saki, S.A., Brune, J.F., Bogin Jr., G.E., Gilmore, R.C., Grubb, J.W., Zipf Jr., R.K., and Marts, J.A. "Gob Ventilation Boreholes Design Optimization for Longwall Coal Mining." In *Proceedings of the 15th North American Mine Ventilation Symposium,* edited by E. Jong, E. Sarver, S. Schafrik, and K. Luxbacher, 453-460. Virginia Polytechnic Institute and State University, Blacksburg, VA: SME, 2015.

Salamon, M. "Mechanism of Caving in Longwall Coal Mining. Rock Mechanics Contributions and Challenges." In *Proceedings of the 31st U.S. Symposium on Rock Mechanics,* edited by W.A. Hustrulid and G.A. Johnson, 161-168. Colorado School of Mines, Golden, CO: A.A. Balkema, 1990.

Schatzel, S.J., Karacan, C.Ö., Goodman, G.V., Mainiero, R.J, and Garcia, F. "The Borehole Monitoring Experiment: Field Measurements of Reservoir Conditions and Responses in Longwall Panel Overburden During Active Mining." In *Proceedings of the 12th U.S./North American Mine Ventilation Symposium*, edited by K.G. Wallace, Jr., 93-101. University of Nevada, Reno, NV: SME, 2008.

Simpson, D. *Coal Bed Methane - In Gas Well Deliquification, 2nd Ed.* Gulf Publishing: Houston, TX, 2008.

Smith, A.C., Diamond, W.P., Mucho, T.P., and Organiscak, J.A. *Bleederless ventilation systems as a Spontaneous Combustion Control Measure in U.S. Coal Mines* IC 9377. Bureau of Mines, 1994.

Smith, A.C., and Yuan, L. "Modeling the Effect of Seal Leakage on Spontaneous Heating in a Longwall Gob Area." In *Proceedings of the 13th US/North American Mine Ventilation Symposium*, edited by S. Hardcastle and D.L. McKinnon, 479-484. Laurentian University, Sudbury, Ontario: SME, 2010.

Stevenson, J.W. "Effects of Bleeder Entries During Atmospheric Pressure Changes." *Mining Engineering* Vol. 6 (1968): 61-64.

Szlązak, J. "The determination of a co-efficient of longwall gob permeability". *Archives of Mining Sciences* Vol. 46, No. 4 (2001): 451-468.

Taylor, C.D., Chilton, J.E., and Mal, T. "Evaluating Performance Characteristics of Machine-Mounted Methane Monitors by Measuring Response Time." In *Proceedings of the North American/9th U.S. Mine Ventilation Symposium*, edited E.D. Souza, Kingston, Canada: A.A. Balkema, 2002.

Timko, R.J., and Derick, R.L. "The Methods to Determine the Status of Mine Atmospheres: An Overview." *Preprint of the Society for Mining, Metallurgy and Exploration Annual Meeting* (2006): 06-062.

Tu, J., Yeoh, G.H., and Liu, C. *Computational Fluid Dynamics: A Practical Approach*. Elsevier: Oxford, UK, 2008.

Turn, S.R. *An Introduction to Combustion: Concepts and Applications 3rd Ed*. McGraw-Hill: New York, 2012.

U.S. Environmental Protection Agency (USEPA). *Guidebook on Coalbed Methane Drainage for Underground Mines*. EPA White Paper by Mutmansky, J.M. 1999. Accessed online in July 2015: www.epa.gov/cmop.

U.S. Energy Information Administration. *Annual Energy Outlook 2017 with Projections to 2050*. DOE/EIA-0383. U.S. Department of Energy, Washington, DC. 2017.

U.S. Energy Information Administration. *Annual Coal Report 2015 – Independent Statistics and Analysis.* U.S. Department of Energy, Washington, DC. 2016.

Wachel, E.W. "Establishing Longwall Gob Porosity from Compaction in Western Coal Mines." Master's Thesis. Colorado School of Mines, 2012.

Wala, A.M., Yingling, J.C., Zhang, J., and Ray, R. "Validation Study of Computational Fluid Dynamics as a Tool for Mine Ventilation Design." In *Proceedings of the 6th International Mine Ventilation Congress*, edited by R.V. Ramani, 519-525. Pittsburgh, PA: SME, 1997.

Wallace, J.M. and Hobbs, P.V. *Atmospheric Science: An Introductory Survey 2nd Ed*. Elsevier: London, UK., 2006.

Wasilewski, S. “A Study of Changes in Barometric Pressure Underground Mines.” In *Occupational Safety and Environmental Protection in Mining* Vol. 4 (2009): 3-13 (In Polish).

Wasilewski, S. “Influence of Barometric Pressure Changes on Ventilation Conditions in Deep Mines.” *Arch. Min. Sci.* Vol. 59 No. 3 (2014): 621-639.

Wendt, M. and Balusu, R. “CFD Modeling of Longwall Goaf Gas Flow Dynamics.” *Coal and Safety Journal* Vol. 20 (2002): 17-34.

Wheatley, L.F. “Investigation Report Underground Coal Mine Explosion McClure No. 1 Mine, Clinchfield Coal Company.” Virginia Department of Mines, Minerals and Energy, 1983.

White, F.M. *Fluid Mechanics 7th Ed*. McGraw-Hill: New York, 2011.

Windridge, F.W., Parkin, R.J., Neilson, P.J., Roxborough, F.F., and Ellicot, C.W. “Report on an Accident at Moura No. 2 Underground Mine.” Warden’s Inquiry, Queensland, Australia, 1994.

Woodward, D.N., and Sheffield, T. “Report of Investigation Methane Ignition/Explosion/Mine Fire Accident, July 9, 2007 at Buchanan Mine #1, Consolidation Coal Company. ID No. 44-04856.” U.S. Department of Labor, MSHA, 2008.

Worrall, Jr., D.M. “Modeling Gas Flows in Longwall Coal Mines using Computational Fluid Dynamics.” Ph.D. diss., Colorado School of Mines, 2012.

Worrall, D.M., Wachel, E., Ozbay, U., Munoz, D., and Grubb, J.W. “Computational Fluid Dynamics Modeling of Sealed Longwall Gob in Underground Coal Mine – A Progress Report.” In *Proceedings of the 14th North American Mine Ventilation Symposium*, edited by F. Calizaya and M. G. Nelson, University of Utah, Salt Lake City, UT: SME, 2012.

Yuan, L., Smith, A.C., and Brune, J.F. “Computational Fluid Dynamics Study on the Ventilation Flow Paths in Longwall Gobs.” In *Proceedings of the 11th US/North American Mine Ventilation Symposium,* edited by J.M. Mutmansky and R.V. Ramani, 591-598. University Park, PA: Taylor and Francis, 2006.

Yuan, L. and Smith, A.C. “Modeling the effect of barometric pressure changes on spontaneous heating in bleederless longwall panels.” *Preprint of the Society for Mining, Metallurgy and Exploration Annual Meeting* (2010): 10-210.

Zipf, Jr., R.K. and Mohamed, K.M. “Composition Change Model for Sealed Atmosphere in Coal Mines.” In *Proceedings of the 13th U.S./North American Mine Ventilation Symposium,* edited by S. Hardcastle and D.L. McKinnon, 493-500. Sudbury, Ontario: SME, 2010.

Zipf, Jr. R.K., Marchewka, W., Mohamed, K., Addis, J., and Karnack, F. “Tube Bundle System for Monitoring of Coal Mine Atmosphere.” *Mining Engineering* 65-5: 57-63. Littleton, CO: SME, 2013a.

Zipf, Jr., R.K., Ochsner, R., Krog, R., Marchewka, W., Valente, M., and Jensen, R. “Tube Bundle System Studies at Signal Peak Energy Bull Mountains #1 Mine.” *Trans. Soc. Min. Metall. and Explor.* Vol. 334 (2013b): 489-497.

APPENDIX A

USER-DEFINED FUNCTION (UDF) OF PRESSURE VARIATION

```
/*
-----------------------------------------------------------------------------------------------
| PRESSURE PROFILE FOR BAROMETRIC SIMULATION                                                  |
| Added by Sam Lolon on 4/28/2016 to gilmore-marts.c file                                     |
| Note: This UDF for a 10-second flat, 1000 Pa sudden drop for 190 seconds                    |
| Seven boundary conditions; Methane Inlet remains unchanged                                  |
-----------------------------------------------------------------------------------------------
*/
DEFINE_PROFILE(inlet_entry1,t,i)
{
real x[ND_ND];
face_t f;
real y = CURRENT_TIME;
begin_f_loop(f,t)
        {
                F_CENTROID(x,f,t);
                if (y <= 0 && y <= 0) {
                        F_PROFILE(f,t,i) = 3332.132;
                }
                        if (y > 0 && y <= 9000) {
                        F_PROFILE(f,t,i) = 2332.132;
                }
        end_f_loop(f,t)
        }
}
DEFINE_PROFILE(inlet_entry2,t,i)
{
real x[ND_ND];
face_t f;
real y = CURRENT_TIME;
begin_f_loop(f,t)
        {
                F_CENTROID(x,f,t);
                if (y <= 0 && y <= 0) {
                        F_PROFILE(f,t,i) = 3332.198;
                }
                if (y > 0 && y <= 9000) {
                        F_PROFILE(f,t,i) = 2332.198;
                }
        end_f_loop(f,t)
        }
```

```
}
DEFINE_PROFILE(inlet_entry3,t,i)
{
real x[ND_ND];
face_t f;
real y = CURRENT_TIME;
begin_f_loop(f,t)
        {
                F_CENTROID(x,f,t);
                if (y <= 0 && y <= 0) {
                        F_PROFILE(f,t,i) = 3467.582;
                }
                if (y > 0 && y <= 9000) {
                        F_PROFILE(f,t,i) = 2467.582;
                }
        end_f_loop(f,t)
        }
}
DEFINE_PROFILE(inlet_entry4,t,i)
{
real x[ND_ND];
face_t f;
real y = CURRENT_TIME;
begin_f_loop(f,t)
        {
                F_CENTROID(x,f,t);
                if (y <= 0 && y <= 0) {
                        F_PROFILE(f,t,i) = 3335.524;
                }
                if (y > 0 && y <= 9000) {
                        F_PROFILE(f,t,i) = 2335.524;
                }
        end_f_loop(f,t)
        }
}
DEFINE_PROFILE(inlet_entry5,t,i)
{
real x[ND_ND];
face_t f;
real y = CURRENT_TIME;
begin_f_loop(f,t)
        {
                F_CENTROID(x,f,t);
                if (y <= 0 && y <= 0) {
                        F_PROFILE(f,t,i) = 3328.255;
                }
```

```
                if (y > 0 && y <= 9000) {
                        F_PROFILE(f,t,i) = 2328.255;
                }
        end_f_loop(f,t)
        }
}
DEFINE_PROFILE(outlet_entry1,t,i)
{
real x[ND_ND];
face_t f;
real y = CURRENT_TIME;
begin_f_loop(f,t)
        {
                F_CENTROID(x,f,t);
                if (y <= 0 && y <= 0) {
                        F_PROFILE(f,t,i) = 2331.556;
                }
                if (y > 0 && y <= 9000) {
                        F_PROFILE(f,t,i) = 1331.556;
                }
        end_f_loop(f,t)
        }
}
DEFINE_PROFILE(outlet_bleeder,t,i)
{
real x[ND_ND];
face_t f;
real y = CURRENT_TIME;
begin_f_loop(f,t)
        {
                F_CENTROID(x,f,t);
                if (y <= 0 && y <= 0) {
                        F_PROFILE(f,t,i) = 2241;
                }
                if (y > 0 && y <= 9000) {
                        F_PROFILE(f,t,i) = 1241;
                }
        end_f_loop(f,t)
        }
}
```

APPENDIX B

UDF OF EXPLOSIBILITY COLOR FOR METHANE-AIR MIXTURE

```
/*
-----------------------------------------------------------------------------------------------
| EXPLOSIVE METHANE-AIR MIXTURES (EGZ)                                                        |
| STORES in (user-define-memory 2) – udm-2                                                    |
| Modified by Sam Lolon on 06/05/2016 from (cal_explosive_mix_NEWER)                          |
| for methane-air species and filename changed to gilmore-marts-sam.c.                        |
| N2 and O2 component are removed. Three transition zones are included                        |
-----------------------------------------------------------------------------------------------
*/
*/
DEFINE_ON_DEMAND(calc_explosive_methane_air)
{
Domain *d; Thread *t; cell_t c;

  real px; real py; real u; real v;
  real u1; real v1; real w;
 real Y_CH4, Y_O2, Y_N2, MW_CH4, MW_O2, MW_N2, MW_Mix, X_CH4, X_O2, Y_Air,
 MW_Air, X_Air;
  real explode;
  d = Get Domain(1);
  thread_loop_c(t,d) {
          begin_c_loop(c,t) {
                  /* Y_X = Mass Fraction of Species X || X_X = Mole Fraction of Species X */
                  Y_CH4=C_YI(c,t,0);
/* Y_N2=C_YI(c,t,1); */
                  Y_Air=1.0-Y_CH4;
/* Y_Air=1.0-Y_CH4-Y_N2; */
                  MW_CH4= 16.043;
                  MW_O2= 31.9988;
                  MW_N2= 28.0134;
                  MW_Air=28.966;
                  MW_Mix= 1/(Y_CH4/MW_CH4+Y_Air/MW_Air);
/* MW_Mix= 1/(Y_CH4/MW_CH4+Y_Air/MW_Air+Y_N2/MW_N2); */
                  X_CH4=(Y_CH4*MW_Mix)/MW_CH4;     /* X = Mole Fraction of X */
                  X_Air=(Y_Air*MW_Mix)/MW_Air;
                  px= X_CH4;
                  X_O2=0.2095*X_Air;
                  py=X_O2;
                  u = 0.8529*px+0.0606; /* Near Explosive to Explosive Slope */
                  v=-0.21*px+0.21;  /* Upper Explosive Limit  */
                  u1=0.8864*px+0.0445;  /* Near Explosive to Requires Air Slope */
```

```
v1=-1.3929*px+0.195;
w=v1;
/*v1=-1.2647*px+0.1771; Cyan to Yellow Slope Transition */

/*w=-1.8545*px+0.2095; Continuation of Slope Oxygen Rich to Oxygen Poor */

/* Explosive Zone - RED */
if (py>u && px>0.055 && py<v)  {
        explode=0.69E0;
        C_UDMI(c,t,2) = explode;
}
/* Near Explosive Zone - PURPLE */
else if (py>u1 && py<u && py<v && py>v1)  {
        explode=0.56E0;
        C_UDMI(c,t,2) = explode;
}
/* Lower Near Explosive Zone - ORANGE */
else if (px>0.040 && px<0.055 && py<v && py>v1)  {
        explode=0.81E0;
        C_UDMI(c,t,2) = explode;
}
/* Bottom Near Explosive Zone - DARK BLUE */
else if (py>u1 && px>0.04 && py<v1)  {
        explode=0.44E0;
        C_UDMI(c,t,2) = explode;
}
/* Fuel Rich Inert - YELLOW */
else if (py<u1 && py>v1 && px>0.055)  {
        explode=1.0E0;
        C_UDMI(c,t,2) = explode;
}
/* Oxygen Lean Inert - Green A  */
else if (py<v1 && px>0.04) {
        explode = 0.19E0;
        C_UDMI(c,t,2) = explode;
}
/* Oxygen Lean Inert - DARK  GREEN  */
else if (py<0.08 && px<0.04) {
        explode = 0.0E0;
        C_UDMI(c,t,2) = explode;
}
/* Oxygen Lean Inert - Green B  */
else if (py<w && px<0.04) {
        explode = 0.19E0;
        C_UDMI(c,t,2) = explode;
}
```

```
                /* Oxygen Rich Inert - CYAN */
                else if (py>w) {
                        explode = 0.31E0;
                        C_UDMI(c,t,2) = explode;
                }
                /* Explosive Zone - BLACK */
                else{
                        explode = 2.66E0;
                        C_UDMI(c,t,2) = explode;
                }
        }  end_c_loop(c,t) }
}
```

APPENDIX C

MESH ASSEMBLY JOURNAL CODE

```
; A journal file to import meshed parts and assemble the full bleeder model
; Created by Sam Lolon on 05/11/2016
;
;-------------------------------------------------------------------------------------------------------------
; IMPORT THE MESH FILES
;-------------------------------------------------------------------------------------------------------------
/file/read "headgate-entry.msh"
/mesh modify-zones/append-mesh "mine-entry.msh"
/mesh modify-zones/append-mesh "tailgate-entry.msh"
/mesh modify-zones/append-mesh "bleeder.msh"
/mesh modify-zones/append-mesh "face.msh"
/mesh modify-zones/append-mesh "gob.msh"
/mesh modify-zones/append-mesh "gob-void.msh"
/mesh modify-zones/append-mesh "strata.msh"
;
;
;-------------------------------------------------------------------------------------------------------------
; SET INTERFACES BETWEEN CONNECTING PARTS
;-------------------------------------------------------------------------------------------------------------
; [mapped] [periodic repeats] [coupled wall] [matching] [only if matching=yes]
/define/mesh-interfaces/create int-face-gob interface-shield-gob () interface-gob-shield () no no no no
/define/mesh-interfaces/create int-entry3-gob interface-entry3-gob () interface-gob-entry3 () no no no yes yes
/define/mesh-interfaces/create int-entry3-hgvoid interface-entry3-hgvoid () interface-hgvoid-entry3 () no no no yes yes
/define/mesh-interfaces/create int-entry3-face interface-entry3-shield () interface-shield-entry3 () no no no yes yes
/define/mesh-interfaces/create int-entry4-gob interface-entry4-gob () interface-gob-entry4 () no no no yes yes
/define/mesh-interfaces/create int-entry4-tgvoid interface-entry4-tgvoid () interface-tgvoid-entry4 () no no no yes yes
/define/mesh-interfaces/create int-entry4-face interface-entry4-shield () interface-shield-entry4 () no no no yes yes
/define/mesh-interfaces/create int-hgxcut-hgvoid interface-hgxcuts-hgvoid () interface-hgvoid-hgxcuts () no no no no
/define/mesh-interfaces/create int-tgxcut-tgvoid interface-tgxcut1-tgvoid interface-tgxcuts-tgvoid () interface-tgvoid-tgxcuts () no no no no
/define/mesh-interfaces/create int-gob-hgvoid interface-hgvoid-gob () interface-gob-hgvoid () no no no yes yes
```

/define/mesh-interfaces/create int-gob-tgvoid interface-tgvoid-gob () interface-gob-tgvoid () no no no yes yes
/definemesh-interfaces/create int-gob-bleeder interface-bleeder-gob () interface-gob-bleeder () no no no yes yes
/define/mesh-interfaces/create int-entry5-bleeder1 interface-entry5-bleeder1 () interface-bleeder1-entry5 () no no no yes yes
/define/mesh-interfaces/create int-entry5-bleeder2 interface-entry5-bleeder2 () interface-bleeder2-entry5 () no no no yes yes
/define/mesh-interfaces/create int-entry2-bleeder1 interface-entry2-bleeder1 () interface-bleeder1-reg102hg () no no no yes yes
/define/mesh-interfaces/create int-entry2-bleeder2 interface-entry2-bleeder2 () interface-bleeder2-reg103hg () no no no yes yes
/define/mesh-interfaces/create int-gob-strata interface-gob-upperseam () interface-upperseam-gob () no no no yes yes
;
;----------